Synthesis of Diphenyl Ethers for the Detection of Ions by Photophysical Methods.

A thesis submitted

by

Ashok Kumar
(Reg. No. 901609001)

In partial fulfillment of the
requirement for the degree of
Doctor of Philosophy

Supervision of
Prof. Manmohan Chhibber

School of Chemistry and Biochemistry
Thapar Institute of Engineering and Technology
Patiala – 147004 Punjab, India
March 2023

Dedicated to
My
Beloved family

Acknowledgements

With humble thanks, I owe it all to Almighty God for granting me the wisdom, health and strength to undertake this research task and who kindly helping me to complete my thesis.

Completion of this doctoral dissertation was not possible without the support of several people. I would like to express my sincere gratitude to all of them. First of all, I am extremely grateful to my research guide, **Prof. Manmohan Chhibber** for the valuable guidance, scholarly input, and consistent encouragement I received throughout the research work. Your advice on both research as well as on my career has been priceless. Sir, I consider it a great opportunity to do my doctoral program under your guidance and to learn from your research expertise. Thank you Sir, for all your help and support.

I would also like to thank my doctoral committee members, **Prof. Satnam Singh, Prof. Haripada Bhunia, and Dr. Bhupesh Goyal** for serving as my committee members even in hardship. I also want to thank you for letting my defense be an enjoyable moment, and for your brilliant comments and suggestions, thanks to you.

I am profoundly obliged to **Prof. Satnam Singh**, Professor and Head, School of Chemistry and Biochemistry, Thapar Institute of Engineering and Technology, Patiala for their good wishes and motivation.

Special regards to my beginning teachers and teachers of the School of Chemistry and Biochemistry for providing suggestions and taking interest in the progress of work along with the lab facility. Special thanks to **Dr. Davinder Kumar** for his assistance in completing the analytical calculations of my project.

The thesis would not have come to successful completion, without the help I received from the staff of the Department of Chemistry and Biochemistry. I would like to specially acknowledge **Mr. Chander Singh Thakur** for always being there to help.

I am thankful to all my lab mates and colleagues for their help and cooperation. I would like to acknowledge my dear ones, **Dr. Aadil Batla, Dr. Sanjeev Kumar, Mr. Sunil Dutt, Dr. Shagun Kainth, Dr. Rupinder Kaur, Dr. Vanshita Goel, Dr. Pawandeep Kaur, Dr. Shivali, Miss Aashima Mahajan, and Mr. Dinesh Kumar** for always standing by my side and sharing a great relationship as compassionate friends. I will forever cherish the warmth shown by them, whose smiling faces always made me refreshed.

Most of the results described in this thesis would not have been possible without the help of laboratories at the institutes like **SAI,** Thapar Institute of Engineering and Technology, Patiala, **SAIF**, Punjab University, Chandigarh is gratefully acknowledged for investigating detection studies.

I gratefully acknowledge the Thapar Institute of Engineering and Technology, Patiala for providing me with financial support.

A special thanks to my family. Words cannot express how grateful I am to my father Mr. Karam Chand my mother Mrs. Satya Devi, my Sister **Reeta Devi, Usha Devi, Pinki Devi, prem lata Mr. Baneet Mehta, and Wood be Nisha Rana** for all the sacrifices that you've made on my behalf. Your prayer for me was what sustained me thus far.

Despite all this cooperation rendered generously by one and all, I am solely responsible for any errors and shortcomings of this dissertation.

Ashok Kumar

Candidate's Declaration

I, hereby declare that the work presented in the thesis entitled **"Synthesis of Diphenyl Ethers for the Detection of Ions by Photophysical Methods"**, in partial fulfillment of the requirement for the award of the degree of Doctor of Philosophy at the School of Chemistry and Biochemistry, Thapar Institute of Engineering and Technology, Patiala, is an authentic record of my work under the supervision of Prof. Manmohan Chhibber, School of Chemistry and Biochemistry, Thapar Institute of Engineering and Technology, Patiala, India. The matter embodied in this thesis has not been submitted in part or full to any other university or institute for the award of any degree in India or abroad.

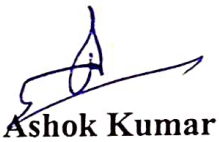

Ashok Kumar
(Regd. No. 901609001)

Certificate

This is to certify that the thesis entitled **"Synthesis of Diphenyl Ethers for the Detection of Ions by Photophysical Methods",** being submitted by Mr. Ashok Kumar in the partial fulfillment of the requirement for the award of the degree of Doctor of Philosophy to the School of Chemistry and Biochemistry, Thapar Institute of Engineering and Technology, Patiala, is a record of **candidate's** work carried out by his under my supervision and guidance. The matter presented in this thesis has not been submitted in part or full for the award of any degree in any other university or institute.

(Supervisor) 24/3/2023.

Prof. Manmohan Chhibber
School of Chemistry and Biochemistry
Thapar Institute of Engineering and
Technology, Patiala – 147004, Punjab
(India)

Prof. Satnam Singh 24/3/23
Head
School of Chemistry and Biochemistry
Thapar Institute of Engineering and
Technology, Patiala – 147004, Punjab
(India)

Table of Contents

List of Figures

List of Scheme's

List of Table's

Abbreviations

Abbreviated Form	Full form
ACN	Acetonitrile
Ala	Alanine
A^o	Angstrom
B3LYP	Becke 3 Lee-Yang and Parr
CH_3COOH	Acetic acid
Compd	Compound
DFT	Density Functional Theory
^oC	Degree Celsius
DMF	Dimethylformamide
DMSO	Dimethylsulfoxide
EPA	Environmental Protection Agency
Eq.	Equation
Equiv.	Equivalent
HEPES	4-(2-hydroxyethyl)-1-piperazineethanesulfonic acid
HOMO	Highest occupied molecular orbital
HPLC	High pressure liquid chromatography
HSAB	Hard soft acid base
Hz	Hertz
Ile	Isoleucine
IR	Infra-red
IUPAC	International Union of Pure and applied chemistry
Kcal/mol	Kilo calorie/mole
leu	Lucine
LUMO	Lowest unoccupied molecular orbital
Lys	Lysine
MeOH	Methanol
MHz	Mega-hertz
mL	Millilitre
mM	Milimolar
mm	Millimeter
nM	Nano-molar
nm	nanometer
NMR	Nuclear Magnetic Resonance
pH	Potential of Hydrogen
Phe	Phenyl Alanine
ppm	Part per million
Pro	Proline
THF	Tetrahydrofuran
TLC	Thin Layer Chromatography
Trp	Tryptophan
UV	Ultra-violet
val	Valanine
WHO	World Health organization
µM	Micro-Molar

Abstract

The selective recognition of cations and anions is vital due to their diverse application in chemistry, biology and the environment. Diphenyl ethers present an attractive architecture with the right balance between rigidity and flexibility due to aromatic planer rings, rotation around the ether linkage, and an inbuilt cavity. Also, the substituents on the phenyl rings can alter the electron density inside the void.

Synthesis of several diphenyl ethers has recently been reported, along with their applications to detect ions. However, the literature lacks a systematic study around the motif by varying substituents on phenyl rings. The present work, presented in three units, explored the selectivity, sensitivity, detection limit, solvent effect and other parameters for environmentally and biologically essential ions by changing the functional group on the molecules.

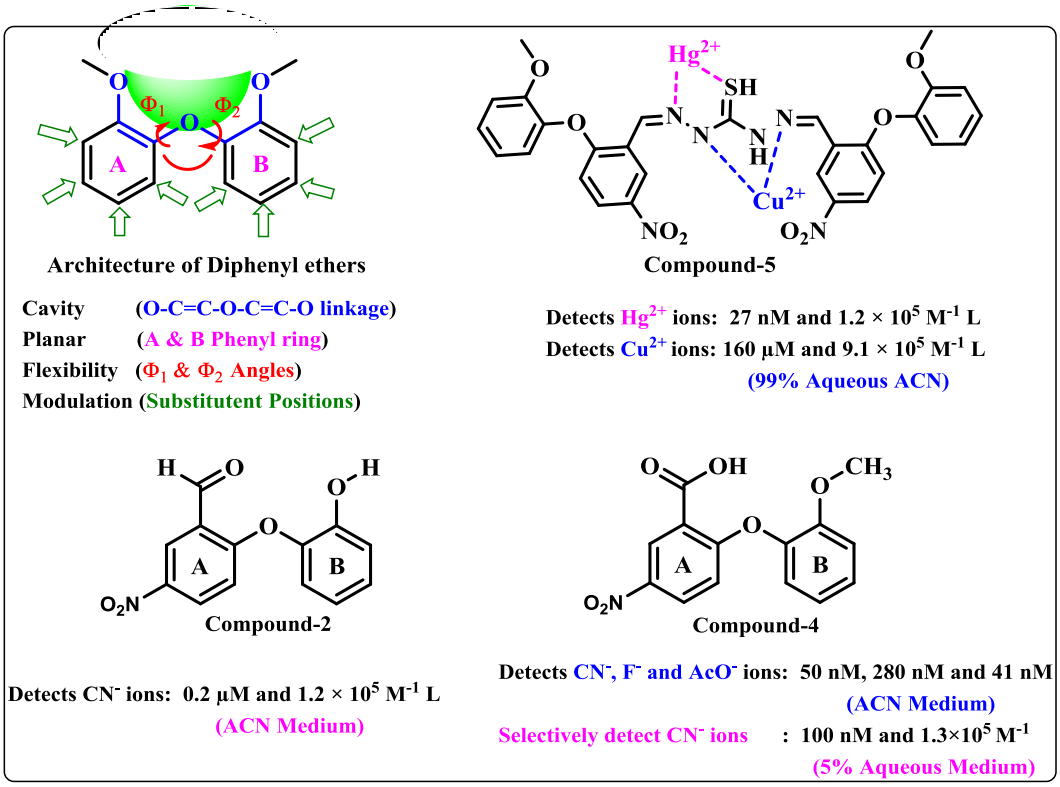

Section-I describes the importance, background, rationale, and recent literature about detecting essential ions. It also details the methodology, techniques and calculations used to conduct the experiments.

Section-II defines the detection of cations with initial studies on optimizing functional groups on diphenyl ethers for recognizing Hg^{2+} and Pb^{2+} ions in an aqueous medium. The molecules' narrow pH range (7.5 to 9.0) to respond to cations constrained their real-life application. Nonetheless, the studies based on pH, solvents and computational data added value to exploring the interaction mechanism. The detection limit of toxic and biologically important cations, Hg^{2+} and Cu^{2+} ions respectively, was refined using a thiocarbohydrazides-based dimeric diphenyl ether **(**Compound-**5)** in an aqueous medium. It could detect Hg^{2+} and Cu^{2+} ions with a minimum concentration limit of 27 nM and 160 µM and an association constant of 1.2×10^5 M^{-1} L and 9.1×10^5 M^{-1} L. The work demonstrated and validated the detection of Hg^{2+} ions in non-invasive biological samples (urine) as a real-life application.

Section-III initiates studies with seven diphenyl ethers containing acidic protons to detect anions via a proton abstraction mechanism. Two compounds displayed selectivity for cyanide ion (Compound-**2)** and cyanide, fluoride and acetate ions (Compound-**4**) with detection limits in the nanomolar range using an acetonitrile medium. Further optimization under different pH and solvent conditions made compound-**4** more selective in detecting the cyanide ions in the neutral pH range. The optimization studies not only explored the proposed proton abstraction mechanism but also detected CN^- ions reasonably with a minimum detection limit of 100 nM and a binding constant equal to 0.5×10^5 M^{-1}.

Theoretical calculations, NMR titrations and IR spectra were used as additional tools to get an insight into the binding sites and interaction mechanism.

Section-I

Introduction & Materials

Chapter-1

Introduction & Literature Review

Chapter-1

Introduction and Literature Survey

1.1. Introduction

The selective recognition of cations and anions is vital due to its diverse application in chemistry, biology and environment. [1-3]

The alkali (Na^+, K^+, Mg^{2+} and Ca^{2+}) and transition metal ions (Cu^{2+}, Zn^{2+}, Mn^{2+}, Fe^{3+} and many more) are essential for many biological processes.[4-6] Detecting these ions is vital for clinical diagnostics and understanding their natural role.[7] Heavy metal ions such as Hg^{2+}, Pb^{2+} and Cd^{2+} are of particular interest due to their ability to form a complex with nitrogen, sulphur and oxygen-containing biological receptors and cause toxicity. The resulting change in the molecular structure of proteins and enzyme inhibition leads to toxicological effects.[8-10] The toxicity of the metal ions can be related to the famous statement of Paracelsus, a Swiss physician and philosopher, that said, "*Everything is poisonous, and nothing is not dangerous; only the dose decides whether something is poisonous or not.*" The concentration of the vital metal ions requires stringent limits in biological systems. Any deviation from the limits can change the equilibrium state to one of deficiency or excess. The latter is the source of metal toxicity.

The body's inability to remove excess essential metal ions like Na^+ or K^+ causes one of the most prevalent electrolyte abnormalities causing congestive heart failure, renal failure, chronic kidney disease, and hypertension.[11] Zinc is present in muscle, liver, and brain. Still, high amounts of this metal ion reduce copper intake to induce myeloneuropathy.[12] Other necessary elements include Co, Mn, Fe, Cu, and Mo in biological processes. Higher concentrations of cobalt cause acute toxicity, such as hypothyroidism and polycythaemia,[13] Mn causes neurotoxicity, and Fe and Cu shortage causes Wilson disease.[14]

Lead poisoning affects neurological, haematopoietic, renal, endocrine, and skeletal systems.[15] Cadmium is a carcinogen that causes illness, emphysema, renal failure, bone abnormalities, and immunosuppression.[16] Recent studies also indicate a rise in cancer risks and death in environmentally exposed populations.[17] Mercury toxicity, referred to as Minamata sickness, causes neurological disorder with symptoms of ataxia, numbness in the hands and feet, general muscular weakness, narrowing of the field of vision, and hearing and speech loss.[18]

Anions also play an essential role in various biological and chemical processes. It includes hormone transfer, protein production, DNA control, and many enzyme functions.[19] These and the corresponding cations are released into the environment through industrial processes of electrocoating, metallurgy, pharmaceutical synthesis, mining and fumigation.[20] Cyanide, fluoride, phosphate and acetate are critical anions that need identification methods in water, biological and environmental samples due to their adverse effects.

Cyanide, for example, is highly toxic by all routes of administration, affecting circulatory, pulmonary and central nervous systems. It inactivates cytochrome oxidase and suppresses cellular respiration to cause anoxia.[21] Phosphate, on the other hand, is one of the essential biological electrolytes for all living creatures. Many disorders like hyperparathyroidism, vitamin D insufficiency, Fanconi syndrome, female ovulation, uremic condition, dental caries and production of dental calculus require the awareness of phosphate levels in bodily fluids for their diagnosis.[22] However, the inorganic phosphate from fertilizers causes excessive growth (eutrophication) of aquatic plants and algae, disrupting marine life. Also, the organophosphate pesticides in agricultural activities percolate in ground waters, causing severe health problems.[23]

Fluoride is another critical anion absorbed quickly by the body but eliminated gradually. The excess fluoride exposure causes acute stomach and renal issues.[24] Fluoride in drinking water beyond permissible limits causes crippling bone disease-fluorosis in many geographical locations. The anion is also vital for the uranium purification and analysis of nerve agent Sarin (isopropyl ethylphosphonofluoridate).[25-27] Dental health and the treatment of osteoporosis also require knowledge of the fluoride concentration in biological samples .[28-30]

As discussed for the anions, the non-essential metal ions sneak into biological systems through industrial and anthropogenic emissions. Lead adsorbs onto the particulate matter from lead-based paints and anti-knock compounds used in gasoline to be breathed and ingested. The need for the power and coal-based industry is the most significant source of anthropogenic mercury emissions besides the gold mining and chemical industry. Cadmium is taken up by some plants like tobacco, rice, wheat, peanuts, and cocoa quickly from the soil, even at low concentrations. Consumption of such eatables is the most common nonindustrial source of exposure for cadmium. Thus, there is a need to develop low-cost and effective methods to determine these ions at their lowest detection limits. Using receptors with the ability to bind these ions is one of the practical techniques.

1.2. Receptors

Identifying and quantifying ions is significant from an industrial and environmental point of view. The use of high-end and exclusive instruments like inductively coupled plasma(ICP-ES, ICP-MS),[31] total reflection X-ray fluorimetry (TXRF),[32] stripping voltammetry (ASV)[33] mass spectrometry,[34] atomic fluorescence spectrometry,[35] high-performance liquid chromatography[36] and atomic absorption spectrometry[37] for the detection of ions is quite prevalent. In spectrophotometric complexing agents, the receptors selectively bind to the ions, offering a promising solution for such detections due to simple, non-destructive, rapid and low concentration-response operations.[38] Here, an analyte can selectively bind or react with the receptor to deliver change in the latter's optical properties detected by UV-vi or fluorescence spectroscopy.[38, 39]

The receptor molecule contains a heteroatom (nitrogen, oxygen, sulphur, phosphorous) in the form of amines, alcohols, thiols, ethers, thioethers, pyridine, pyrimidine, quinoline, triazole, isoxazole, etc. or a functional group containing carbonyl, carboxyl, ester, amide, thiocarbonyl, imine, diethoxyphosphoryl to bind with the cation or an anion selectively. Alkali, alkaline earth, lanthanides and transition metals in the first row, up to cobalt, prefer to coordinate with hard O-containing ligands and less likely to be coordinate with soft N-containing ligands. Transition metals in succeeding rows, however, prefer N-donors.

A sea of receptors that bind to ions are available in the literature. The following paragraphs discuss receptors that specifically bind to Hg^{2+}, Cu^{2+} and Pb^{2+} ions in the present work context.

1.2.1. Detection of Hg^{2+} Ions

A few receptors reported in the literature detect Hg^{2+} ions selectively using UV-Visible and fluorescence spectroscopy.

With fluorescence techniques, Bhalla et al. modified pyrene using 15-crown-5-ether to selectively detect Hg^{2+} ions up to 40 nM **[Figure-1.1 (a)]**.[40] This efficiency of the receptor was attributed to the electron-rich oxygen atoms of the crown ether unit that enhanced the fluorescence via the PET mechanism. The scope of crown ethers was widened to increase sensitivity for Ag^{+}, Hg^{2+}, and Cd^{2+} ions by replacing oxygen with other heteroatoms. For example, N, N-dibenzyl-4,13-diaza-18-crown-6 shows increased affinity for Hg^{2+} ion when oxygen atoms of an 18-crown-6 are replaced by nitrogen **[Figure-1.1 (b)].**[41] The replacement with nitrogen atoms influenced the cavity formed in the crown ring and side arm donor

provides three-dimensional solvation that may leads to the selective interaction with Hg^{2+} ions.

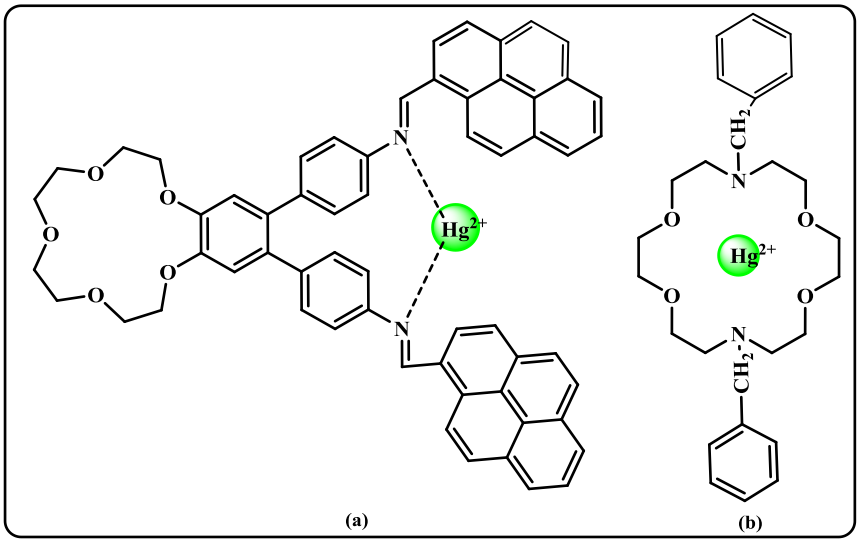

Figure-1.1: Bhalla and Gupta et. al. modified the crown ether receptor with **a)** pyrene and **b)** an N-N-dibenzyl group to improve the selectivity towards Hg^{2+} ions.

Vincens and co-workers reported modification of the calixarenes with pyrenes and spiro-lectum unit **[Figure-1.2 (a)]** for the selective detection of Hg^{2+} ions using absorption and emission spectroscopy.[42]

Benz-imidazole and benzo-thiazole-based derivatives signal the detection of ions in the presence of heteroatoms. **Figures-1.2 (b)** shows an example reported by Ergun et al. that selectively detects Hg^{2+} ions using synthesized benzimidazole-based with a detection limit of 39 nM in a 1:1 stoichiometric ratio **[Figure-1.2 (b)]**.[43]

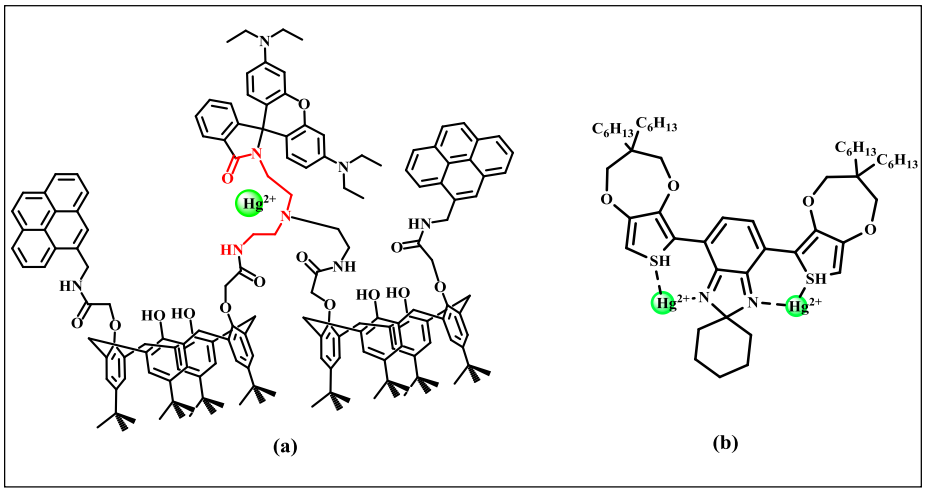

Figure-1.2: (a) Modification of the calixarenes with pyrenes and spiro-lectum unit and **(b)** benzimidazole-based receptor for the selective detection of Hg^{2+} ions.

Yao and co-workers reported on a new benzothiazole-based receptor for the simultaneous detection of Hg^{2+} and Cu^{2+} ions using fluorescence techniques. Fluorescence quenching confirmed the copper complex formation with the receptor unit while deprotecting the thio-acetal group with mercury gave a new fluorescence peak. **[Figure-1.3 (a)]**.[44]

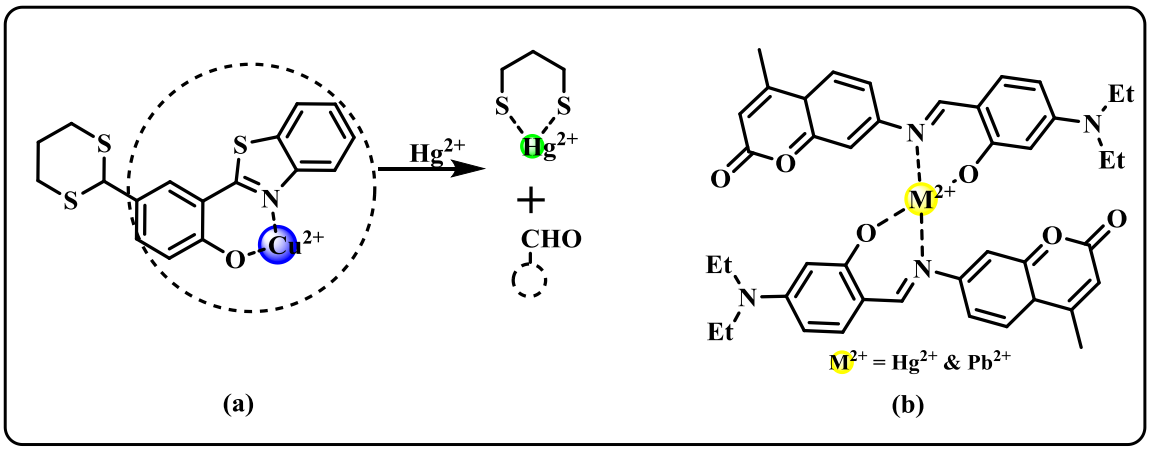

Figure-1.3: (a) Benzo-thiozole based receptors for the detection of Cu^{2+}/ Hg^{2+} ions respectively and **(b)** coumarin based receptors for the Selective metal detection of Hg^{2+}/ Pb^{2+}ions.

Coumarin, a known signalling unit, has been manipulated for metal ion detection by incorporating 4-(diethylamino) and salicylaldehyde moieties by Muthusamy et al. The motif, as shown in **Figure-1.3 (b)** can detect Hg^{2+} and Pb^{2+} ions in an aqueous medium up to a minimum detection limit of 8.3 and 10.5 nM, respectively. The receptor uses intramolecular proton transfer and photo-induced electron transfer mechanisms for detection.[45]

Many researchers, including this work, have used the carboxylate group as a recognition site for detecting Hg^{2+} ions. A detailed literature survey has been presented later in chapter-**4**. Sayani Das et al. reported hemicyanine-based receptor **[Figure-1.4 (a)]** for detecting up to 50 nM of Hg^{2+} ions in a 100% aqueous buffer solution. The group validated their results by ^{1}H-NMR titration and DFT, displaying a binding ratio of 1:2.[46]

Naphthalene, a fluorescent signal unit, has been extensively used for ion detection. Tai Wei et al. reported on a similar receptor **[Figure-1.4 (b)]** for detecting Hg^{2+} ions at µM concentration. In DMSO same receptor could sense to a minimum detection limit of 55 nM.[47]

Besides benzothiazole and coumarin discussed above, indole, another heterocycle, has been extensively explored as a functional material. Needless to mention that indole is a pharmaceutically active motif used in many medicines. The presence of unsaturated pi electrons in this chromophore makes it a potential signalling unit for developing into a sensor. **Figure-1.4 (c)** shows an example of indole and coumarin-tagged motifs for

recognizing metal ions. Joshi et al. synthesized a molecule that could sense Hg^{2+} ion sensing using absorption studies up to 0.1 µM with an association constant of $6.4 \times 10^3\ M^{-1}$.[48]

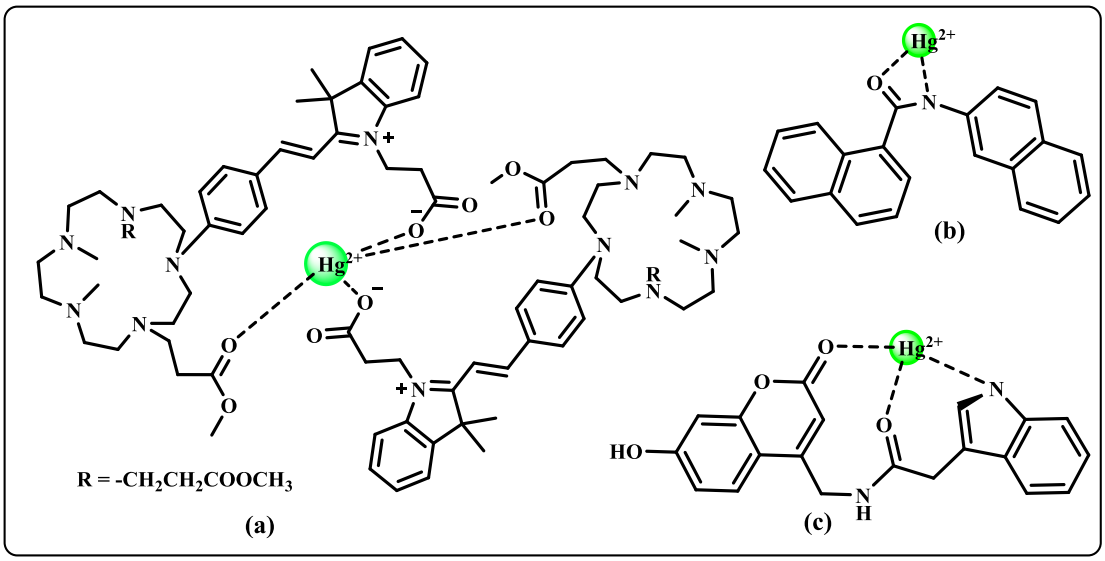

Figure-1.4: (a) Hemicyanin-based receptor used carboxylate ions for the selective detection of Hg^{2+} ions. **(b)** Naphthalene-based fluorescent receptors and **(c)** coumarin-tagged indole signalling unit for Hg^{2+} and Fe^{3+} ions detection.

1.2.2. Detection of Cu^{2+} Ions

Copper is one of the essential elements in biological systems. Its deficiency or excess can cause many medical conditions that may harm life. In literature, it has been established that nitrogen as a heteroatom in the receptor helps to recognize Cu^{2+} ions.[49]

Rhodamine, a fluorescent scaffold, is a popular transducer due to its high absorption coefficient. Its high excitation and emission wavelengths, quantum yield, and process of non-fluorescent spiro-lactam ring opening to fluorescent amide make it an attractive receptor. Wang et al. synthesized rhodamine-based absorption and fluorescence sensor for dual channel detection of Cu^{2+} and Co^{2+} ions having a minimum detection limit and an association constant for the Cu^{2+} as 85 nM and $5.93 \times 10^5\ M^{-1}$, respectively **[Figure-1.5 (a)]**.[50] The group validated the proposed stoichiometry for the copper complex as 1:1 and the cobalt complex as 2:1. Similarly, Mergu et al. synthesized a Schiff-based receptor to detect Cu^{2+} ions with a minimum detection range of 1.0 µM **[Figure-1.5 (b)]**.[51]

Azine, a nitrogen-containing derivative, selectively detects Cu^{2+} ions in 20% aqueous / DMSO medium up to 35 nM using colorimetric and fluorescent techniques with a stoichiometric of 2:1 **[Figure-1.6 (a)]**.[52] Yuxin Guo's group developed a pyrene-based Schiff

base for detecting Cu^{2+} ions by colorimetric and absorption methods **[Figure-1.6 (b)]** having a minimum detection limit of 8.5 µM with a binding constant of $0.4\times10^{5}\ M^{-1}$.[53]

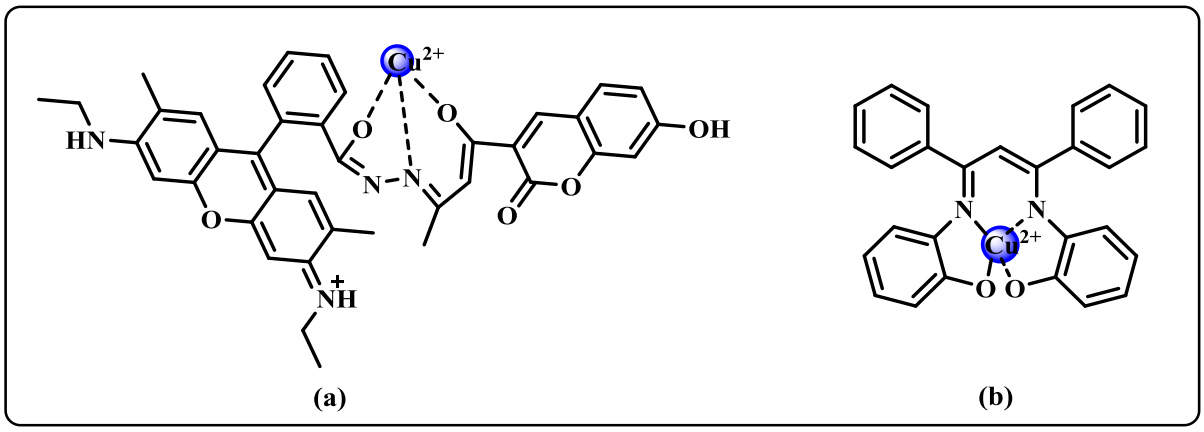

Figure-1.5: (a) A rhodamine based dual-channel sensor for Cu^{2+} and Co^{2+} ions and **(b)** Schiff based receptors for selective Cu^{2+} ions detection.

The NMR titration studies confirmed the stability of the complex formation, while DFT calculations displayed a stoichiometric ratio of 1:1. Quinoline units have been used as a building block for receptor design due to their unique signaling properties for detecting metal ions. Owais group reported selective detection of copper with a detection limit of 1.03 µM in a stoichiometric ratio of 1:1 **[Figure-1.6 (c)]**. The colorimetric change from colorless to light green gave a binding constant for the receptor metal complex of $1.43\times10^{4}\ M^{-1}$.[54]

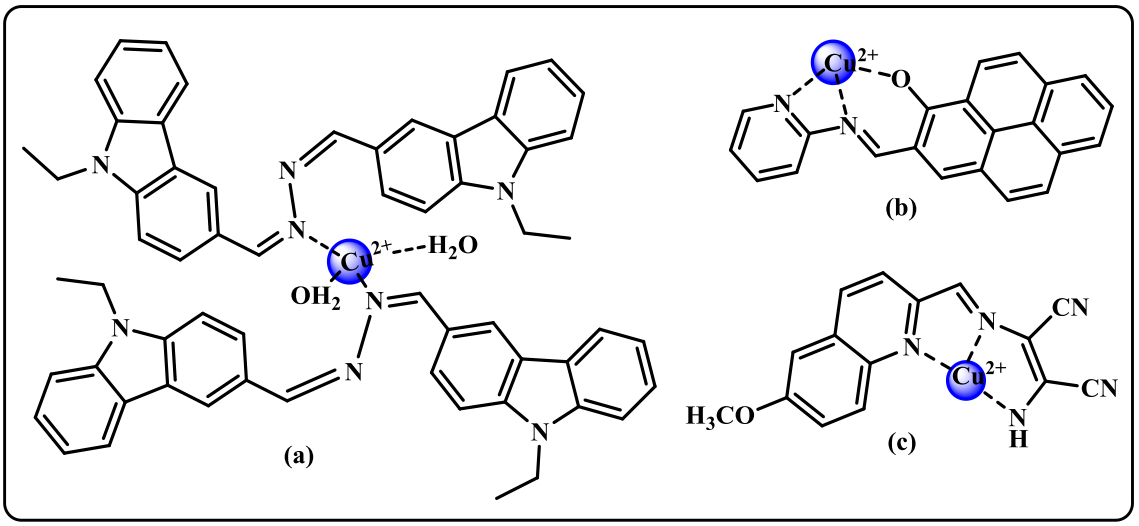

Figure-1.6: (a) Selective detection of Fe^{3+} and Cu^{2+} ions upto 3.0 and 35 nM respectively with azine based receptors **(b)** Pyrene-based optical sensor for the selective detection of metal ions such as Cu^{2+} ion with their minimum detection limits at 8.5 µM in a stoichiometric ratio of 1:1. **(c)** Quinolone-based optical sensor for selective Cu^{2+} ions detection with their minimum detection limits that are 1.03 µM in a 1:1 stoichiometric ratio.

1.2.3. Detection of Pb^{2+} Ions

Deshpande's group created a spiropyran-based receptor for the selective detection of Pb^{2+} ions with a detection limit of 40 nM and a binding constant value of 2×10^5 M^{-1}. The binding was justified using a 2:1 stoichiometric ratio and further confirmed by the NMR titration experiments **[Figure-1.7 (a)]**.[55] Another coumarin-based receptor with a 1:1 binding stoichiometry, 1.9 nM detection limit, and 6.76×10^6 M^{-1} binding constant was reported by Kumar et al. for detecting Pb^{2+} ions. The system used a 20 mM phosphate-buffered solution using DMSO/H_2O (1:9 (v/v), pH 8.0) **[Figure-1.7 (b)]**.[56] A fluorene-bearing pyridine-2,6-dicarboxamide receptor was reported in 2021 for Cu^{2+} and Pb^{2+} ion detection. The potential of the receptor and its parameters were calculated Using optical methods. The association constant for Cu^{2+} and Pb^{2+} complexes was 8.89×10^3 M^{-1} and 5.65×10^8 M^{-2}, respectively. The detection limit for both the complexes was reported as 1.49 and 2.31 µM, respectively [**Figure-1.7 (c)]**.[57]

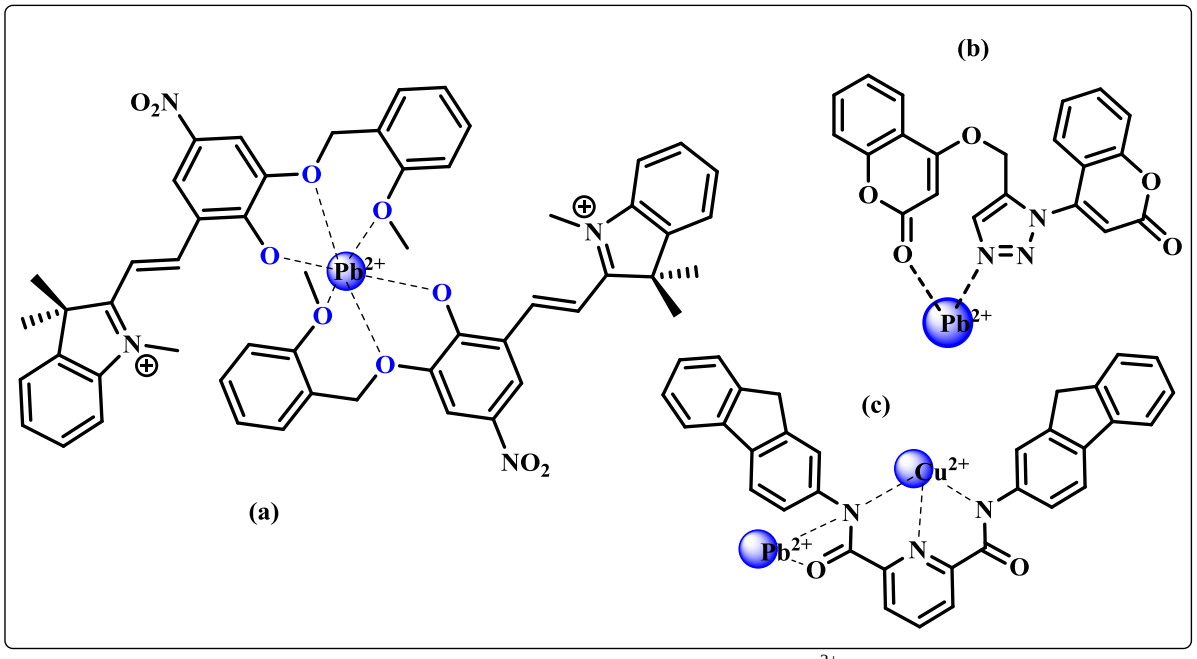

Figure-1.7: (a) Spiropyran-based receptor for the selective detection of Pb^{2+} ions with a detection limit of 40 nM in a 2:1 stoichiometric ratio **(b)** Coumarins-based receptor with a detection limit of 6 µM in a 1:1 stoichiometric ratio. **(c)** A fluorescent-based receptor to detect Cu^{2+} and Pb^{2+} ions in stoichiometric ratios of 1:1 and 1:2, respectively.

1.3. Diphenyl Ether as a Receptor

The organic moieties discussed above are a limited number of several others reported in the literature to capture ions. Many others include the use of 1-(2-aminoethyl) thioureas,[58] benzimidazole,[43, 59] BODIPY,[60, 61] dansylamides,[62] hydroxyl chromones,[63] thiophene,[64, 65]

porphyrin,[66, 67] naphthalenediimide,[68, 69] naphthyridine[70, 71] and naphthalimides,[71, 72] groups. The optical receptors using these organic groups have detection range of 10^{-5} to 10^{-10} M.

Phenyl ethers for detecting cations and anions have been reported recently.[73, 74] These molecular motifs present an attractive architecture that can be moulded into a cavity **[Figure-1.8 (a)]** with suitable rigidity due to aromatic planer rings **[Figure-1.8 (b)]**. Additionally, rotation around ether linkage [angles Φ and Ψ in **Figure-1.8 (c)]** imparts the desired flexibility to accommodate ions of varying along with as many as ten substituent positions on the phenyl rings to change the electron density in the cavity by use of acceptor or donor groups **[Figure-1.8 (d)]**.

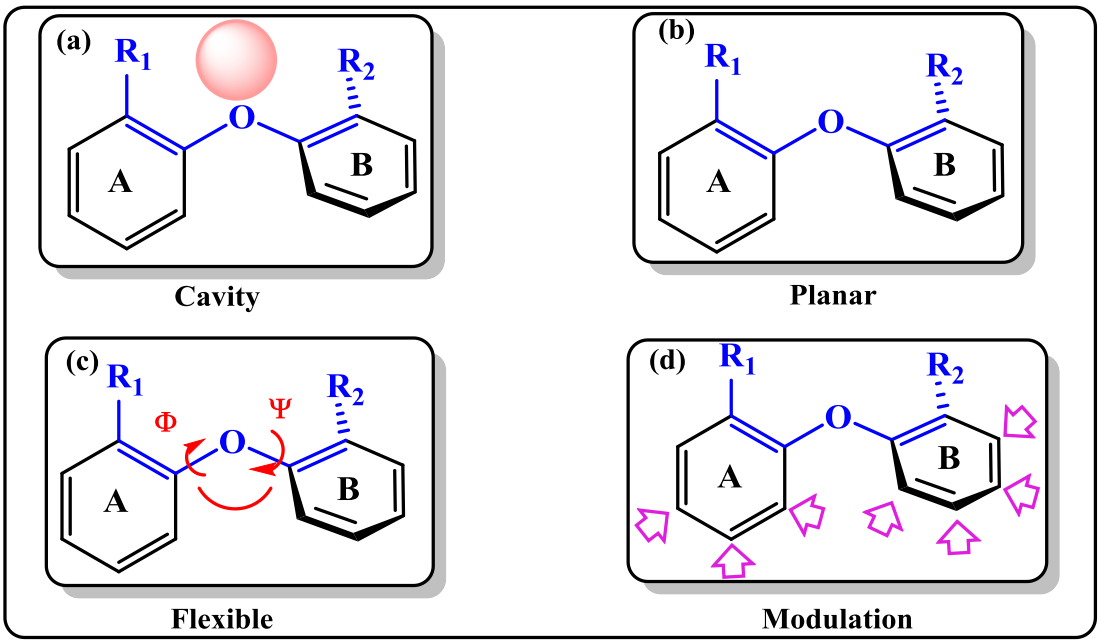

Figure-1.8: Advantage of using diphenyl ethers for ion sensing **(a)** The heteroatom-lined cavity can be used to trap ions. **(b)** Planer phenyl rings offer desired rigidity. **(c)** Rotation around angles Φ and Ψ gives flexibility. **(d)** Substituents on the phenyl ring offer the advantage of modulating the electron density in the cavity to be influenced by different solvents and to attach other chromophores.

Recently, various diphenyl ethers have appeared in the literature as receptors for different ions. Diphenyl ether-based ionophores, as shown in **Figure-1.9 (a)** are selective for Fe^{2+} ions. At the same time, the addition of the nitro group at the meta position **Figure-1.9 (b)** changed its selectivity to Ca^{2+} ions.[75, 76] Triphenyl ethers also act as ionophores due to the formation of the cavity between two ether linkages. Modifying the substituent group at the phenyl ring helps to improve the cavity and strong binding with metal ions. Triphenyl ethers shown in **Figure-1.9 (c & d)** are selective for Cu^{2+} and Ca^{2+} ions.

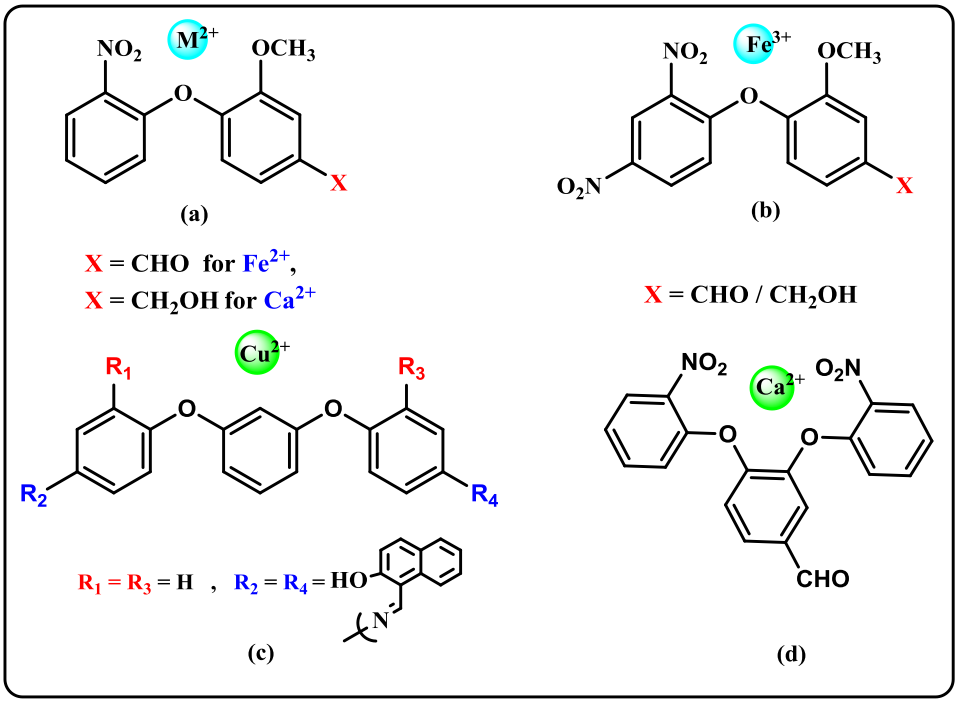

Figure-1.9: (a & b) Diphenyl ether receptors known for Fe^{2+} , Ca^{2+} and Fe^{3+} ion detections.**(c & d)**Triphenyl ether molecules representing the ion detection by varying the functional group at $R_{(1,2,3\ and\ 4)}$ positions.

Colorimetric-based selective detection of the fluoride ions is reported in the literature, complemented by UV-Visible spectroscopy. The detection displayed a change up to 20 µM with an association constant of 2.8×10^4 M^{-1}. The deprotonation-based detection had an acidic proton are linked to the signalling unit that influenced the electronic property of the receptor resulting the absorption change was observed as shown in **Figure-1.10**.[77]

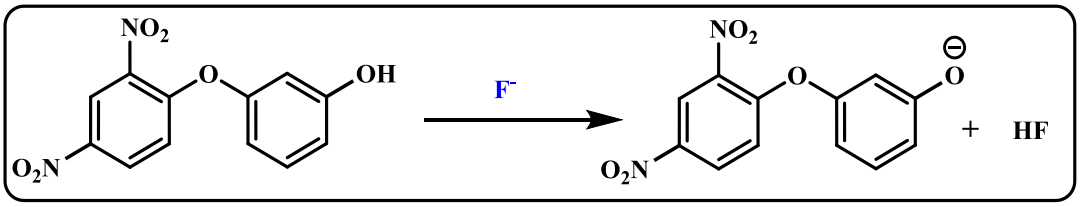

Figure-1.10: Diphenyl ether's acidic hydrogen content causes a hydrogen bond to form with a fluoride ion and then deprotonate, as shown by the colour shift from colourless to yellow and then to blue.

1.4. Effect of a functional group for ion detection (Systematic studies)

The selectivity and sensitivity of the receptors to trap specific ions vary as a function of the organic group present on its skeleton. The electron donor and acceptor groups manipulate a receptor for its selectivity towards an ion and change their detection limits or binding constants.

Kundu et al. synthesized five diphenyl ether derivatives using different groups at R_1 and R_2 positions to make ionophores. The variation of donor or acceptor led to improved sensitivity, corroborating results with the theory. **Figure-1.11** shows the structure of five substituents on position-X having both electron-donating and withdrawing groups that responded to both Fe^{3+} and Cu^{2+} ions. Replacement of substituted phenolic group by naphthyl ring (Compound-3) gave selectivity for the Cu^{2+} ions. It can be attributed to the steric effect of the bulky naphthyl group in compound-3.[78]

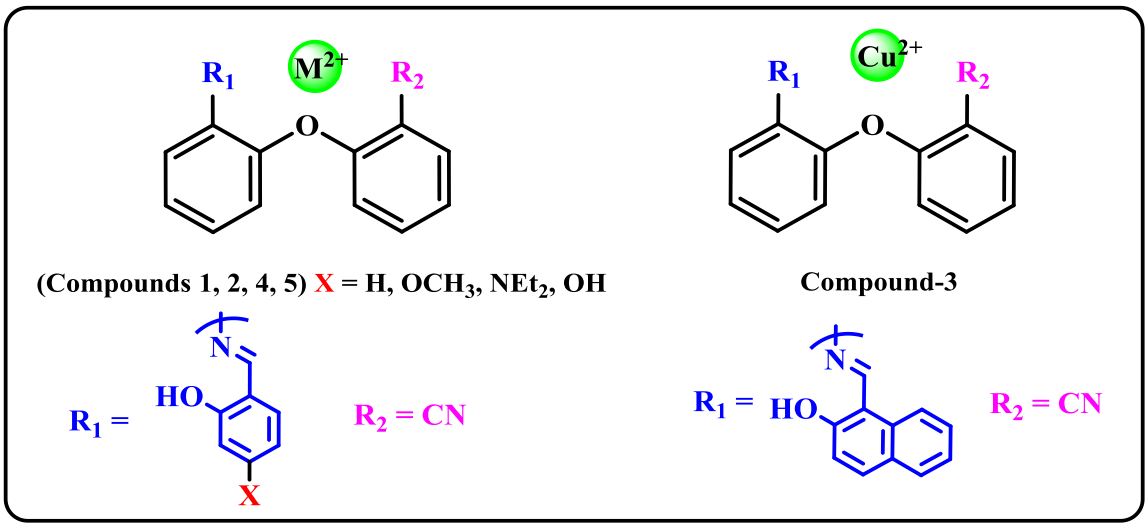

Figure-1.11 : Series of five diphenyl ether-based receptors for detecting Fe^{3+} and Cu^{2+} ions.

Figure-1.12 shows that a systematic study on the salen receptor displayed that a change in the substituent changed the selectivity for different metal ions by colorimetric or fluorimetric methods.[79]

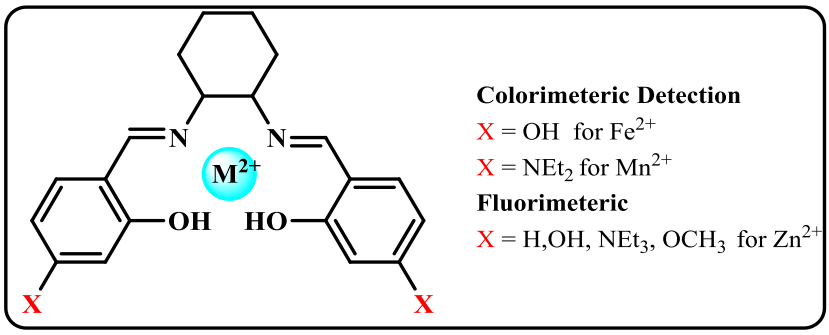

Figure-1.12: Optimized the metal ions detection by varying the substituents on salen group.

A similar systematic study performed by Jefferies and co-workers. reported a series of water-soluble receptors capable of recognizing metal ions (Cu^{2+}, Ni^{2+}, Cr^{3+} and Co^{2+}). The same

skeleton changed its selectivity for identifying Ag^{+} and Co^{2+} ions by replacing the aliphatic linker with the phenyl ring **(Figure- 1.13)**.[80]

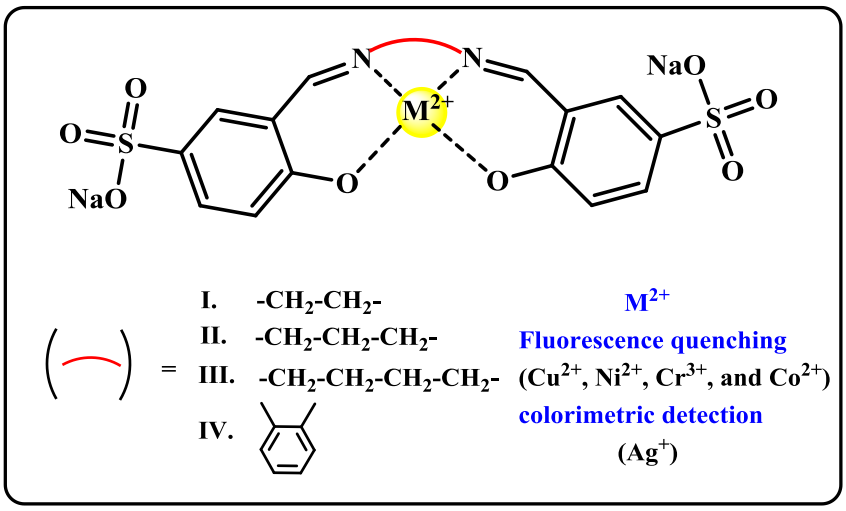

Figure-1.13: Schiff base receptors detect Ag^{+} and Co^{2+} ions while changing the linker between two Schiff base Nitrogen with various groups.

Liu et al. developed a naphthalimide-based receptor that changed its selectivity from Zn^{2+} to Hg^{2+} ions by changing the carboxylate group with ether carboxylate one. Both fluorescence-based sensors detected both Zn^{2+} to Hg^{2+} ions in the µM range **(Figure- 1.14)**.[81, 82]

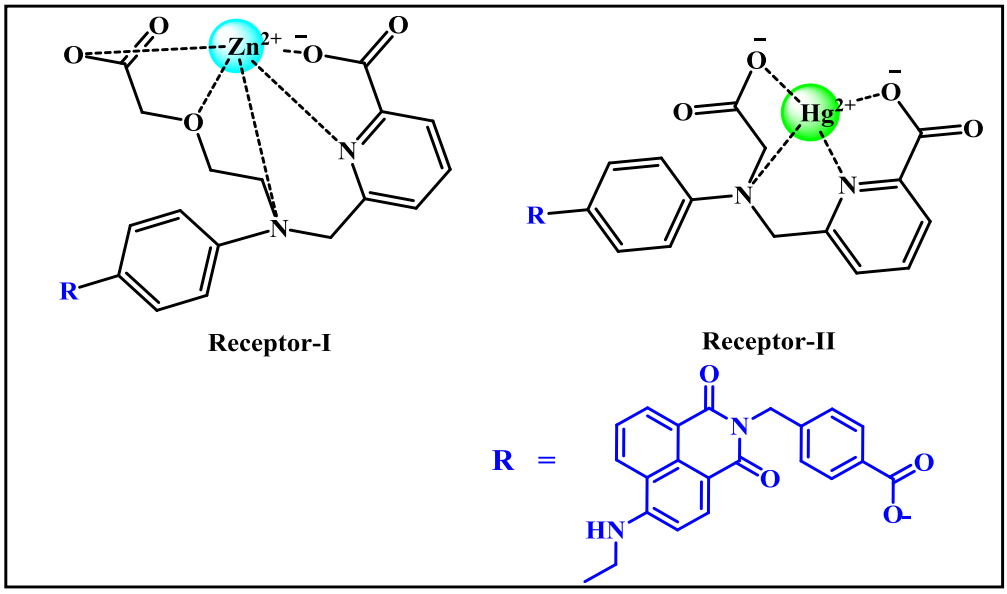

Figure-1.14: Selective change in the metal interaction by varying the recognition sites with naphthalimide-based receptors for (a) Zn^{2+} and (b) Hg^{2+} ions.

1.5. Effect of Solvents for the detection of ions

Solvents influence the spectral properties of the receptor due to their polarity. Hydrogen bonding is one of the primary influencers that develops short-range interactions around the

receptor to create the first solvation shell. It alters the receptor's molecular energy level, directly affecting its photophysical properties. Protic and aprotic solvents help to distinguish the response of various receptors. Aprotic solvents with partial positive and negative charges can strengthen a receptor's polar characteristics, while protic ones directly create hydrogen bonds to exploit their sensing characteristics. For example, polar solvents (e.g. DMSO, Methanol) can cause a 100-fold increase in fluorescence quantum yield for the n-π* transitions compared to non-polar solvents (e.g. Hexane) The formation of exciplex systems due to intra and intermolecular hydrogen-bond formation causes this change. The following literature cites some examples where a modification of the solvent system brought about a difference in selectivity.

S. Bayindir improvised the selectivity of the rhodamine-based receptor for Hg^{2+} ions by changing the solvent system from pure ACN to ACN: H_2O (1:1 v/v) **(Figure-1.15)**. Pure ACN medium detected Hg^{2+} and Cu^{2+} ions with a binding ratio of 1:1 and detection limit calculated as 3.36 μM and 2.31 μM, respectively.[83]

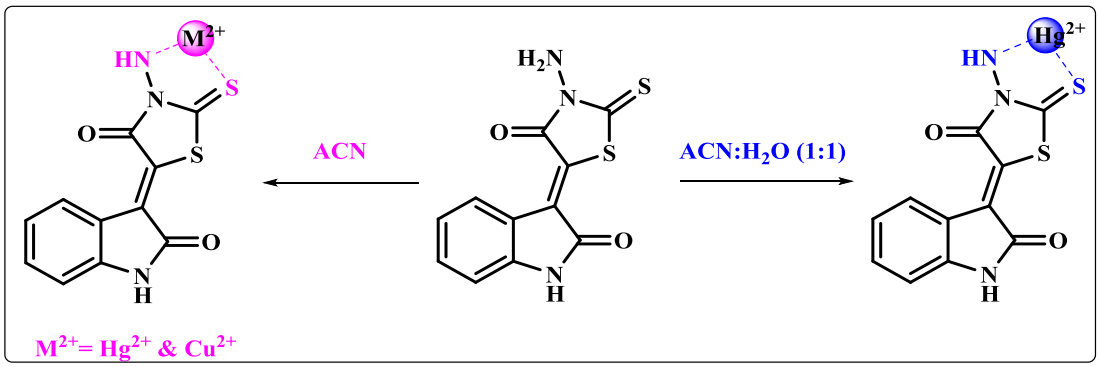

Figure-1.15: Solvent dependent selective detection of Hg^{2+} ions in aqueous medium [ACN:H_2O (1:1)].

A Schiff base receptor switched the selective detection of Al^{3+} and Zn^{2+} ions on changing the solvent from protic to aprotic, as shown in **(Figure-1.16)**. Al^{3+} was detected using a MeOH and H_2O solvent system, while Zn^{2+} ions required a DMF-H_2O mixture.[84]

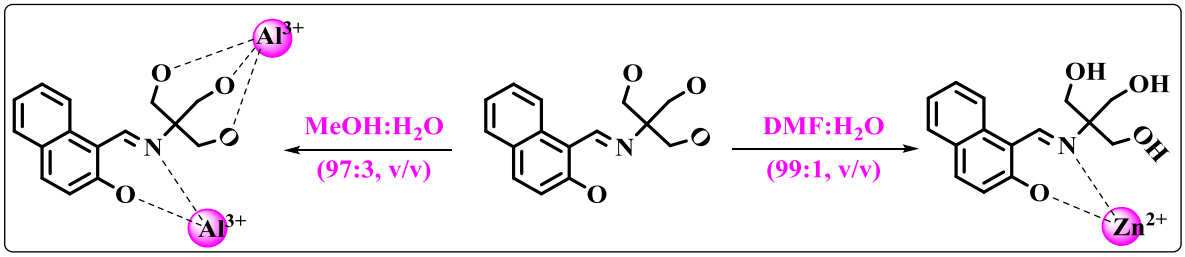

Figure-1.16: Different solvent mixtures are used for solvent dependent duel detection of Al^{3+} and Zn^{2+} ions with receptor generated from Schiff bases.

Chen et al. reported a receptor detecting Co^{2+} and Cu^{2+} ions in two separate solvent systems **(Figure-1.17)**. The rhodamine-based molecule detected two Cu^{2+} ions in the DMF-HEPES buffer system with a detection limit of 0.2 µM. In contrast, the ACN-HEPES buffer sensed Co^{2+} ions in 1:1 stoichiometry and a detection limit of 44 nM.[85]

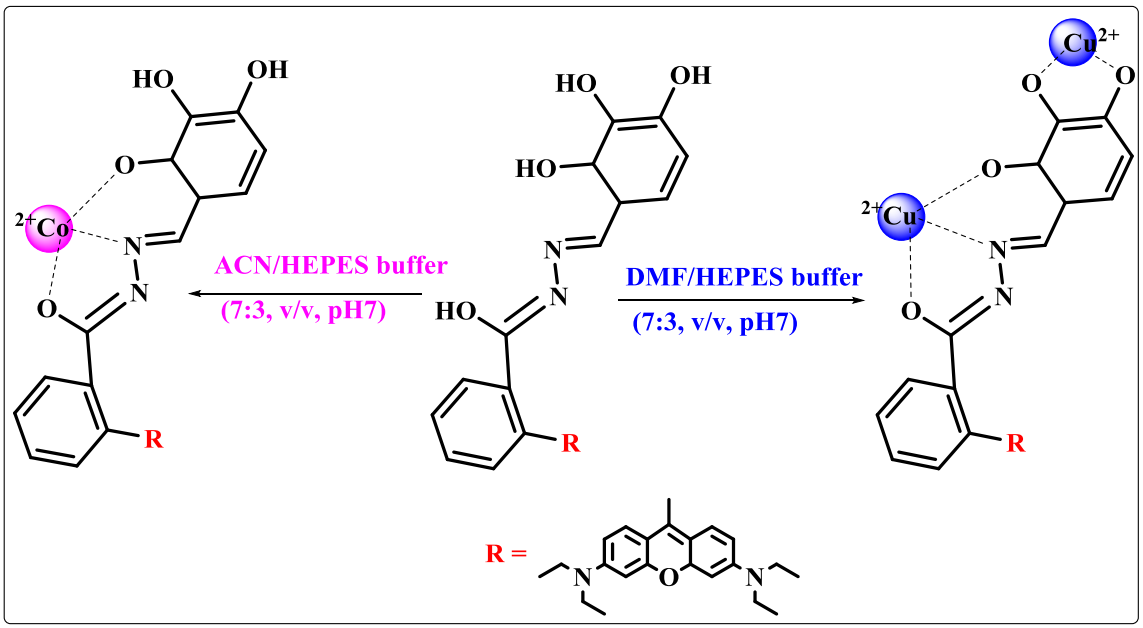

Figure-1.17: Solvent strategy to detect Cu^{2+} and Co^{2+} ions selectively in 1:2 and 1:1 stiochimetric ratio solvent mixtures ACN:HEPES Buffer and DMF: HEPES Buffer solution.

A thiourea-based receptor displayed a colourimetric selection of anions by change of the solvent systems [86]. The molecule recognized CN^- ions selectively in protic solvent, while in aprotic solvents, it detected F^-, CH_3COO^-, and $H_2PO_4^-$ as additional anions (**Figure-1.18)**.

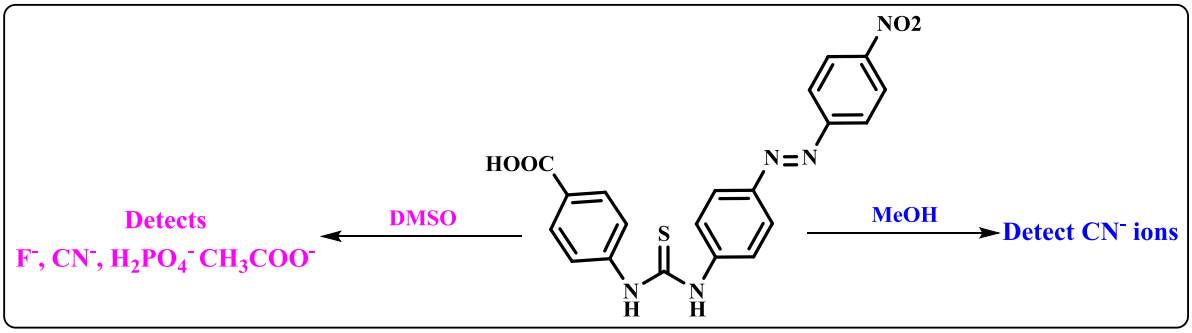

Figure-1.18: Example of thiohydrazide-based receptors showing dynamic behavior using different solvents with anions.

The present work explored systematic studies with different solvents to examine the properties of synthesized receptors.

1.6. Techniques

Generally, two types of methods are employed in the detection of ions. The first one uses the instruments for direct metal ion detection, while the other uses the aid of optical indicators like a complexing agent, fluorophore or chromophore. In the latter method, optical detection techniques are popular that apply absorption, fluorescence, and luminescence. Despite being effective, optical ion sensing has some drawbacks.[87] For example, when actual (real-life) samples are analyzed, an optical indicator may be selective for unknown species and give a false positive. Therefore it is essential to validate the method using a real-life sample. The presence of acidic or basic moieties (hydrogen, hydroxide) on the optical indicator necessitates adequate pH management.

The work presented here used optical detection techniques as a primary source of investigation. Nuclear magnetic resonance (NMR) and infrared spectroscopy (IR) were used as additional tools to investigate further the interactions between the optical indicators (receptors) and the ions. The following paragraphs describe the general details of the technique and the calculations employed to conduct the research.

1.6.1. Absorption and Emission Spectroscopy

Absorption spectroscopy uses ultraviolet (190–400 nm) and visible (400–800 nm) radiation to electronically excite the molecules. The technique, also called electronic spectroscopy, provides valuable insight into the interactions between an optical receptor and the ion when the wavelength of the absorbed radiation is compared with its native structure. This information, combined with Beer-Lambert's law, estimates the concentration of the species present in a solution. The law inversely correlates the concentration of the analyte with the absorbance and the path length of the light during illumination using an expression $A = \varepsilon. b. c$. Here A stands for absorbance, ε for the molar absorbance coefficient (wavelength-dependent) in mol^{-1} L cm^{-1}, b for the route length in cm, and c for the absorber concentration in mol L^{-1}.[88]

The linear relationship between absorbance (A) and concentration (c) of the analyte samples (optical receptor) in the presence and absence of the interacting ions provides information related to the chemistry between the two species. The influence of the solvent, pH, photo-degradation or any reaction between the ions can also be predicted using this technique.[88, 89] Most instruments have tungsten filament or deuterium lamp as the source of light and glass or quartz material to hold the sample. However diverse instruments use a variety of detectors

like a photomultiplier,[90] photodiode array (PDA),[91] charged-coupled devices (CCD), and paired emitter detector diode (PEDD).[92]

The ability of certain molecules to relax by releasing the photon of light after electronic excitation is called fluorescence. Another related process called phosphorescence also occurs for specific molecules. Both electronic and vibrational states participate in such molecules. Such fluorophores can also be used as optical receptors to probe the interaction with different ions by observing fluorescence enhancement or depreciation. Some natural aromatic molecules like tyrosine, tryptophan and luciferins also show similar phenomena.

The diphenyl ethers used in this work display absorption in the UV range (260 nm to 360 nm). Therefore, most investigations were carried out using an Analytica Jena Specord-205 UV-Visible spectrophotometer. The weak emission intensity checked on the Spectro fluorophotometer (Shimadzu RF-6000) for these molecules prevented the use of the fluorescence technique in investigations.

1.6.2. Physical Calculations

Different parameters like the limit of detection, binding constant, and stoichiometry define the interaction of ions with optical receptors. The methods are well established in the literature to calculate these criteria.

Limit of Detection: Quantifying the minimum amount of any species (elements, ions, or molecules) in an analyte either in the free or combined form (as a biological or material matrix) is referred to as the limit of detection. Initially, the calculation for the limit of detection model was adopted by the International Union of Pure and Applied Chemistry (IUPAC) in 1975 (I), and the American Chemical subcommittee reaffirmed this standard in 1980.[93] After this, the identification of the minimal detection limit is an important process in the analytical procedures.[94]

Binding Constant: Benesi and Hildebrand proposed the Benesi-Hildebrand (B-H) technique in 1949.[95] It has become a prominent approach for calculating the association constant (Ka) and stoichiometry binding interactions and is widely employed in many aspects of binding systems. The data gathered from various spectroscopic methods like UV-Vis, fluorescence, infrared, and NMR[96, 97] can be used in the B-H calculation.

For any new species XY governed by Beer-Lambert law, formed from the interaction of X and Y (Expression-1), the Benesi-Hildebrand equation can be expressed as expression-2 if the binding is 1:1.

X + Y = XY…… (1)

B-H equation,

$[X]/\Delta A=1/[[Y]K(\varepsilon XY-\varepsilon X)]+1/(\varepsilon XY-\varepsilon X)$……..(2)

Where ΔA is the change in absorbance during complexation, [X] and [Y] are the initial concentrations of X and Y, εX and εXY are the absorption coefficients of X and XY, respectively.

For binding interactions other than 1:1, B-H binding interactions can be extended as expression–3. For the general one-step binding interactions in the form of

X+nY = XYn,……..(3)

Therefore extended B-H equation is:

$[X]/\Delta A=1/[[X])\ nK\ (\varepsilon XYn-\varepsilon X)]+1/(\varepsilon XYn-\varepsilon X)$ ……..(4)

The plot for [1/ΔA vs (1/[Y]) n is expected to be a straight line for a 1:n complexation. Further, the binding constant was calculated from the slope and intercept of this straight line.

Stoichiometry (Job's Plot): The practice of continuous variations is generally associated with the name Job, who published a detailed application of the method to study a wide range of coordination compounds.[98] A wide range of analytical and instrumental analyses use this approach. Ostromisslenskv employed the principle of continuous variations in 1911 to establish the 1:1 stoichiometry of the adduct formed between nitrobenzene and aniline. [99] Denison, in 1912, also used this method to study various liquid mixtures. The approach involves mixing aliquots of two equimolar stock solutions of metal and ligand in a fixed volume. The solutions are prepared to keep the total analytical concentration of metal and ligand constant while the ligand-metal ratio varies in each sample as per expression-5 below.

$C_M+C_L, = k$ …… (5)

C_M and C_L are the analytical concentrations of metal and ligand, respectively, and k is a constant. The absorbance is displayed as a function of the ligand or metal mole fraction in graph to obtain a bell-shaped curve. Maxima in the curve at 0.5 equivalents/mole fractions

indicate a 1:1 stoichiometry of the ligand and the mole fraction, while maxima at 0.67 and 0.75 gave 2:1 and 3:1 stoichiometry, respectively.

Two experimental crosschecks ensure the reliability of the data for this technique. The data should be evaluated at more than one wavelength[100] and more than one metal and ligand concentration. The value of *k* as per expression-5 should be different. For the method to be applicable, the position of the maximum on the mole fraction axis must be invariant as a function of the recommended changes.

Isosbestic point: It is the point at which the wavelength, frequency or wavenumber of UV active unit doesn't altered during the chemical or physical change (or is the equilibrium state of the receptor and its complexes). And the point is observed in overlaid spectra when a chromophoric precursor is converted to a product with a different spectrum, so that it is often assumed that an isosbestic point occurs only when the precursor is quantitatively converted to a single product. The isosbestic point describe in our studies confirms the interaction of metal ions or anions with the UV active receptors.

1.6.3. NMR Techniques

Nuclear magnetic resonance, one of the comprehensive methods for structure determination, is also used to study intra and intermolecular interactions between different chemical species nowadays.[101] In supramolecular chemistry, this spectroscopic technique provides information about the orientation of the guest species inside the cavity. Other parameters related to the physicochemical properties of the inclusion complexes can also be predicted.[102, 103] Bodner et al. investigated changes in bonding for mono-substituted benzene derivatives upon complexation with Cr(CO) using ^{13}C NMR spectroscopy.[104]

Researchers use NMR titration to understand the atomic level interaction between host and guest molecules. Gupta et al. predicted the involvement of aldehyde oxygen when the coumarin-based receptor recognized the Mg^{2+} ion. **Figure-1.19** shows the deshielding of the aldehyde proton on sequential addition of Mg^{2+} ions in the receptor due to their mutual interaction.[105]

Another group complimented the UV-Visible detection of Hg^{2+} ions using NMR spectroscopy. The receptor (2-((E)-(3-(1H-imidazole-1-yl) propylamine) methyl)-5-(diethylamino) phenol) displayed disappearance of the hydroxy proton (H_{13}) on sequential addition of Hg^{2+} ions (0.0-1.0 Equiv) due to enhanced interactions **Figure-1.20**. Similarly,

the imidazole ($H_{10–12}$) and the other non-aromatic protons of $H_{6–9}$ displayed an apparent downfield shift indicating the binding of the phenolic O, $N_{imidazole}$, and N_{imine} with Hg^{2+}. [106]

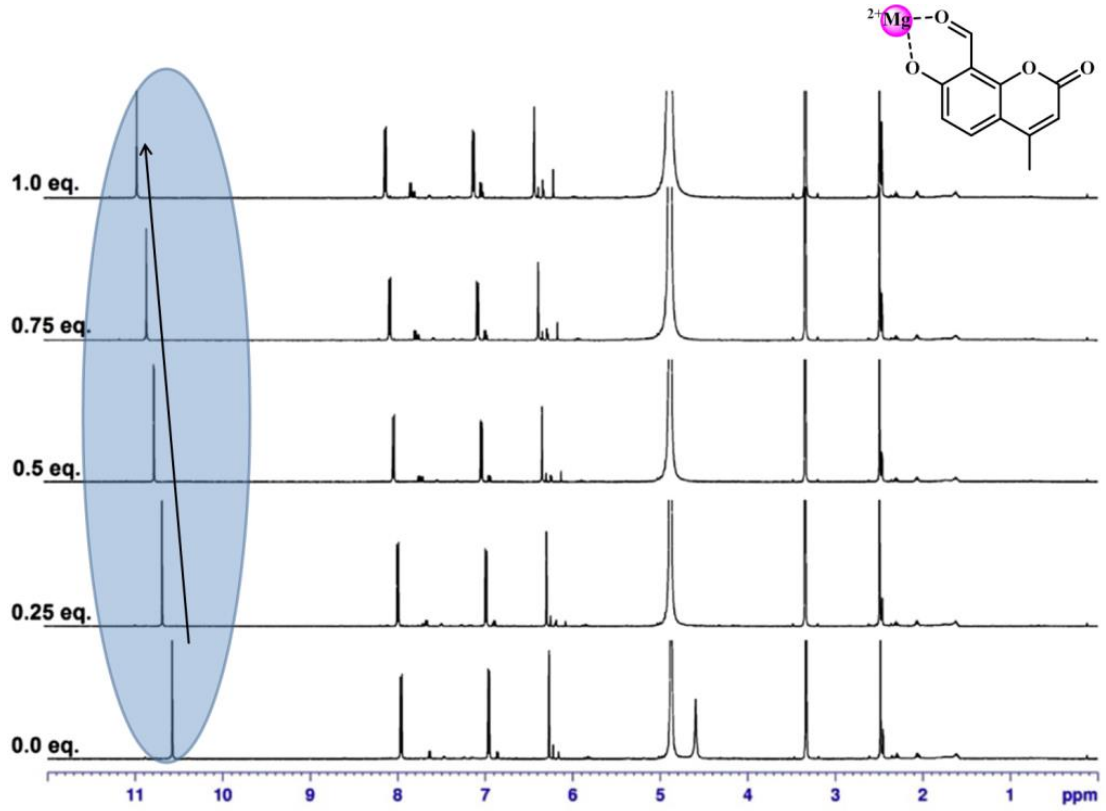

Figure-1.19: Deshielding shift in the aldehyde peak of coumarin receptor using ^1H NMR proton confirming the complex formation with Mg^{2+} ions.

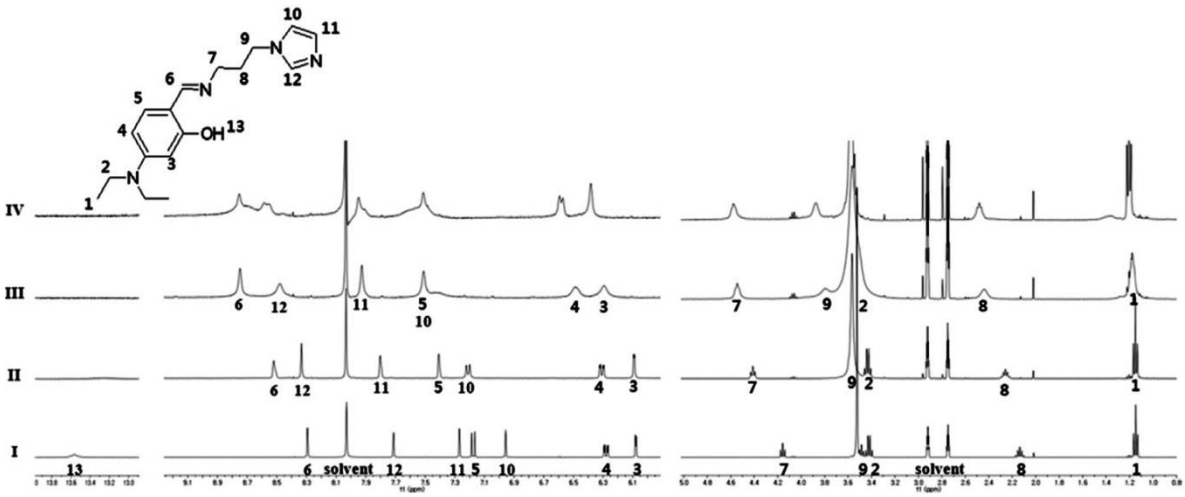

Figure-1.20: The optimization of aromatic and aliphatic peaks shifting and disappearing in NMR spectra reveals the Hg^{2+} interaction with the receptor molecule and identifies its interacting sites.

1.6.4. I.R. Techniques

Infrared spectroscopy is also a complementary technique, researchers used to identify molecular interactions based on vibrational spectroscopy. The infrared light-induced vibrations of the heteroatoms bonded to the recognition get altered when they interact with guest or analyte species. Thus, comparing the infrared spectra of the native molecule with the analyte-bound one helps to estimate the molecular interactions.

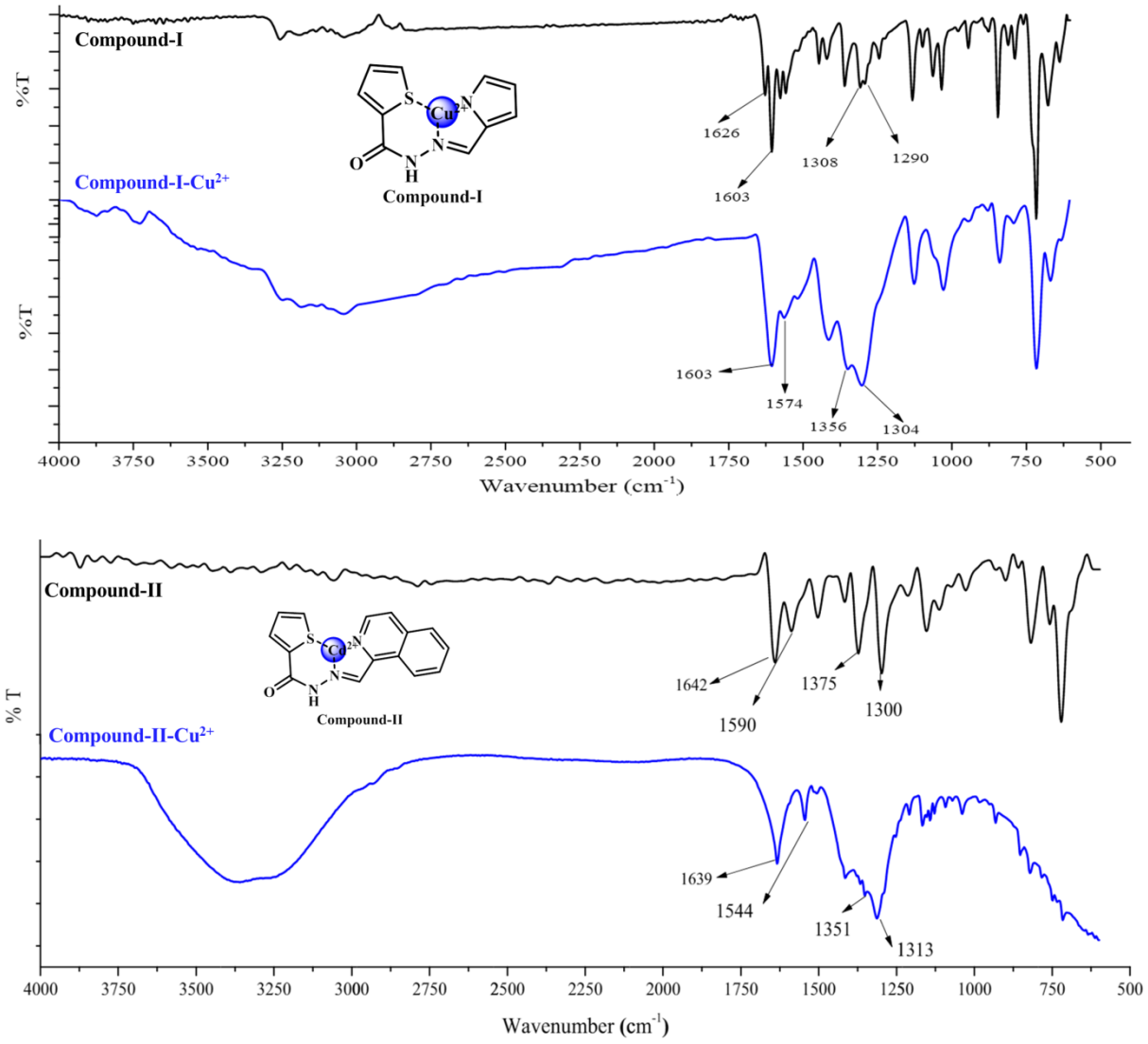

Figure-1.21: Detection of Cu^{2+} and Cd^{2+} ions by a reported receptor was confirmed by a shift in the stretching peaks of the C=O and C-N bond.

Tekuri et al. reported detection of Cu^{2+} and Cd^{2+} ions in the minimum detection limit of 2.8 and 0.2 µM using a UV-Visible spectrophotometer. The group validated the predicted interaction site by comparing its IR spectra with the native molecule. The IR spectra

displayed the shifting of the stretching peak for C=O and C-N bond as shown in **Figure-1.21**.[107]

Mahajan et al. reported a sipro-lectum based receptor for the selective detection of Hg^{2+} ions, and validated receptor metal complex using I.R studies the C=N peaks was observed from 1590 to 1605, 1637 to 1690 cm^{-1} besides the disappearance of carbonyl peak at 1705 cm^{-1} due to the enhanced interaction with the metal ions. [108]

The work presented here also confirmed the interaction of the cations and anions with synthesized receptors using NMR titrations and IR comparison.

References:

1. McConnell, A. J.; Beer, P. D., *Angew. Chem. Int. Ed.* **2012,** *51*, 5052-5061.
2. Desvergne, J. P.; Czarnik, A. W., *Chemosensors of ion and molecule recognition*. Springer Science & Business Media: **2012**; Vol. 492.
3. Du, J.; Hu, M.; Fan, J.; Peng, X., *Chem. Soc. Rev.* **2012,** *41*, 4511-4535.
4. Sigel, H.; Sigel, A., *Z. Naturforschung B* **2019,** *74*, 461-471.
5. Pothulapadu, C. A. S.; Jayaraj, A.; Priyanka, R. N.; Sivaraman, G., *ACS omega* **2021,** *6*, 24473-24483.
6. Yang, C.-X.; Ren, H.-B.; Yan, X.-P., *Anal. chem.* **2013,** *85*, 7441-7446.
7. Lake, R. J.; Yang, Z.; Zhang, J.; Lu, Y., *Acc. chem. Res.* **2019,** *52*, 3275-3286.
8. Engwa, G. A.; Ferdinand, P. U.; Nwalo, F. N.; Unachukwu, M. N., *Poisoning in the modern world-new tricks for an old dog* **2019,** *10*, 70-90.
9. Sharma, B.; Singh, S.; Siddiqi, N. J., *Bio. Med. Res. Int.* **2014,** *15*, 2014-2030.
10. Prashanth, L.; Kattapagari, K. K.; Chitturi, R. T.; Baddam, V. R. R.; Prasad, L. K., *J. NTR Univ. health sci.* **2015,** *4*, 75-82.
11. Weiner, I. D.; Wingo, C. S., *J. Am. Soc. Nephrol.* **1997,** *8*, 1179-1188.
12. Hedera, P.; Fink, J. K.; Bockenstedt, P. L.; Brewer, G. J., *Archives of Neurology* **2003,** *60*, 1303-1306.
13. Paustenbach, D. J.; Tvermoes, B. E.; Unice, K. M.; Finley, B. L.; Kerger, B. D., *Crit. Rev. Toxicol.* **2013,** *43*, 316-362.
14. Dusek, P.; Roos, P. M.; Litwin, T.; Schneider, S. A.; Flaten, T. P.; Aaseth, J., *J. Ttrace Elem. Med. Biol.* **2015,** *31*, 193-203.
15. Assi, M. A.; Hezmee, M. N. M.; Sabri, M. Y. M.; Rajion, M. A., *Vet. world* **2016,** *9*, 660.
16. Bertin, G.; Averbeck, D., *Biochimie* **2006,** *88*, 1549-1559.
17. Järup, L.; Åkesson, A., *Toxicol. Appl. Pharmacol.* **2009,** *238*, 201-208.
18. Nabi, S., In *Toxic Effects of Mercury*, Springer: **2014**; pp 187-199.
19. Bianchi, A.; Bowman-James, K.; García-España, E.; García-Espana, E., *Supramolecular chemistry of anions*. Wiley-vch: **1997**.
20. Capelo, R.; Rohlman, D. S.; Jara, R.; García, T.; Viñas, J.; Lorca, J. A.; Contreras Llanes, M.; Alguacil, J., *Int. J. Environ. Res. Public Health* **2022,** *19*, 4732.
21. Simeonova, F. P.; Fishbein, L.; Organization, W. H., *Hydrogen cyanide and cyanides: human health aspects*. World Health Organization: 2004.
22. Kawasaki, H.; Sato, K.; Ogawa, J.; Hasegawa, Y.; Yuki, H., *Anal. Biochem.* **1989,** *182*, 366-370.
23. Mulkerrins, D.; Dobson, A.; Colleran, E., *Environ. Int.* **2004,** *30*, 249-259.
24. Michigami, Y.; Kuroda, Y.; Ueda, K.; Yamamoto, Y., *Ana. Chim. Acta* **1993,** *274*, 299-302.
25. Xu, S.; Chen, K.; Tian, H., *J. Mater. Chem.* **2005,** *15*, 2676-2680.
26. Sohn, H.; Létant, S.; Sailor, M. J.; Trogler, W. C., *J. Am. Chem. Soc.* **2000,** *122*, 5399-5400.
27. Zhang, S.-W.; Swager, T. M., *J. Am. Chem. Soc.* **2003,** *125*, 3420-3421.
28. Kirk, K. L., *Biochemistry of the Elemental Halogens and Inorganic Halides* (Volume A) Biochemistry Halogenated Organic Compounds: **1991**.
29. Kleerekoper, M., Endocrinol. Metab. *Clin. North Am.* **1998,** *27*, 441.
30. Leymarie, F.; Jolly, D.; Sanderman, R.; Briancon, S.; Marchand, A.; Guillemin, F.; Eschard, J.; Suurmeijer, T.; Poitrinal, P.; Blanchard, F., *Br. J. rheumatol.* **1997,** *36*, 1106-1112.
31. Faraji, M.; Yamini, Y.; Saleh, A.; Rezaee, M.; Ghambarian, M.; Hassani, R., *Anal. Chim. Acta* **2010,** *659*, 172-177.

32. Sitko, R.; Janik, P.; Zawisza, B.; Talik, E.; Margui, E.; Queralt, I., *Anal. chem.* **2015,** *87*, 3535-3542.
33. Zinoubi, K.; Majdoub, H.; Barhoumi, H.; Boufi, S.; Jaffrezic-Renault, N., *J.Electroanal. Chem.* **2017,** *799*, 70-77.
34. Zhang, Y.; Zeng, G. M.; Tang, L.; Chen, J.; Zhu, Y.; He, X. X.; He, Y., *Anal. chem.* **2015,** *87*, 989-996.
35. Leopold, K.; Harwardt, L.; Schuster, M.; Schlemmer, G., *Talanta* **2008,** *76*, 382-388.
36. Hu, B.; Hu, L.-L.; Chen, M.-L.; Wang, J.-H., *Biosens. Bioelectron.* **2013,** *49*, 499-505.
37. Qin, D.; Gao, F.; Zhang, Z.; Zhao, L.; Liu, J.; Ye, J.; Li, J.; Zheng, F., *Spectrochim. Acta Part B: At. Spectrosc.* **2013,** *88*, 10-14.
38. Kim, J. S.; Quang, D. T., *Chem. Rev.* **2007,** *107*, 3780-3799.
39. Wang, J.; Qian, X.; Cui, J., *J. Org. Chem.* **2006,** *71*, 4308-4311.
40. Bhalla, V.; Tejpal, R.; Kumar, M.; Sethi, A., *Inorg. chem.* **2009,** *48*, 11677-11684.
41. Gupta, V. K.; Chandra, S.; Agarwal, S., Mercury selective electrochemical sensor based on a double armed crown ether as ionophore. *niscpr* **2003,** *43*, 813-818. (Http://nopr.niscpr.res.in/handle/123456789/18196)
42. Othman, A. B.; Lee, J. W.; Wu, J.-S.; Kim, J. S.; Abidi, R.; Thuéry, P.; Strub, J. M.; Van Dorsselaer, A.; Vicens, J., *J. Org. Chem.* **2007,** *72*, 7634-7640.
43. Ergun, E. G. C.; Ertas, G.; Eroglu, D., *J.Photochem. Photobiol. A: Chem.* **2020,** *394*, 112469.
44. Gu, B.; Huang, L.; Su, W.; Duan, X.; Li, H.; Yao, S., *Anal. Chim. Acta* **2017,** *954*, 97-104.
45. Muthusamy, S.; Rajalakshmi, K.; Zhu, D.; Zhu, W.; Wang, S.; Lee, K.-B.; Xu, H.; Zhao, L., *Sens. Actuators B Chem.* **2021,** *346*, 130534.
46. Das, S.; Sarkar, A.; Rakshit, A.; Datta, A., *Inorg. Chem.* **2018,** *57*, 5273-5281.
47. Wei, T.-B.; Gao, G.-Y.; Qu, W.-J.; Shi, B.-B.; Lin, Q.; Yao, H.; Zhang, Y.-M., *Sens. Actuators B Chem.* **2014,** *199*, 142-147.
48. Joshi, S.; Kumari, S.; Sarmah, A.; Pant, D. D.; Sakhuja, R., *J. Mol. Liq.* **2017,** *248*, 668-677.
49. Kowser, Z.; Rayhan, U.; Akther, T.; Redshaw, C.; Yamato, T., *Materials Chemistry Frontiers* **2021**, *5*, 2173-2200.
50. Wang, Y.; Wu, H.; Wu, W.-N.; Mao, X.-J.; Zhao, X.-L.; Xu, Z.-Q.; Xu, Z.-H.; Fan, Y.-C., *Spectrochim. Acta Part A Mol. Biomol. Spectrosc.* **2019,** *212*, 1-9.
51. Mergu, N.; Gupta, V. K., *Sens. Actuators B Chem.* **2015,** *210*, 408-417.
52. Christopher Leslee, D. B.; Karuppannan, S.; Vengaian, K. M.; Gandhi, S.; Subramanian, S., *Luminescence* **2017,** *32*, 1354-1360.
53. Guo, Y.; Wang, L.; Zhuo, J.; Xu, B.; Li, X.; Zhang, J.; Zhang, Z.; Chi, H.; Dong, Y.; Lu, G., *Tetrahedron Letters* **2017,** *58*, 3951-3956.
54. Farhi, A.; Firdaus, F.; Saeed, H.; Mujeeb, A.; Shakir, M.; Owais, M., *Photochem. Photobiol. Sc.* **2019,** *18*, 3008-3015.
55. Deshpande, S. S.; Jachak, M. A.; Khopkar, S. S.; Shankarling, G. S., *Sens. Actuators B Chem.* **2018,** *258*, 648-656.
56. Kumar, A.; Parveen, I.; Ahmed, N., *Luminescence* **2018,** *33*, 713-721.
57. Rahimi, H.; Hosseinzadeh, R.; Tajbakhsh, M., *J. Photochem. and Photobiol. A Chem.* **2021,** *407*, 113049.
58. Lee, M. H.; Lee, S. W.; Kim, S. H.; Kang, C.; Kim, J. S., *Org. Lett.* **2009,** *11*, 2101-2104.
59. Satapathy, R.; Wu, Y.-H.; Lin, H.-C., *Org. lett.* **2012,** *14*, 2564-2567.
60. Sulak, M.; Kursunlu, A. N.; Girgin, B.; Karakuş, Ö. Ö.; Güler, E., *J. Photochem. Photobiol. A Chem.* **2017,** *349*, 129-137.
61. Cantürk, C.; Üçüncü, M.; Emrullahoğlu, M., *RSC Advances* **2015,** *5*, 30522-30525.

62. Tharmaraj, V.; Pitchumani, K., *Anal. Chim. Acta* **2012,** *751*, 171-175.
63. Svechkarev, D.; Dereka, B.; Doroshenko, A., *J. Phys. Chem. A* **2011,** *115*, 4223-4230.
64. Shigemoto, A. K.; Killjoy, A. A.; Dayton, J.; Virca, C. N.; McCormick, T. M., *Mol. Syst. Des. Eng.* **2020,** *5*, 1024-1036.
65. Udhayakumari, D.; Suganya, S.; Velmathi, S.; MubarakAli, D., *J. Mol. Recog.* **2014,** *27*, 151-159.
66. Zhu, X. J.; Fu, S. T.; Wong, W. K.; Guo, J. P.; Wong, W. Y., *Angew. Chem.* **2006,** *118*, 3222-3226.
67. Balaji, T.; Sasidharan, M.; Matsunaga, H., *Analyst* **2005,** *130*, 1162-1167.
68. Zong, L.; Xie, Y.; Li, Q.; Li, Z., *Sens. Actuators B Chem.* **2017,** *238*, 735-743.
69. Li, Q.; Peng, M.; Li, H.; Zhong, C.; Zhang, L.; Cheng, X.; Peng, X.; Wang, Q.; Qin, J.; Li, Z., *Org. lett.* **2012,** *14*, 2094-2097.
70. Mahapatra, A. K.; Hazra, G.; Das, N. K.; Sahoo, P.; Goswami, S.; Fun, H.-K., *J. Photochem. Photobiol. A Chem.* **2011,** *222*, 47-51.
71. Shi, Y. G.; Duan, Y. L.; Chen, J. H.; Wu, X. H.; Zhou, Y.; Zhang, J. F., *Bull. Korean Chem. Soc.* **2013,** *34*, 63-67.
72. Bahta, M.; Ahmed, N., *J. Photochem. Photobiol. A Chem.* **2019,** *373*, 154-161.
73. Liu, Y.; Yu, Y.; Zhao, Q.; Tang, C.; Zhang, H.; Qin, Y.; Feng, X.; Zhang, J., *Coord. chem. rev.* **2021,** *427*, 213601.
74. Daunert, S.; Wallace, S.; Florido, A.; Bachas, L. G., *Anal. Chem.* **1991,** *63*, 1676-1679.
75. Kaur, H.; Chhibber, M.; Mittal, S. K., *MAPAN* **2018,** *33*, 43-55.
76. Sharma, R.; Chhibber, M.; Mittal, S. K., *RSC Advances* **2015,** *5*, 21831-21842.
77. Sharma, R.; Mittal, S. K.; Chhibber, M., *J. Electrochem. Soc.* **2015,** *162*, B248.
78. Kundu, A.; Hariharan, P.; Prabakaran, K.; Anthony, S. P., *Sens. Actuators B Chem.* **2015,** *206*, 524-530.
79. Hariharan, P.; Anthony, S. P., *Spectrochim. Acta Part A Mol. Biomol. Spectrosc.* **2015,** *136*, 1658-1665.
80. Reimann, M. J.; Salmon, D. R.; Horton, J. T.; Gier, E. C.; Jefferies, L. R., *ACS omega* **2019,** *4*, 2874-2882.
81. Liu, D.; Yin, X.; Deng, X.; Shi, J.; Zhu, H.; Shang, Z.; Chen, J.; Yang, G.; He, H., *Inorg. Chem. Comm.* **2019,** *106*, 43-47.
82. Liu, D.; Zhu, H.; Shi, J.; Deng, X.; Zhang, T.; Zhao, Y.; Qi, P.; Yang, G.; He, H., A *Anal. Methods* **2019,** *11*, 3150-3154.
83. Bayindir, S., *J. Photochem. Photobiol. A Chem.* **2019,** *372*, 235-244.
84. Kim, D. H.; Im, Y. S.; Kim, H.; Kim, C., *Inorg. Chem. Comm.* **2014,** *45*, 15-19.
85. Chan, W. C.; Saad, H. M.; Sim, K. S.; Lee, V. S.; Ang, C. W.; Yeong, K. Y.; Tan, K. W., *Spectrochim. Acta Part A Mol. Biomol. Spectrosc.* **2021,** *262*, 120099.
86. Gimeno, N.; Li, X.; Durrant, J. R.; Vilar, R., *Chem. A Eur. J.* **2008,** *14*, 3006-3012.
87. Cho, E. J.; Tao, Z.; Tehan, E. C.; Bright, F. V., *Anal. Chem.* **2002,** *74*, 6177-6184.
88. Tissue, B. M., *Mater. Charact.* **2002,** *3*, 7888-7896 .
89. Sommer, L., *Stud. Anal. Chem.* **1989,** *15*, 354-365.
90. Christian, G.; Dasgupta, P., Schug, KA. *Anal. Chem. Ed., Wiley*, **2014,** *12*, *826-834*.
91. Grossman, W. E., *J. Chem. Ed.* **1989,** *66*, 697.
92. Holonyak Jr, N.; Bevacqua, S. F., *Appl. Phys. Lett.* **1962,** *1*, 82-83.
93. Long, G. L.; Winefordner, J. D., *Anal. chem.* **1983,** *55*, 712A-724A.
94. Li, J.; Song, Y.; Cai, Y., *Environ. Poll.* **2020,** *257*, 113570.
95. Benesi, H. A.; Hildebrand, J., *J. Am. Chem .Soc.***1949,** *71*, 2703-2707.
96. Ajayaghosh, A.; Carol, P.; Sreejith, S., *J. Am. Chem. Soc.* **2005,** *127*, 14962-14963.
97. Balta, D. K.; Temel, G.; Goksu, G.; Ocal, N.; Arsu, N., *Macromolecules* **2012,** *45*, 119-125.
98. Maccarthy, P.; Hill, Z., *J. Chem. Ed.* **1986,** *63*, 162-167.
99. MacCarthy, P.; Mark Jr, H. B., *Soil Sci. Soc. Am. J.* **1976,** *40*, 267-276.

100. Job, P., *Ann. chim* **1928,** *9* , 113-134.
101. Saenger, W., *Angew. Chem. Int. Ed. English* **1980,** *19*, 344-362.
102. Brewster, M. E.; Loftsson, T., *Adv. drug deliv. rev.* **2007,** *59*, 645-666.
103. Cesari, A.; Casulli, M. A.; Hashimoto, T.; Hayashita, T., *Int. J. Mol. Sci.* **2022,** *23*, 6045.
104. Bodner, G. M.; Todd, L. J., *Inorg. Chem.* **1974,** *13*, 360-363.
105. Gupta, V. K.; Mergu, N.; Kumawat, L. K.; Singh, A. K., *Sens. Actuators B Chem.* **2015,** *207*, 216-223.
106. Choi, Y. W.; You, G. R.; Lee, M. M.; Kim, J.; Jung, K.-D.; Kim, C., *Inorg. Chem. Comm.* **2014,** *46*, 43-46.
107. Tekuri, V.; Trivedi, D. R., *Analytica chimica acta* **2017,** *972*, 81-93.
108. Mahajan, P. G.; Shin, J. S.; Dige, N. C.; Vanjare, B. D.; Han, Y.; Choi, N. G.; Kim, S. J.; Seo, S. Y.; Lee, K. H., *J. Photochem. Photobiol. A Chem.* **2020**, *397*, 112579-112590.

Gaps in Research

Although several diphenyl ethers have been synthesized and their applications studied for the detection of various cations and anions, a systematic study around a motif by varying substituents on a phenyl ring is still required. The literature cites many examples of the same motif acting as a receptor for different ions by varying the electron density of the functional groups. Therefore, it was envisaged that altering the functional group can change the ions' lower detection limit. Thus, the present proposal aimed to complement the lack of previous work on diphenyl ethers.

The following objectives were finalized.

1. Synthesis and characterization of diphenyl ethers.
2. Screening of environmentally and biologically important ions using photophysical methods.
3. To study the effect of different substituents on the receptor molecules for the sensing property

Chapter-2

Material and Methods

Chapter-2

Methods to Synthesize and Characterize Diphenyl Ether Derivatives And Their Use for the Detection of Ions.

(Materials and Methods)

2.1. Introduction

Diphenyl ethers are scarcely-known natural products of marine, plant and animal origin **(Figure-2.1)**. Triclosan, a synthetic diphenyl ether, has been long known for its antibacterial activity. The revelation of triclosan's ability to exclusively inhibit bacterial fatty acid biosynthesis (FAS) has led to the synthesis of many of its derivatives.[1, 2] However, recent reports of alternative pathways to FAS in certain bacteria have reduced the scope of phenyl ether molecules from the broad to the narrow spectrum. In industry, these molecules are used as flame retardant materials and in high-temperature reactions.

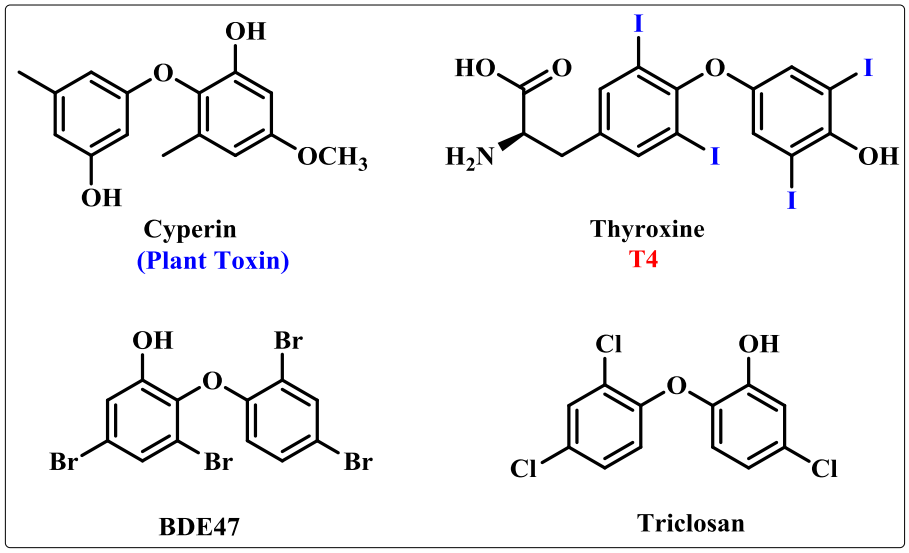

Figure-2.1: Examples of a few diphenyl ethers originated from plant animals and marine sources.

Diverse methods are known for the synthesis of these molecules. One of the earliest methods reported for the synthesis of diphenyl ethers, about a century ago by Ullmann, is still used in its present manifestations. It involves using alkali metal phenolate, an aryl halide, in the presence of copper or its compounds as catalysts at elevated temperatures. To date, three broad classes for synthesizing this class of compounds are known. As discussed above, it all started with metal-mediated arylation of phenols, followed by nucleophilic aromatic substitution reactions and finally oxidative couplings of phenols.[3-6] Present work has utilized

nucleophilic aromatic substitution reaction for the synthesized diphenyl ether skeleton followed by functional group manipulation to get desired groups.

2.2. Synthesis

Compound-**1 (Scheme 2.1**) was envisaged to contain a cavity lined by three oxygen atoms and an electron-withdrawing nitro group. The electronegative oxygens in the trap would capture cations, and manipulating the substituent group on ring-A will help manage the electron density inside the void.

Compound-**1** was thus synthesized by nucleophilic aromatic substitution of the bromo group on compound-A by phenoxide anion of the o-methoxy phenol (Compound-B) in DMF using potassium carbonate as the base **(Scheme 2.1**). 18-crown-6 was used as the phase transfer catalyst to enhance the basicity of potassium carbonate. Purification by column chromatography gave the white product that was characterized using ^{1}H, ^{13}C NMR and HPLC. The NMR data of 99.72 % pure product was consistent with its proposed structure. In line with the objectives of the work, groups on compound-**1** were transformed into other functionalities to study the structure-activity relationship.

The methoxy group on compound-**1** was converted to the corresponding hydroxy group **(**compound-**2)** in the presence of 48% aqueous hydrobromic acid using acetic acid as solvent under reflux conditions **(Scheme 2.1**). The yield, in this case, was only 25 % due to degradation of the product under reflux conditions. Reduction of the aldehyde in compound-**1** to corresponding benzyl alcohol **(**compound-**3)** was carried out using sodium borohydride in the presence of methanol. The same aldehyde was oxidized to the corresponding acid **(**compound-**4)** using aqueous potassium permanganate under reflux conditions.

All the synthesized derivatives of the parent compound-**1** were characterized using ^{1}H and ^{13}C NMR and analyzed for their purity using HPLC. The yield for all the compounds ranged from 28 to 95%.

Scheme 2.2 shows further transformation steps with the functional groups of compound-**3** for the desired aim of this work. The benzyl alcohol in compound-**3** was converted to corresponding methyl ether using methyl iodide and sodium hydroxide as a base in dimethyl sulfoxide. Similarly, demethylation of the methoxy group gave corresponding phenol (compound-**3b**) in 48% aqueous hydrobromic acid as described for compound-**2** above. The reduction of the nitro group in the positive pressure of H_2 gas using palladium charcoal as a

catalyst gave corresponding amine **(**compound-**3c)**. All the compounds were characterized using ^{1}H and ^{13}C NMR.

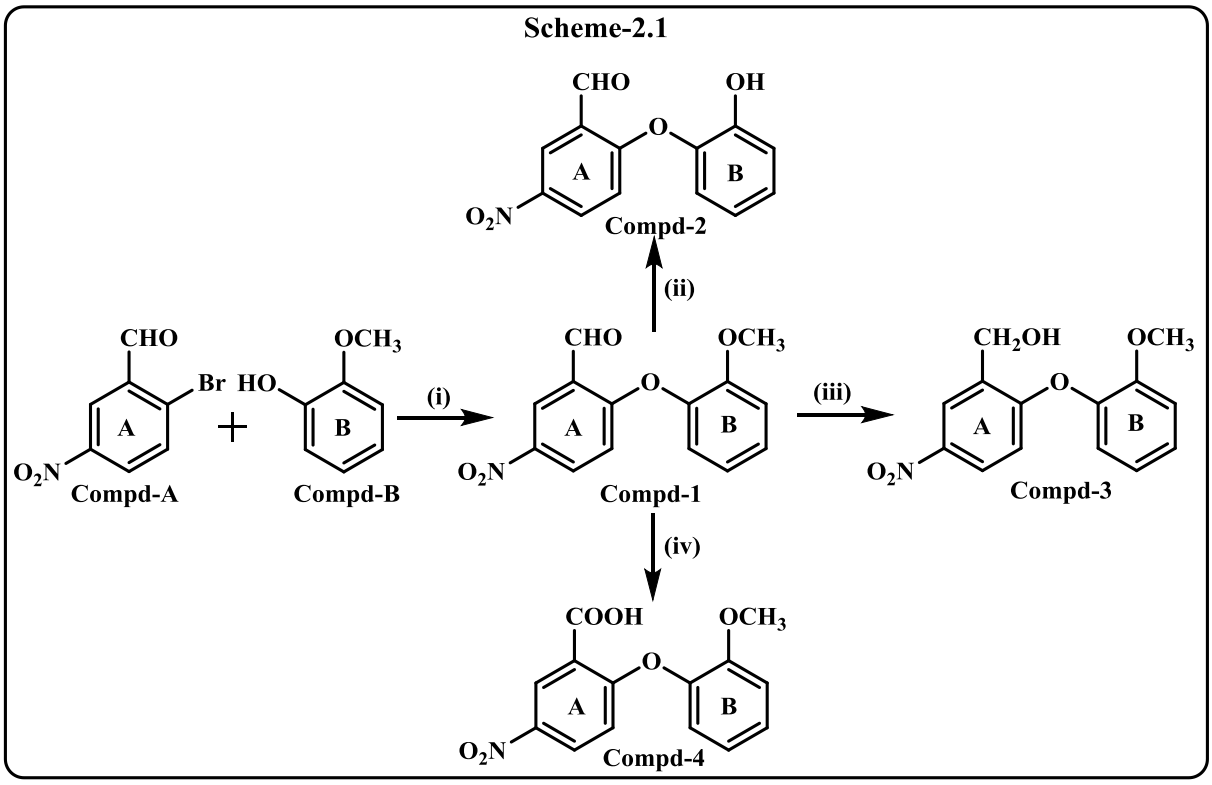

Scheme-2.1: Reagents; (i) K_2CO_3, 18-Crown-6, DMF (ii) CH_3COOH, 48% Aqueous HBr (aq) (iii) $NaBH_4$, MeOH (iv) $KMnO_4$, H_2O refluxed

Compound-**4**, in Scheme-2.1, was converted to the corresponding synthetic analogues using similar methodologies as for compound-**3. Scheme-2.3** shows methylation of compound-**4** using sodium hydroxide and methyl iodide in DMSO medium to a corresponding ester **(**compound-**4a)** in good yield (73%). Demethylation of compound-**4** with 48% aqueous hydrobromic acid in acetic acid under refluxing condition gave corresponding phenol compound-**4b** in 40 % yields. Finally the reduction of nitro to corresponding amino in compound-**4** using tin chloride in ethanol gave corresponding amino acid as compound-**4c** in 51 % yields. All the compounds were characterized using ^{1}H and ^{13}C NMR, HPLC and Infrared spectroscopy.

The modification of **compound-1** to the corresponding thio-derivative was done by making its Schiff base by reacting it with dithiocarbohydrazide in a mixture of methanol and water under reflux conditions for 24 hours to get a product (Compound-**5**) in 23 % yield **(Scheme-2.4).** The product was obtained after column chromatography purification and characterized using ^{1}H and ^{13}C NMR, HPLC and Infrared spectroscopy.

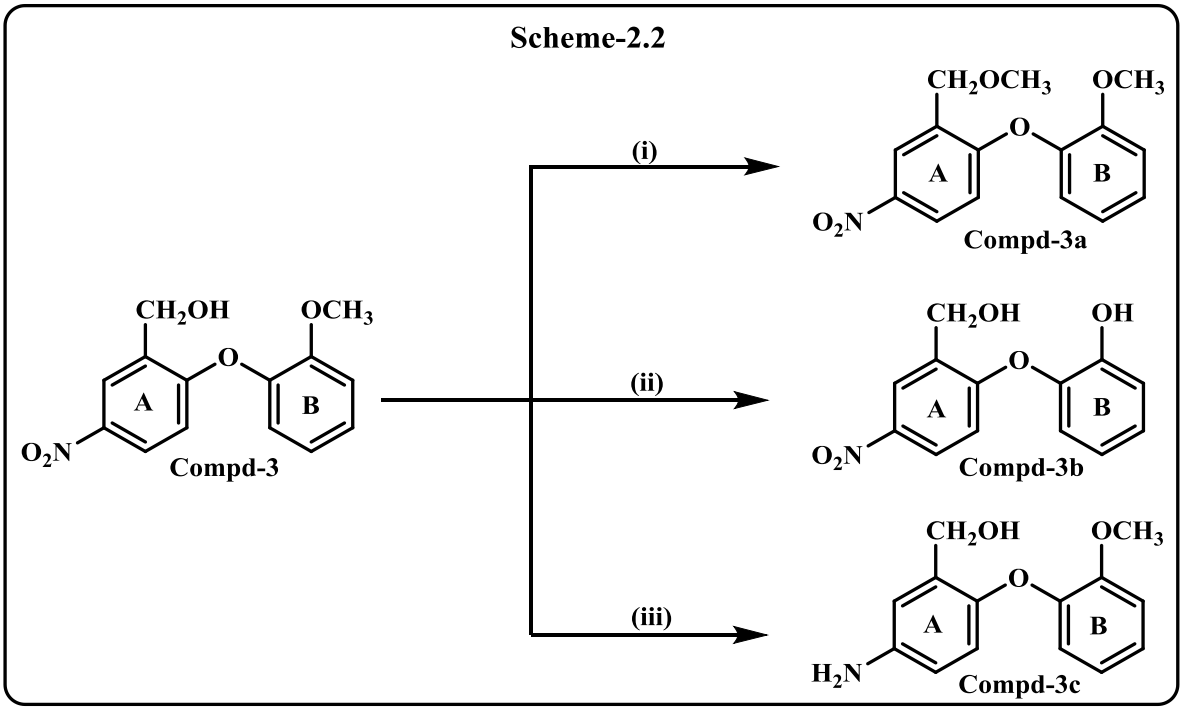

Scheme-2.2: Reagents; (i) CH_3I, NaOH, DMSO (ii) CH_3COOH, 48% Aqueous HBr (iii) 10% Pd/C MeOH (6-7 hrs).

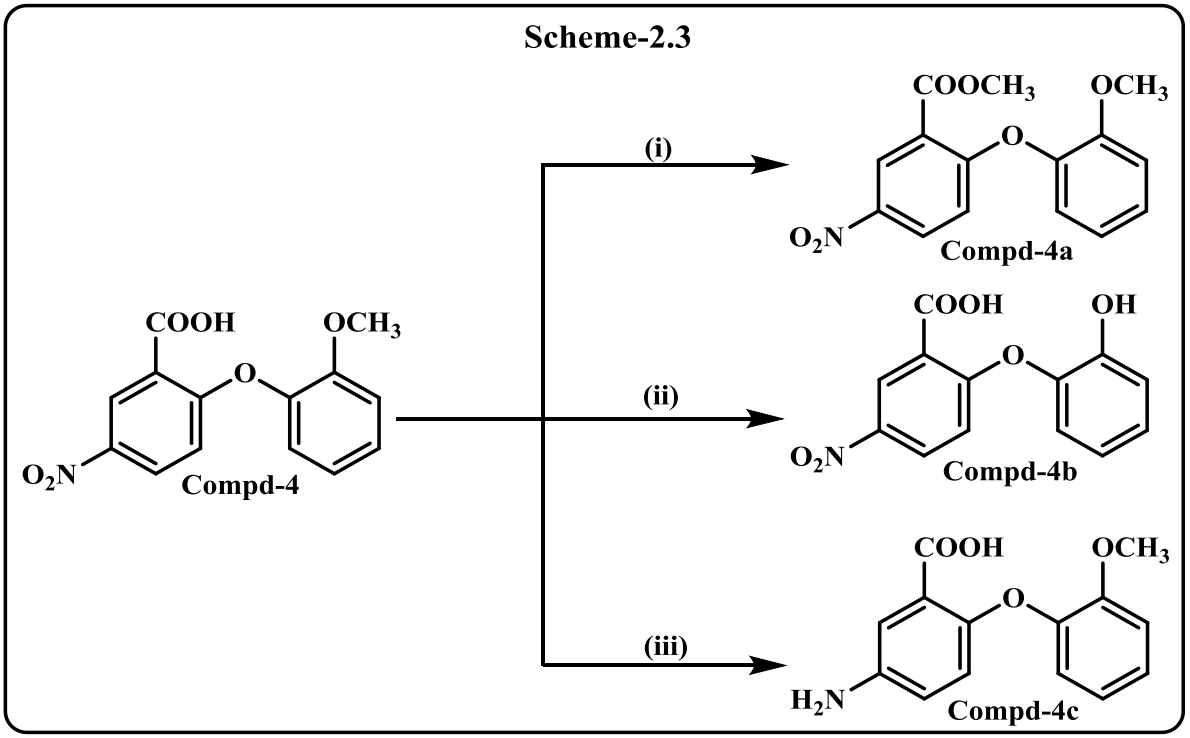

Scheme-2.3: Reagents; (i) CH_3I, NaOH, DMSO (ii) CH_3COOH, 48% Aqueous HBr (iii) $SnCl_2$, MeOH, 70 ^oC, 5% $NaHCO_3$.

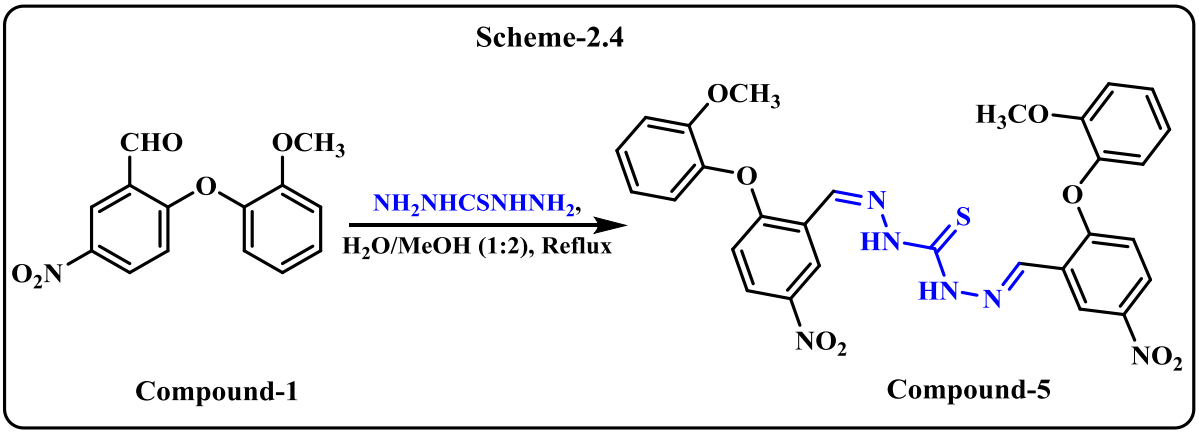

Scheme-2.4: Reagents; $NH_2NHCSNHNH_2$, H_2O: CH_3OH (7:3 v/v), Reflux 70ºC.

2.3. Characterization

The synthesized compounds were characterized for their structure and purity by NMR, IR spectroscopy and HPLC. 2-Bromo-5-nitro benzaldehyde required for the synthesis of **Compound-1** was prepared by the nitration of 2-fluoro benzaldehyde. It was confirmed for its nitro position by ^{1}H NMR. **Figure-2.2** displays two doublets at 8.7 and 6.7 ppm and a double doublet at 8.2 ppm corresponding to protons-**a, c** and **b,** respectively. The J value of 2.7 Hz for proton **a** corresponded to the meta coupling due to proton-**b**. The proton-**b** displayed a double doublet due to meta and ortho coupling with protons-**a** and **c,** respectively, with J values corresponding to 8.9 and 3.0 Hz. The proton **c** displayed a doublet due to coupling with proton-**b** at ortho position corresponding to a J value of 8.7 Hz. Thus, absence of any other aromatic protons corresponding to the ring-A or B and compliance of the J values with reported literature confirmed the position of nitro group in compound-**1**.[7]

The disappearance of methoxy singlet at 3.75 ppm in ^{1}H NMR and at 55.85 ppm in ^{13}C NMR confirmed the synthesis of phenolic compound-**2** from its precursor compound-**1.** Similarly, the disappearance of methoxy singlets at 3.74 ppm and 3.84 ppm in ^{1}H NMR confirmed the formation of phenolic compounds **3b** and **4b** by demethylation of their corresponding precursors **(**compounds **3** and **4** respectively**)**. The disappearance of ^{13}C NMR signal around 55 ppm for the above two compounds was also in compliance with the proposed structures for the compounds **3b** and **4b**.

The structure of compound-**3** was confirmed by the disappearance of the aldehyde proton at 10.67 ppm (for the precursor compound-**1**) and the simultaneous appearance of methylene protons (-CH_2-) at 4.90 ppm. This also corroborated with the appearance of benzylic carbon at 60.82 ppm in place of aldehyde carbon at 185.78 ppm in the precursor compound-**1**.

Methylation of compound-**3** to its corresponding ester **(**compound-**3a)** was confirmed by the appearance of a singlet peak for three protons at 3.48 ppm in ^{1}H NMR at 58.97 ppm in ^{13}C NMR.

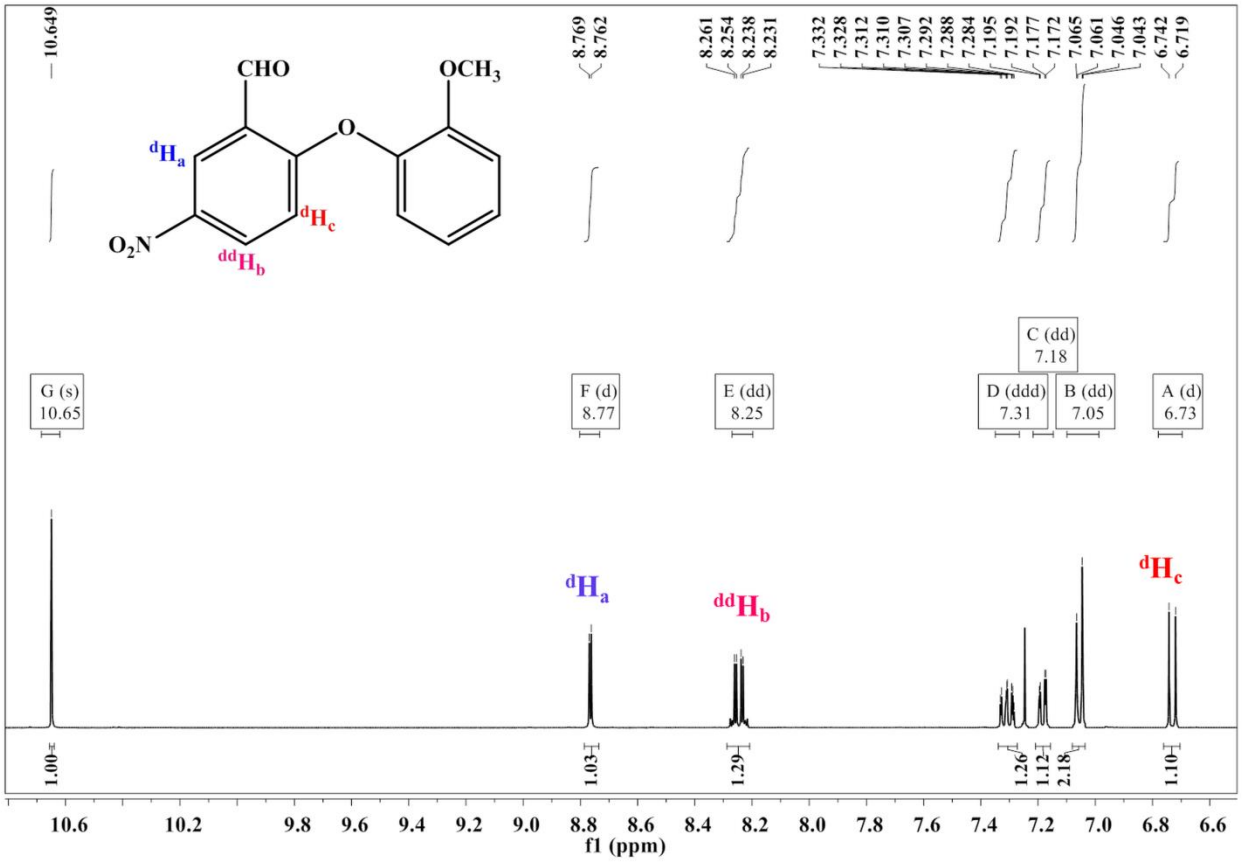

Figure-2.2: ^{1}H NMR for the compound-**1** (Aromatic region) synthesized by nitration of 2-bromo benzaldehyde. The J values for the protons H_a, H_b and H_c agree with literature values to confirmed the position of nitro group.

2.4. Materials and Instrumentation

All reagents used in the synthesis were purchased from Avra (India), SD Fine Chemicals (India) and Aldrich used without further purification. Purification of products obtained via organic reactions was by column chromatography using silica as a stationary phase. TLC analysis was done for reaction monitoring on silica gel 60 F_{254} plates. Column chromatography using product extraction was performed on a rota-evaporator (Roteva). All the synthesized products were analyzed for identification and purity by ^{1}H and ^{13}C NMR spectrometer (Jeol 400 MHz), infrared spectrometer, HPLC (Thermo-Fischer ultimate-3000) and CHN analysis were performed for purification purposes. The mobile phase used for purity analysis was ACN : water = 8:2 using C-18 and C-8 column (250 x 4.6 mm) with a constant flow rate of 1 ml / min. All photophysical studies were performed on Analytic Jena (Specord 200 UV-Visible) double-beam spectrophotometer.

2.5. Scheme-2.1

2.5.1. 2-(2-Methoxy phenoxy)-5- nitrobenzaldehyde (Compound-1)

To a solution of compound-B, 2-methoxy phenol, (103 mg, 0.54 mmol) in DMF (7 mL) were added K_2CO_3 (110 mg, 1.12 mmol), 18-crown-6 (10 mg, 0.04 mmol) and Compound-A, 5-nitro-2-bromobenzaldehyde (108 mg, 0.47 mmol). The reaction mixture was stirred at room temperature for 12 h and after completion of the reaction (TLC monitoring), the mixture was diluted with CH_2Cl_2 (50 mL), and washed with water (3 x 50 mL). The lower organic layer was separated and traces of moisture removed using anhydrous sodium sulphate. The crude product was concentrated using rota-evaporator to get white solid that was purified using silica gel column chromatography (Solvent system : Gradient increase up to 12% of ethyl acetate in hexane) to get compound-**1** in 76.5%(113 mg, mp 109-113 ^oC) yield.

Purity (HPLC) - 99.72% . ^1H NMR ($CDCl_3$) δ 10.67 (s,1H (CHO)), 8.78 (d, J = 3.2, 1H), 8.26 (dd, J = 1.85, 8.24(o,m), 1H), 7.33 (m, 1H), 7.20 (d, J = 7.06, 1H), 7.06 (d, J = 7.8, 2H), 6.75 (d, J = 9.2, 1H), 3.75 (s,3H); ^{13}C NMR ($CDCl_3$) δ 187.52, 165.00, 151.26, 142.49, 141.73, 130.03, 127.6, 124.5, 122.69, 121.51, 115.66, 113.03, 55.85. IR Spectra $\nu_{(C-H)\ aromatic}$ = 2998-3109 cm^{-1}, (OCH_3) $\nu_{(C-H)}$ = 2840,2889 cm^{-1}, (CHO) $\nu_{(C=O)}$ = 1689 cm^{-1}, (NO_2) $\nu_{(N-O)}$ = 1525cm^{-1}, (CH_3) $\nu_{(C-N)\ stretch\ \&\ (C-H)\ bending}$ = 1316 -1496 cm^{-1}, (COC) $\nu_{(C-O)}$ = 1198-1286 cm^{-1}, CHN Anal. Calcd. For $C_{14}H_{11}NO_5$ (273.24): C 61.54, H 4.06, and N 5.13; Found: C 61.40, H 3.98, and N 5.01.

2.5.2. 2-(2-Hydroxy phenoxy)-5-nitrobenzaldehyde (Compound-2)

To **Compound-1** (100 mg, 0.91 mmol) in acetic acid (7 mL) was added 48% aqueous HBr (6 mL) and the reaction mixture refluxed for 4 hours at 130 ^oC. After completion of the reaction, the mixture was washed with a brine solution to remove the excess of HBr solution and then diluted in 1M NaOH solution (100 mL) to solubilize the product. The aqueous layer was washed with ethyl acetate (3 x10 mL) to remove any unreacted product, and excess HCl was added (pH = 4). The crude product was extracted using ethyl acetate (50 mL) and dried over sodium sulphate,, then concentrated using a rota-evaporator. The light brown coloured product, compound-**2**, was obtained after silica gel column chromatography (Solvent system: Gradient increase from 30% to 40% of ethyl acetate in hexane) in 25% (59 mg, mp 84-88 ^oC) yield.

Purity (HPLC)-96.43 % . ^1H NMR ($CDCl_3$) δ 10.05 (s,1H (CHO)), 8.65 (d, J = 4.0, 1H), 8.33 (dd, J = 4.0, 8.0, 1H), 7.49 (m, 1H), 7.39 (m, 1H), 6.93 (d, J = 8.0, 1H), 6.75 (d, J = 9.2,

1H); ^{13}C NMR ($CDCl_3$) δ 185.78, 163.00, 145.09, 143.38, 130.39, 128.47, 125.13, 123.71, 116.27. IR Spectra $\nu_{(O-H)}$ = 3250 cm^{-1}, $\nu_{(C-H)\ aromatic\ \&\ methoxy}$ = 2849-3086 cm^{-1}, (CHO) $\nu_{(C=O)}$ = 1670 cm^{-1}, (NO_2) $\nu_{(N-O)}$ = 1509cm^{-1}, (CH_3) $\nu_{(C-H)\ bending}$ = 1410 -1494 cm^{-1}, (COC) $\nu_{(C-O)}$ = 1212-1285 cm^{-1}, CHN Anal. Calcd. For $C_{13}H_9NO_5$ (259.22): C 60.24, H 3.50, and N 5.40; Found: C 60.11, H 3.53, and N 5.38.

2.5.3. (2-(2-Methoxyphenoxy)-5-nitrophenyl) methanol (Compound-3)

To compound-**1** synthesized above (303 mg, 1.1 mmol) in methanol (12mL) was added $NaBH_4$ (82 mg, 21 mmol). The reaction mixture was stirred at room temperature and after completion of the reaction methanol evaporated and to the crude residue CH_2Cl_2 (50ml) added and washed with water (5 x 50 mL). Evaporation of separated CH_2Cl_2 gave crude product that was concentrated using rota-evaporator after drying over anhydrous sodium sulphate. Purification using silica gel column chromatography (Solvent system : Gradient increase up to 20 % of ethyl acetate in hexane) gave compound-**3** in 64.9% (198 mg, mp 79-82 ^oC) yield.

Purity (HPLC)–98.50 % . ^1H NMR ($CDCl_3$) δ 8.33 (d, J = 2.72, 1H), 8.02 (dd, J = 2.72, 9.16, 1H), 7.26 (m, 1H), 7.14 (dd, J = 1.36, 6.88, 1H), 7.02 (d, J = 7.76, 2H), 6.62 (d J = 8.72, 1H), 4.90 (s, 2H), 3.74 (s, 3H), ^{13}C NMR ($CDCl_3$) δ 161.30, 151.44, 142.45, 130.73, 127.11, 124.76, 124.55, 122.93, 121.46, 113.72, 113.09, 60.82, 55.85. IR Spectra $\nu_{(O-H)\ broad}$ = 3272 cm^{-1}, $\nu_{(C-H)\ aromatic\ \&\ methoxy}$ = 2838-3069 cm^{-1}, (NO_2) $\nu_{(N-O)\ \&\ (C-H)\ bending}$ = 1442-1526cm^{-1}, (COC) $\nu_{(C-O)}$ = 1169-1288 cm^{-1}, CHN Anal. Calcd. For $C_{14}H_{13}NO_5$ (289.24): C 61.09, H 4.76, and N 5.09; Found: C 61.12, H 4.68, and N 5.14.

2.5.4. 2-(2-Methoxy phenoxy)-5-nitrobenzoic acid (Compound-4)

To compound-**1** synthesized above (50 mg, 0.18 mmol) in H_2O (10 mL) was added $KMnO_4$ (44mg, 0.28 mmol) dropwise and the reaction mixture refluxed at 60-70 ^oC. After 2 h, 10% KOH solution in water was added to make the reaction mixture alkaline and precipitate the MnO_2 . The precipitates were filtered through celite bed while the reaction mixture was still hot followed by washing with hot water (3 x 15 mL) to recover any residual product. The cooled filtrate was acidified with dilute HCl until no further precipitate formed. White precipitates were dissolved in ethyl acetate (25 mL) washed with water until later was neutral. The traces of moisture were removed from ethyl acetate using anhydrous Na_2SO_4 to get yellow colored crude product that was purified using SiO_2 column chromatography (

Solvent system : Gradient increase up to 18 % of ethyl acetate in hexane) to get compound-**4** in yield 47% (25mg, mp-90-93 ^{o}C).

Purity (HPLC)–99.99 %. ^{1}H NMR ($CDCl_3$) δ 11.77 (s, (COOH)), 9.06 (d, J = 2.76, 1H), 8.41 (dd, J = 2.72, 9.16, 1H), 7.32 (m, 1H), 7.18 (dd, J = 1.8, 7.76, 1H), 7.15 (d, 1H) 7.07-7.03 (m, 2H), 3.84 (s, 3H); ^{13}C NMR ($CDCl_3$) δ 167.22, 166.53, 150.76, 140.16, 138.45, 131.01, 127.94, 127.35, 122.45, 120.93, 118.79,112.54, 111.64, 55.87. IR Spectra $\nu_{(O-H)\ broad}$ = 2500-3200 cm^{-1}, (=C-H) $\nu_{(C-H)\ methoxy\ \&\ aromatic}$ = 2838, 3083 cm^{-1}, (COOH) $\nu_{(C=O)}$ = 1707 cm^{-1}, (NO_2) $\nu_{(N-O)\ \&\ (C-H)\ bending}$ = 1450-1509 cm^{-1}, (COC) $\nu_{(C-O)}$ = 1234-1345 cm^{-1}, bending peak (COOH) $\nu_{(O-H)\ bending}$ = 918 cm^{-1}, CHN Anal. Calcd. For $C_{14}H_{11}NO_6$ (289.24): C 58.14, H 3.83, and N 4.84; Found: C 58.13, H 4.21, and N 5.0.

2.6. Scheme-2.2

2.6.1. 2-(Methoxymethyl)-1-(2-methoxyphenoxy)-4-nitrobenzene (Compound-3a)

To compound-**3** (100 mg, 0.38 mmol) in DMSO (5 mL) was added NaOH (58 mg, 1.45 mmol) and stirred for 10 minutes in an ice bath. After getting a homogeneous solution MeI (206 mg, 1.45 mmol) was added drop-wise and the further stirred for 1 hour at room temperature. After completion of the reaction (TLC monitoring) the mixture was diluted with ethyl acetate (50ml), washed with H_2O (5 x 50 mL) and the organic layer dried over sodium sulphate. A fade yellow crude product was concentrated using rota-evaporator and purification done using silica gel column chromatography (Solvent system : Gradient increase up to 4 % of ethyl acetate in hexane) to get pure compound-**3a** in 44% (46 mg, mp 89-94 ^{o}C) yield.

Purity (HPLC)–88.83 % . ^{1}H NMR ($CDCl_3$) δ 8.39 (s, 1H), 8.0 (dd, J = 4.0, 8.0, 1H), 7.23 (dd, J = 8.0, 4.0, 1H), 7.08 (dd, J = 8.0,4.0, 1H), 7.00 (m, 2H), 6.56 (d, J = 8.0, 1H) 4.70 (s, 2H), 3.50 (s, 3H), 3.45 (s,3H); ^{13}C NMR ($CDCl_3$) δ 160.61, 151.53, 142.73, 142.50, 128.64, 126.87, 124.31, 124.19, 122.69, 121.46, 113.72,113.07, 68.53, 58.97, 55.86. IR Spectra $\nu_{(C-H)\ aromatic\ \&\ methoxy}$ = 2824-3000 cm^{-1}, (NO_2) $\nu_{(N-O)\ \&\ (C-H)\ bending}$ = 1435-1533cm^{-1}, (COC) $\nu_{(C-O)}$ = 1169-1260 cm^{-1}, CHN Anal. Calcd. For $C_{15}H_{15}NO_5$ (289.29): C 62.28, H 5.23, and N 4.84; Found: C 62.24, H 5.14, and N 4.86.

2.6.2. 2-(2-(Hydroxymethyl)-4-nitrophenoxy) phenol (Compound -3b)

To compound-**3** (100 mg, 0.36 mmol) in acetic acid (6 mL) was added HBr (6 mL) and the reaction mixture refluxed for 4 hours at 130 ^{o}C. After completion of the reaction, the mixture was washed with brine solution to remove the excess of HBr solution and then diluted in

NaOH solution (100 mL) to solubilize the product. The aqueous layer was washed with ethyle acetate (3 × 10 mL) to remove any unreacted product and excess HCl added (pH = 4). Crude product was extracted using ethyle acetate (50 mL) and dried over sodium sulphate followed by its concentrated using rota-evaporator. The brown coloured product, compound-**3b**, was obtained after silica gel column chromatography (Solvent system : Gradient increase from 40% to 50% of ethyl acetate in hexane) to get compound-3 in 51% (48 mg, mp 138-141 ^{o}C) yield.

Purity (HPLC)–90.20 % . ^{1}H NMR ($CDCl_3$) δ 8.14 (s, 1H), 7.95 (dd, J = 4.0, 8.0, 1H), 7.12 (t, 1H), 6.99 (m, 2H), 6.89 (t, 1H), 6.71 (d, J = 8.0, 1H) 4.83 (s, 2H); ^{13}C NMR ($CDCl_3$) δ 161.39, 148.76, 141.53, 130.09, 127.36, 125.73, 125.63, 122.45, 122.31, 120.67, 118.02, 115.22, 61.43. IR Spectra (free OH) $\nu_{(O-H)\ sharp}$ = 3493, 3528 cm^{-1}, (OH intra-molecular hydrogen bonded) $\nu_{(O-H)\ broad}$ = 3197 cm^{-1}, $\nu_{(C-H)\ aromatic\ \&\ methoxy}$ = 2837-3079 cm^{-1}, (NO_2) $\nu_{(N-O)\ \&\ (C-H)\ bending}$ = 1445-1512cm^{-1}, (COC) $\nu_{(C-O)}$ = 1143-1249 cm^{-1}, CHN Anal. Calcd. For $C_{13}H_{11}NO_5$ (261.23): C 59.77, H 4.24, and N 5.36; Found: C 59.69, H 4.23, and N 5.39.

2.6.3. (5-Amino-2-(2-methoxyphenoxy) phenyl) methanol (Compound -3c)

To compound-**3** (150mg, 0.54 mmol) in methanol (20 mL) was added 10% Pd/C (20 mg) and the suspension stirred for 4 hours at room temperature in positive pressure of hydrogen gas. It was then diluted with 10% aqueous K_2CO_3 (50 mL) and filtered through celite 545 and further washed with hot water (3 × 20 mL). The alkaline filtrate was neutralized to pH 7 using HCl and extraction done using ethyl acetate. The organic layer was washed with H_2O (3 × 50mL) and the crude product obtained by evaporating solvent using rota-evaporator. Dark brownish product obtained was purified using column chromatography (Solvent system : Gradient increase from 50 % up to 80 % of ethyl acetate in hexane) gave pure compound-**3c** in 90% (120 mg, mp 130-135 ^{o}C) yield.

Purity (HPLC) – 80.36 %. ^{1}H NMR ($CDCl_3$) δ 7.04 (m,1H), 6.95 (m, 1H), 6.83 (m, 3H), 6.65 (d, J = 8.0 1H), 6.58 (dd, J =8.0,4.0, 1H) 4.62 (s, 2H), 3.82 (s, 3H), ^{13}C NMR ($CDCl_3$) δ 150.45, 148.02, 146.38, 132.67, 123.86, 121.14, 119.11, 116.71, 115.99, 112.53, 61.37, 55.97. IR Spectra (NH_2) $\nu_{(N-H)\ sharp}$ = 3365 cm^{-1}, (CH_2OH) $\nu_{(O-H)\ broad}$ = 3272 cm^{-1}, $\nu_{(C-H)\ aromatic\ \&\ methoxy}$ = 2835-3036 cm^{-1}, (CH_3) $_{(C-H)\ bending}$ = 1449-1495cm^{-1}, (COC) $\nu_{(C-O)\ \&\ (C-N)}$ = 1176-1257 cm^{-1}, CHN Anal. Calcd. For $C_{14}H_{15}NO_3$ (245.28): C 68.56, H 6.16, and N 5.71; Found: C 68.50, H 6.14, and N 5.74.

2.7. Scheme-2.3

2.7.1. Methyl 2-(2-methoxyphenoxy)-5-nitrobenzoate (Compound -4a)

To compound-**4** (58 mmol, 168 mg) in DMSO (7 mL) with NaOH (2.3 mmol, 93 mg) was added MeI (46 mmol, 0.14 mL) drop wise over a period of 1 hour at room temperature. After completion of the reaction (TLC monitering), the mixture was dissolved in dichloromethane (100 ml) and washed with water (5 × 50 mL). The organic layer was dried over Na_2SO_4 and evaporation of the solvent gave a white coloured product that was purified using SiO_2 column chromatography(Solvent system : Gradient up to 20 % of ethyl acetate in hexane) to give compound-**4a** in 73% yield (130 mg, mp-98-102 ^oC).

Purity (HPLC) – 96.85 % .^1H NMR ($CDCl_3$) δ 8.81 (d, J = 2.76, 1H), 8.19 (dd, J = 9.16, 2.76, 1H), 7.25 (d, 1H), 7.14 (dd, J = 1.84, 7.8, 1H), 7.03 (m, 1H), 6.73 (d, 9.16), 3.96 (s, 3H), 3.76 (s, 3H); ^{13}C NMR ($CDCl_3$, δ) 164.28, 162.67, 151.21, 142.33, 141.45, 128.32, 127.97, 127.04, 122.47, 121.45, 120.30, 116.05, 113.08, 55.83, 52.65. IR spectra: $\nu_{(C-H)\ aromatic\ \&\ methoxy}$ = 2832-3164 cm^{-1}, (COOH) $\nu_{(C=O)}$ = 1680 cm^{-1}, (NO_2) $\nu_{(N-O)}$ = 1404-1507 cm^{-1}, (COC) $\nu_{(C-O)}$ = 1254-1297 cm^{-1}; CHN Anal. Calcd. For $C_{15}H_{13}NO_6$ (303.27.08): C 59.41, H 4.32, and N 4.62; Found: C 59.40, H 4.32, N 4.58.

2.7.2. 2-(2-hydroxyphenoxy)-5-nitrobenzoic acid (Compound-4b)

To compound-**4** (50 mg, 0.17 mmol) in acetic acid (6 mL) was added HBr (6 mL) and the reaction mixture refluxed for 4 hours at 130 ^oC. After completion of the reaction, the mixture was washed with brine solution to remove the excess of HBr solution and then diluted in KOH solution (100 mL) to solubilize the product. The aqueous layer was washed with ethyl acetate (3 × 10 mL) to remove any unreacted product and excess HCl added (pH = 4). Crude product was extracted using ethyl acetate (50 mL) and dried over sodium sulphate followed by its concentrated using rota-evaporator. The light yellowish product, compound-**4b**, was obtained after silica gel column chromatography (Solvent system : Gradient increase from 50% to 70% of ethyl acetate in hexane) to get compound-**4b** in 38% (20 mg, mp 97-102 ^oC) yield.

Purity (HPLC)–94.02 % . ^1H NMR ($CDCl_3$) δ 8.26 (d, 1H), 8.09 (dd, 1H), 7.15 (m, 2H), 7.04 (dd, J = 8.0 1H), 6.92 (m, 2H) 4.95 (s, 1H), ^{13}C NMR ($CDCl_3$) δ 167.41, 160.18, 149.73, 145.07, 143.48, 128.05, 126.37, 124.82, 121.20, 118.40, 117.26, 116.06. CHN Anal. Calcd. For $C_{13}H_9NO_6$ (275.22): C 56.73, H 3.30, and N 5.09; Found: C 56.77, H 3.24, N 5.09.

2.7.3. 5-Amino-2-(2-methoxyphenoxy) benzoic acid (Compound-4c)

To compound-**4** (100 mg, 0.34 mmol) dissolved in absolute EtOH (6 mL) was added $SnCl_2.2H_2O$ (78 mg, 0.34 mmol) and the reaction mixture refluxed at 70 ^oC under nitrogen atmosphere. After 30 minutes, the reaction mixture was cooled and made alkaline using 5% aqueous $NaHCO_3$. The ethanol was evaporated and ethyl acetate (60 mL) added to extract the organic compound. The organic layer was washed with water (3 × 50 mL) and dried over sodium sulphate to get a light brownish coloured compound that was purified using SiO_2 column chromatography (Solvent system : Gradient increase from 30 % up to 50 % of ethyl acetate in hexane) to get compound-**4c** in yield 51% (45mg, mp-140-144 ^oC).

Purity (HPLC) – 96.70 % . ^1H NMR ($CDCl_3$) δ 10.61 (s, 1H), 7.50 (dd, J = 8.24, 1.84, 1H), 7.27 (d, J = 8.68, 1H), 7.16 (dd J = 1.84, 7.80, 1H), 7.02 (m, 2H), 6.96 (d J = 7.8, 1H), 6.80 (t, J = 7.56, 1H), 3.93 (b, NH_2), 3.82 (s, 3H), ^{13}C NMR: 150.42, 147.41, 146.58, 142.43, 132.58, 123.83, 121.02, 119.38, 118.91, 116.17, 115.36, 112.52, 61.57. IR spectra: (NH,) $\nu_{(N-H)}$ = 3310, cm^{-1}, (=C-H) $\nu_{(C-H)}$ = 2946 cm^{-1}, (OCH_3) $\nu_{(C-H)\ aromatic\ \&\ methoxy}$ = 2845-3113 cm^{-1}, (COOH) $\nu_{(C=O)}$ = 1699 cm^{-1}, (CH_3) $\nu_{(C-H\ bending)}$ = 1437-1491 cm^{-1}, $\nu_{(C-N)}$ = 1337 cm^{-1}, (COC) $\nu_{(C-O)}$ = 1232,1264 cm^{-1}, bending peak (COOH) $\nu_{(O-H)}$ = 920 cm^{-1}; CHN Anal. Calcd. For $C_{14}H_{13}NO_4$ (259.08): C 64.86, H 5.05, and N 5.40; Found: C 64.88, H 5.21, and N 5.58.

2.8. Scheme-2.4

2.8.1. N',2-bis(-2-(2-methoxyphenoxy)-5-nitrobenzylidene)hydrazine-1carbothiohydrazide (Compound-5):

To thiocarbohydrazide (40 mg, 0.3 mmol) in water : methanol (7:3, 10 mL) mixture was added Compound-**1** (200 mg, 0.7 mmol), and the reaction mixture refluxed for 24 hours. TLC monitoring confirmed the product formation. After cooling, the organic product was extracted with ethyl acetate (2 × 50 mL), washed with water (2 × 50 mL) and the organic layer dried over sodium sulphate. After filtration, evaporation of the solvent using a rotatory evaporator gave crude product as a solid brown mass. Purification using column chromatography (Silica Gel stationary phase and 40 % ethyl acetate in hexane) gave the final product in 23 % yield. Yield: 20 mg, Melting range: 328-331^oC,

Purity (HPLC): 96.74% ^1H NMR ($CDCl_3$) δ 9.69 (s,1H (HC=N)), 8.76 (d, J = 2.76, 2H), 8.36 (s, 1H (HC=N)), 8.06 (dd, J = 9.64, 3.2, 2H), 7.29 (m, 2H), 7.11 (dd, J =8.24,1.84 2H), 7.04 (m,4H), 6.66 (d, J = 9.32, 2H), 3.77 (m (s,6H), 2.05 (s, 2H (NH)); ^{13}C NMR :179.25, 161.485, 151.24, 142.55, 141.98, 136.74, 127.27, 126.33, 122.52, 122.11, 121.45, 114.92,

112.99, 55.73. IR spectra: (NH_2,) $\nu_{(N-H)}$ = 3393, cm^{-1}, (=C-H) $\nu_{(C-H)}$ = 2946 cm^{-1}, (OCH_3) $\nu_{(C-H)\ aromatic\ \&\ methoxy}$ = 2938, 2821 cm^{-1}, (C=N) $\nu_{(C=N)}$ = 1650-1693 cm^{-1}, $\nu_{(C=S)}$ = 1570, 1341 and 1265 cm^{-1}, (NO_2) $\nu_{(N-O)}$ = 1455,1455cm^{-1}; CHN Anal. Calcd. For $C_{29}H_{24}N_6O_8S$ (616.61) C, 56.49; H, 3.92; N, 13.63; O, 20.76; S, 5.20.

2.9. Spectroscopic Studies

Preparation of Solutions

Analytical grade salts of nitrate (for cations) and tert-butyl ammonium (for anions) from Sigma Aldrich, India were used to prepare a stock solution (1×10^{-2} mol L^{-1}). The prepared stock was further diluted with the desired solvent to reach the required dilution. All the receptors used for the study were synthesized, purified using column chromatography and analyzed before preparing a stock solution (1×10^{-3} mol L^{-1}) in the desired solvent. Dilutions were done using a micropipette of 1000, 200 and 10 microliter capacities.

UV-Visible Studies: For absorption studies, a UV-Visible spectrophotometer ((Specord-205, Analytic Jena) with a scanning range of 200 to 800 nm was used. The solution taken in the quartz cuvette having a path length of 1.0 cm. The photophysical response of the receptors and ions individually and in combination was optimized by comparing the absorption change observed by adding 10-time excess ions.

Emission Studies: For emission studies, a Spectroflorometer((Shimadzu RF-6000) with a scanning range of 185 to 820 nm was used. The solution taken in the glass cuvette having a path length of 1.0 cm. The emission response of the receptors and ions individually or in combination was optimized by comparing the emission change observed by adding 10-time excess ions.

The following parameters and method protocols were considered to validate the potential of ion-sensing receptors.

2.9.1. Specificity: The capacity of the receptors to sense specific ions in the presence of other interferences was carried out in two different ways. In the first case, the receptor-ion complex was observed for change in the absorption band by adding ten times excess of the interfering ions. In the second case, excessive amounts of the interfering ions were introduced into the receptor, followed by the addition of the ions that the receptor detects selectively to observe any change from the initial absorption. A bar graph plotted for absorbance versus ions summarized the investigation.

Additionally, utilizing titration studies, a common experiment was run to determine the binding constant and its detection limits. This study looked at the variations in absorption at a certain wavelength by adding selective ions one at a time while maintaining a consistent receptor concentration.

The minimum detection limit (LOD): A graph plotted between the receptor's absorbance/emission intensity versus the ion concentration at a specific wavelength for the receptor, and ion titration data gave a linear response due to quenching, amplification, or shifting of the peak. Origin software gave a regression line for the points on the linear graph that was used to determine the LOD using the IUPAC-approved equation shown below.

$$LOD = 3\frac{\sigma}{k} \quad \ldots\ldots\ldots\ldots\ldots\ldots\ldots\ldots (1)$$

where σ is the standard deviation of the response and k is the slope of the linear curve.

2.9.2. Binding Constant: Benesi-Hildebrand equation (Eq-2) calculated the binding constant from the plot of $1/A\text{-}A_0$ verses 1/ [ion] where A_0 is the maximum absorbance of the receptor at the responded wavelength, and A is the absorbance observed at a particular wavelength with change in the concentration of ions [M]. A_{max} is the maximum absorbance change of the receptor that did not change further after adding the respective ion. The association constant K_a ($L\ mol^{-1}$) was determined from the slope of the linear plot.

$$\frac{1}{A - A_0} = \frac{1}{K_a(A_{max} - A_0)[M]^1} + \frac{1}{A_{max} - A_0} \ldots\ldots\ldots\ldots\ldots\ldots\ldots\ldots\ldots\ldots (2).$$

The slope and intercept from this straight line were used to compute the binding constant.

2.9.3. Job's plot: Stoichiometry of the complex was determined by Job's method using the following equation.

$$\Delta A = |A\text{-}(1\text{-}\ X_M).\ A_R^{\circ}\ \text{-}\ X._M.\ A_M^{\circ}\ | \ldots\ldots\ldots\ldots\ldots\ldots\ldots\ldots\ldots\ldots (3)$$

The resultant curve, known as Job's plot, was obtained via mixing aliquots of two equimolar stock solutions of metal and ligand in a fixed volume in the range between 0.1 – 0.9 equivalents provided maxima that show the ligand-metal ratio in solution. The maxima at 0.5 equivalents/mole fractions indicated 1:1 composition for complex, whereas maxima at 0.67 and 0.75 gave 2:1 and 3:1 stoichiometry, respectively.

Calibration Curve: The calibration curve in the analytical method is a linear relationship between concentration (independent variable) and response (dependent variable) using a least squares method. This relationship predicted the unknown concentrations of the analyte

in a complicated matrix. The linearity of the calibration curve was expressed in terms of the coefficient of determination having R^2 value more than 0.9.

2.10. Validation Methods

2.10.1. NMR Titration: The method complemented the results from the photophysical studies to understand the receptor-ion orientation while interacting. NMR spectra were recorded each time after adding an incremental concentration of the selective ion in the fixed concentration of the receptor. The receptor and the receptor-ion complex for ^{1}H NMR bonded to the interacting atoms displayed a shift. The change in the δ value was compared to determine the interaction mechanism.

2.10.2. IR validation: The method also complemented the results from the photophysical studies. The atoms of the receptor molecule changed their vibrational frequencies after interacting with ions. Comparative experiments were carried out utilizing the SHIMADZU instrument to validate the suggested interaction site of the ions in a specific receptor (IR Tracer-100).

2.10.3. Theoretical studies: Virtual modelling was performed in three dimentions to predict the interaction of the native receptors and their complexes with ions using DFT calculations in Gaussian-16. The B3LYP technique and the basis set 3-21G, 6-31G, 6-311G, and 6-311G (d,p) were used for all the synthesized molecules. For transition metal atoms, LANL2MB was used. The computational method calculated the receptor's minimal energy and reactive site in the presence of selective ions. The HOMO-LUMO energy gave the stability of the complex. Time-dependent DFT calculation was performed to understand the electronic properties and photophysical behaviour of the receptors theoretically.

2.11. Real-life sampling: For the real-life application of **compound-5** to detect Hg^{2+} ions in urine, a conventional procedure, as reported in the literature was followed. The presence of UV-Visible active components necessitated dilution of the urine sample. It decreased the detection limit of the receptor from nM to μM for the determination of Hg^{2+} ions. However, the nM concentration was determined using the spiking method, and MPAES did further validation to determine real-life applicability.

References:

1. Srivastava, V.; Srivastava, K.; Singh, P.; Dwivedi, V., *Materials Today: Proceedings* **2022**.
2. Chhibber, M.; Kumar, G.; Parasuraman, P.; Ramya, T.; Surolia, N.; Surolia, A., *Bioorg. & med. chem.* **2006,** *14*, 8086-8098.
3. Cava, M. P.; Afzali, A., *J. Org. Chem.* **1975,** *40*, 1553-1556.
4. Afzali, A.; Firouzabadi, H.; Khalafi-Nejad, A., *Synth. Commun.* **1983,** *13*, 335-339.
5. Pellón, R. F.; Carrasco, R.; Milián, V.; Rodés, L., *Synth. commun.* **1995,** *25*, 1077-1083.
6. Cristau, H.-J.; Cellier, P. P.; Hamada, S.; Spindler, J.-F.; Taillefer, M., *Org. lett.* **2004,** *6*, 913-916.
7. Wachter, N. M.; Khouryawad, N. W.; Tarbox, H. E., In *NMR Spectroscopy in the Undergraduate Curriculum, Volume 4: In-Person and Distance Learning Approaches*, ACS Publications: 2021; pp 67-78.

Section-II

Cation Detections

Chapter-3

Graphical Abstract:

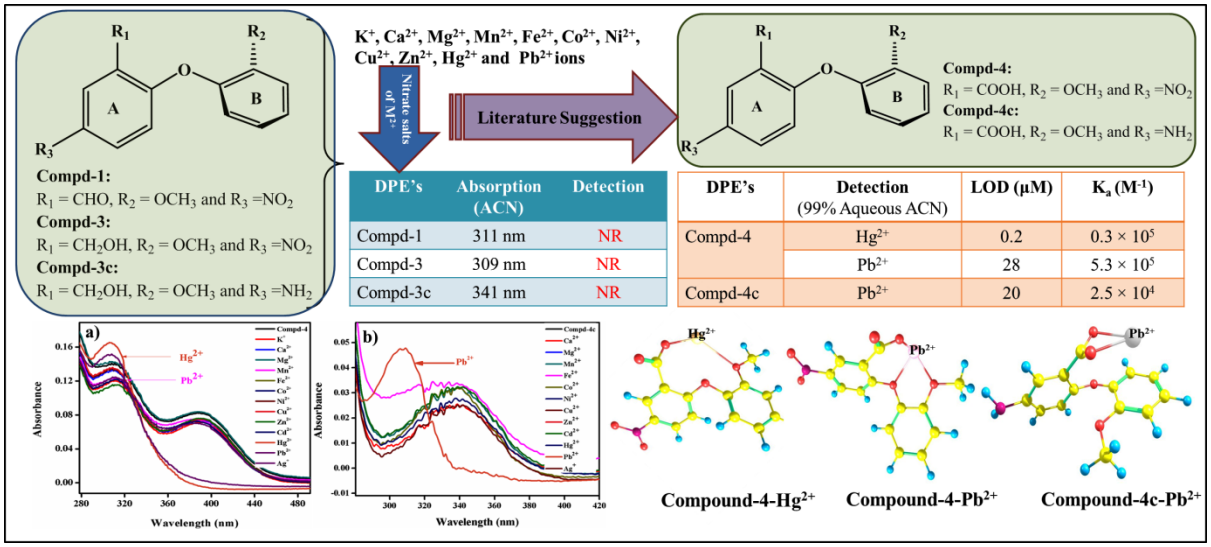

Chapter-3

OPTIMIZATION OF FUNCTIONAL GROUPS ON DIPHENYL ETHERS FOR THE RECOGNITION OF MERCURY AND LEAD IONS

3.1. Introduction

Detection of heavy metal ions is essential due to their highly toxic nature.[1] Both natural and artificial sources are responsible for the spread of such ions in the environment. It includes volcanic eruptions, leaching from the open mines, waste burning, leather tanning, electroplating, preventive medical practices, agricultural and industrial processes and fossil fuel combustion.[2-4] Mercury and lead ions are amongst the most dangerous ions due to their ability to cause adverse effects to human and animal health, even in minute amounts.[5,6] As per WHO guidelines, the minimum permissible limit for these ions in drinking water is 29 nM (Hg^{2+}) and 480 nM (Pb^{2+}).[7] Therefore detection of such ions in an aqueous medium by affordable technique is vital.

Fortunately, metal ions are electron-deficient species having an affinity for electron-rich moieties. Atoms like oxygen, nitrogen, sulphur, and phosphorous carry a lone pair of electrons in most synthetic and natural organic molecules that can serve as bait for the metal ions. The HSAB principle governs the selectivity of the cations for an electron-rich heteroatom. [8]

As discussed in **chapter-1**, optical methods that can detect receptor molecules offer numerous advantages like affordability, easy processing, real-time response and less time consumption. [9] Diphenyl ether molecules decorated with heteroatom-containing functional groups can respond in the UV-Vis region along with the additional advantage of balance between rigidity and flexibility and many opportunities for functional group manipulation on the rings. The work presented in this chapter explored the potential of different functional groups for the selective detection of cations in the aqueous medium. Functional group manipulation on diphenyl ethers gave optimized structures of the two molecules capable of detecting Hg^{2+} and Pb^{2+} ions.

3.2. Design of the receptors

As discussed in the introduction, phenyl ether molecules are rigid and flexible due to planar phenyl rings and flexible ether linkages. Appropriately placed functional groups in these

molecules offer charged cavities of varying sizes for the entrapment of ions and molecules, as shown in **Figure 3.1**.

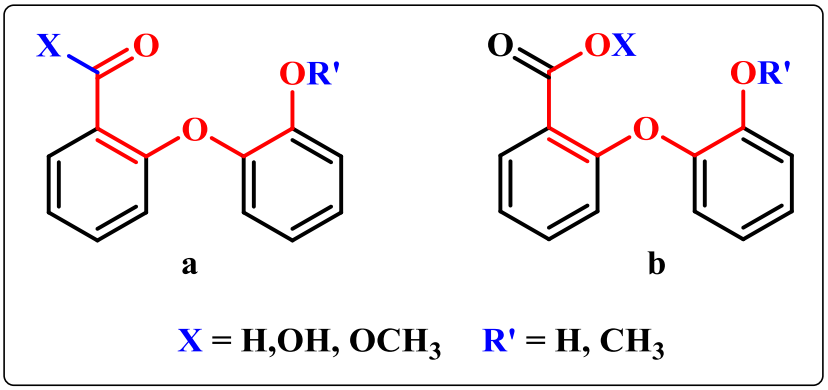

Figure-3.1: Representation of the appropriate positioning of functional group in diphenyl ether, offering a charged cavities of varying sizes for the entrapment of ions.

Therefore, it envisaged synthesizing compound-**1 (Figure-3.2)** and its derivatives with the charged cavities and exploring its potential to detect harmful cations for real-life applications. Compounds **1**, **3** and **3c** absorbed the UV light, giving their respective λ_{max} at 311, 309 and 341 nm in the acetonitrile medium. However, the absorbance of the three molecules did not show any deviation from their native UV-Visible spectra in the presence of nitrate salt of the metal ions having a concentration of 1 mM. (K^{+}, Ca^{2+}, Mg^{2+}, Mn^{2+}, Fe^{2+}, Co^{2+}, Ni^{2+}, Cu^{2+}, Zn^{2+}, Cd^{2+}, Hg^{2+}, Pb^{2+} and Ag^{+}) All three compounds tended to precipitate in the presence of an aqueous medium and, therefore, could not be taken up for further studies.

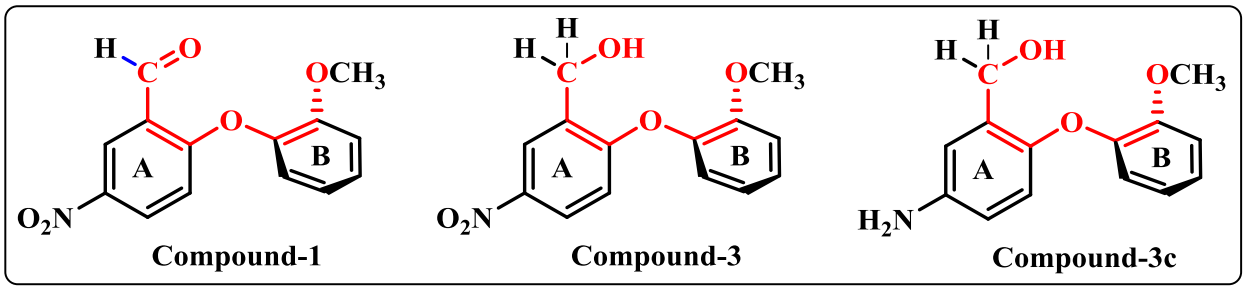

Figure-3.2: Representation of the compound-**1**, **3**, **3c** molecule having charged cavities when functional groups are linked at the appropriate position.

Selective detection of the harmful metal ions by a carboxylate group in an aqueous medium is known in the literature. **Table 3.1** mentions carboxylic acid derivatives for the selective detection of these ions with the solvent conditions, a method employed and the detection limit.

Table 3.1: Examples from the literature for the selective detection of Hg^{2+} and Pb^{2+} ions using carboxylate group in an aqueous medium

Receptors	Solvent system	Technique Used	Metal Detected	LOD/Ka	Ref.
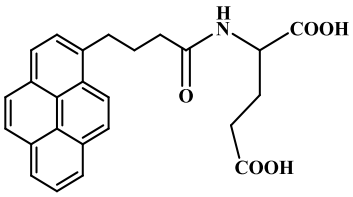	H_2O: DMSO (98:2)v/v	Fluorescence	Pb^{2+}	1.5 µM / 1.15×10^6 M^{-1}	10
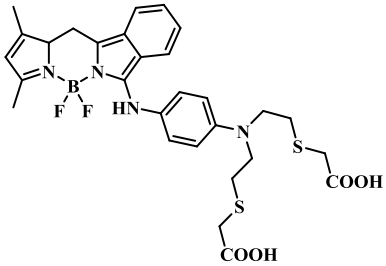	H_2O:MeOH (1:1)v/v	Fluorescence	Hg^{2+}	5.7 nM/ 1.16×10^4 M^{-1}	11
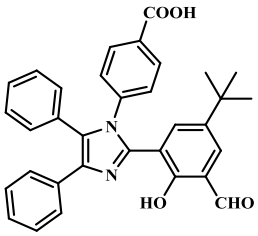	H_2O:ACN (1:1)v/v	Absorbance and Fluorescence	Hg^{2+}	1.5 µM/ Not given	12
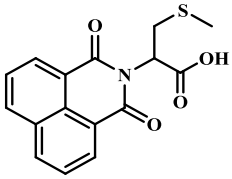	H_2O:MeOH (9:1)v/v	Absorbance and Fluorescence	Hg^{2+}	3.4 nM/ 3.4×10^9 M^{-2}	13
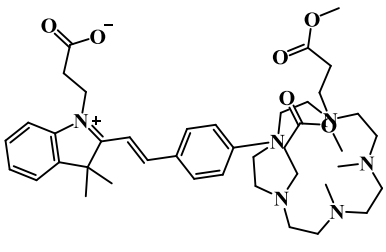	H_2O	Absorbance and Fluorescence	Hg^{2+}	50 nM/ Not given	14
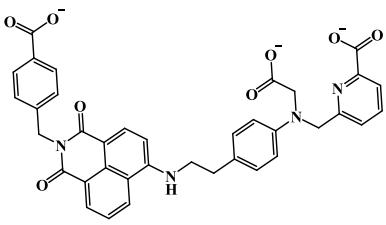	H_2O	Fluorescence	Hg^{2+}	100 nM/ 1.4×10^8 M^{-1}	15

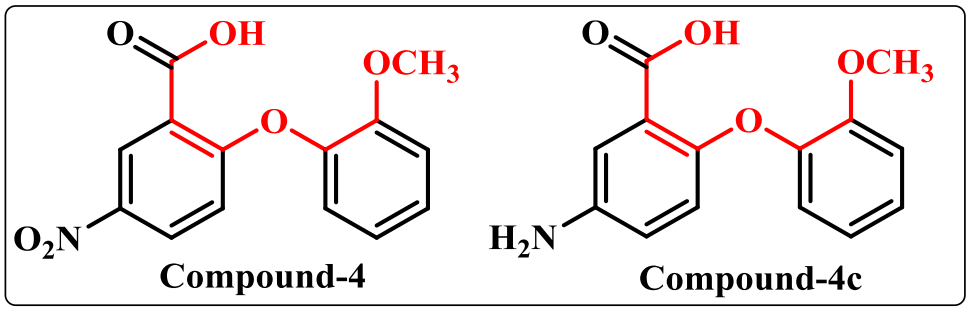

Figure-3.3: The structures of compounds **4** and **4c** include the necessary functionality to create charge holes between the functional group at the ortho position of each phenyl ring and the ether linkage.

Based on the literature, the carboxylic acid derivatives of the above compounds were synthesized as discussed in **chapter-2** to afford compounds **4** and **4c**. Both the compounds showed solubility in 99% aqueous media when dissolved from a stock of ACN having respective λ_{max} at 302, 341nm. In the preliminary studies, compound-**4** displayed an affinity for the Hg^{2+} and Pb^{2+} ions and compound-**4c** for Pb^{2+} ions when evaluated for 0.1mM concentration of the nitrate salts for K^{+}, Ca^{2+}, Mg^{2+}, Mn^{2+}, Fe^{2+}, Co^{2+}, Ni^{2+}, Cu^{2+}, Zn^{2+}, Cd^{2+}, Hg^{2+}, Pb^{2+} and Ag^{+} ions (**Figure-3.4)**.

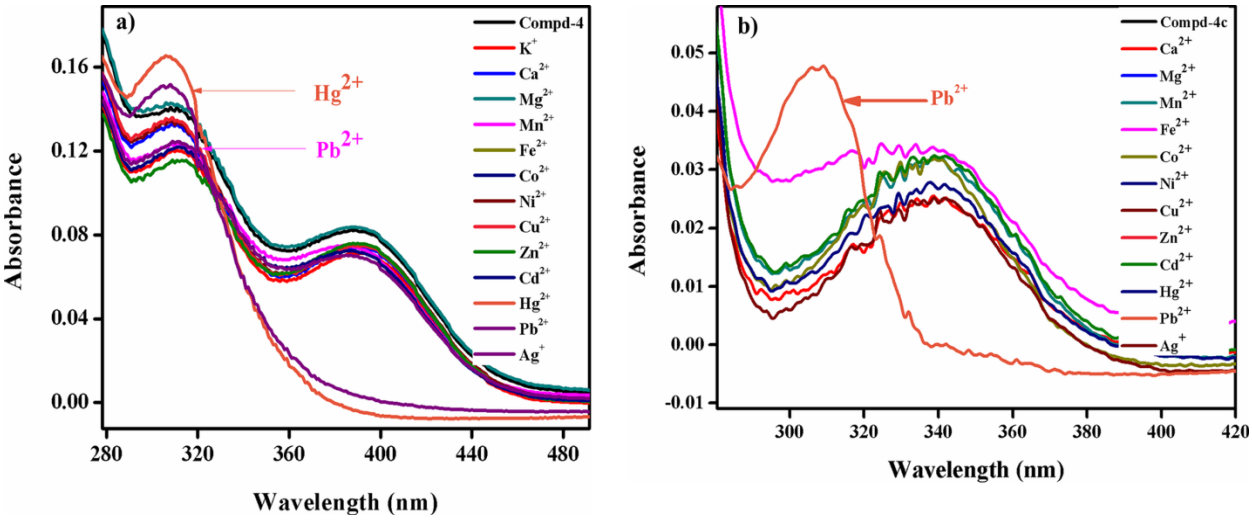

Figure-3.4: Absorption spectra of compound-**4** and **4c** with nitrate salts of various metal ions in 99% aqueous ACN medium.

3.3. Solvochromic Effect

The two compounds required exploration in different solvents and pH conditions to understand and optimize the behavior of metal ions. Native compound-**4** showed an absorption band at 307 nm due to π-π^{*} transition **[Figure-3.5 (a)]** that upon reduction to the

corresponding amino group in compound-**4c,** displayed a redshift to 341 nm **[Figure-3.5 (b)]**. It can be attributed replacement of the electron-withdrawing nitro group with an electron-rich amino moiety.

Figure-3.5 shows absorption spectra for compounds **4** and **4c** in different solvents (MeOH, H_2O, ACN, DCM, DMSO, THF). Compound-**4** showed an insignificant change in its UV specta except in the case of water and DMSO, where a red shift for peaks at 276 and 303 nm, a new peak was observed in at 404 (water) and at 425 nm (DMSO). It can be ascribed to n-π^* transition due to the ionization of the carboxylic acid group in water and polarization due to DMSO. Compound-**4c** did not show change its spectra in any solvents compared to ACN.

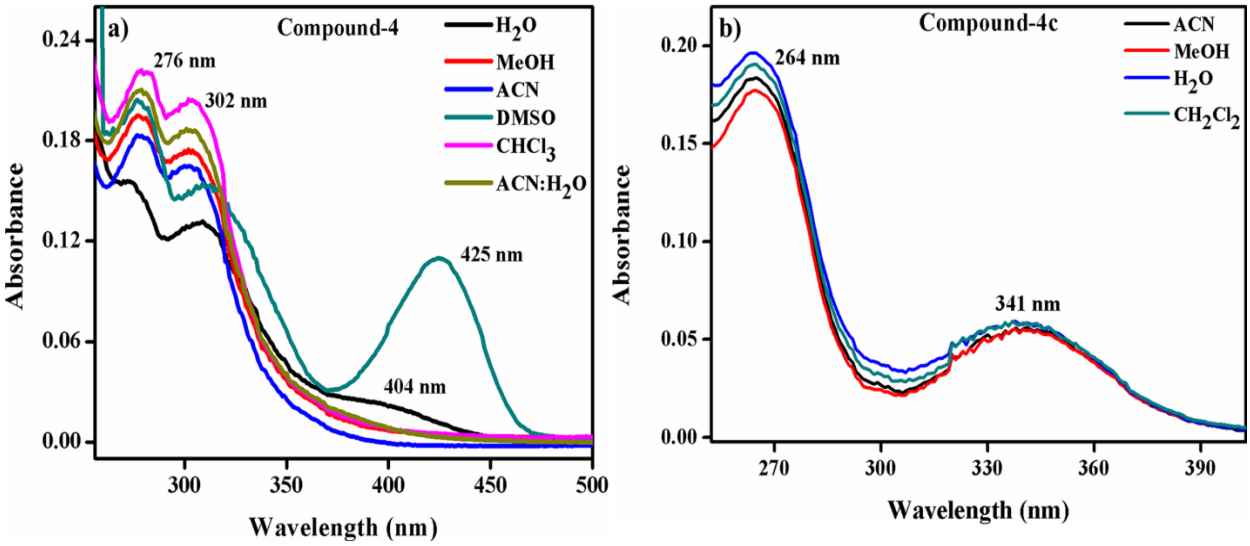

Figure-3.5: Effect of solvents on the absorption peaks of **a)** compound-**4,** where new band was observed at 404 and 425 nm in H_2O and DMSO solvent system and **b)** compound-**4c,** shows similar absorption band at 341 nm with all the solvents .

3.4. pH Effect

It is known that the solubility of metal ions is affected by changes in pH.[16] It was therefore mandatory to determine the operating pH range for compounds **4** and **4c** alone and with the Hg^{2+} and Pb^{2+} ions. **Figure-3.6 (a)** shows a new peak in the basic pH range with a hyperchromic effect as it increased from 8 to 10 for compound-**4.** Compound-**4c** also indicates a significant change in the basic pH range, with a new peak at 341 nm that shows a change with increased pH **[Figure-3.6 (b)]**. The changes in the basic pH can be reasoned with the formation of carboxylate ions. It was confirmed by observing UV-Visible spectra in an acidic medium (pH=4) that displayed spectra similar to that of the native compound.

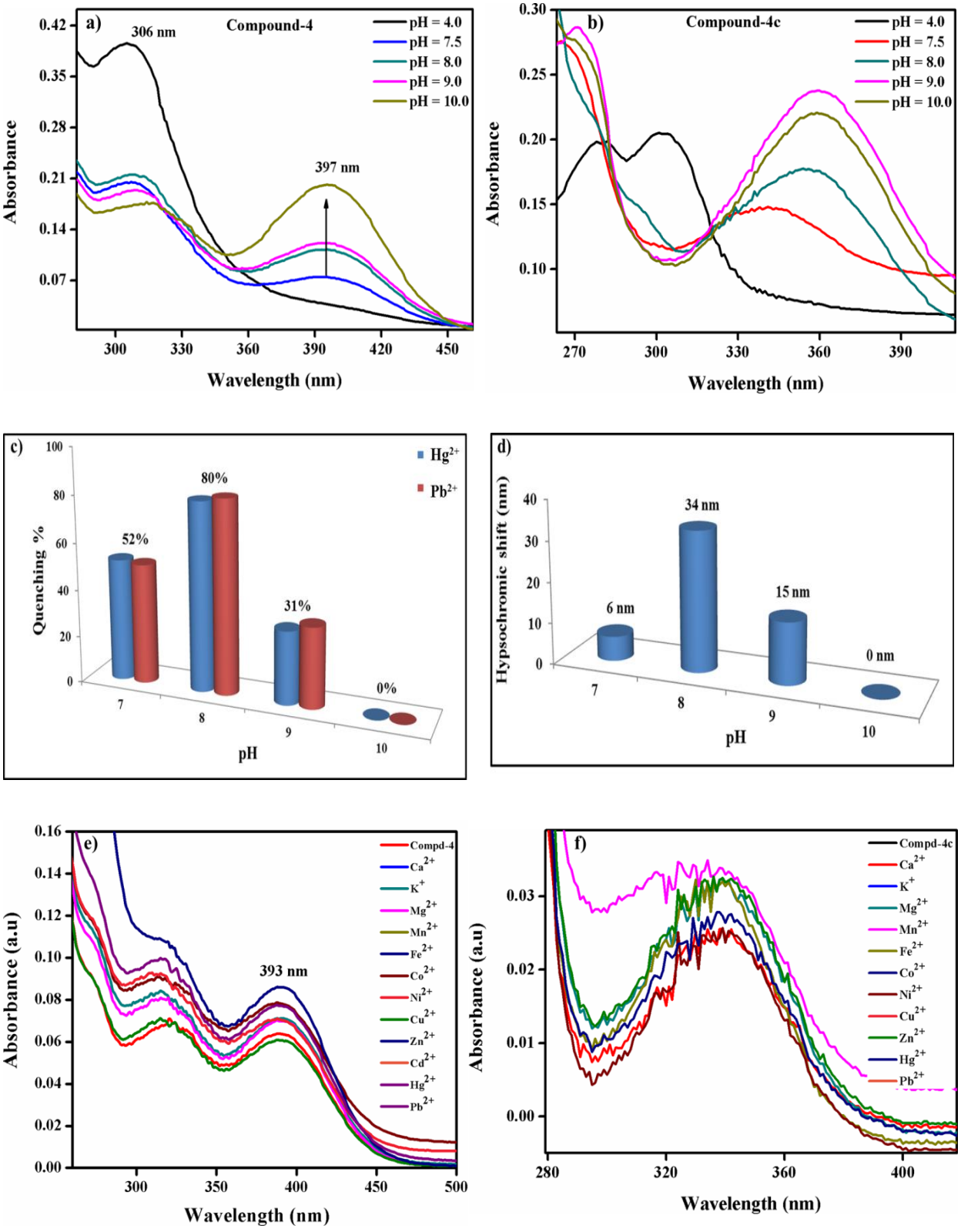

Figure-3.6: (a & b) Displayed the absorption property of compounds **4** and **4c** at different pH values. **(c & d)**Bar chart reprentation of compounds **4** and **4c** having maximum response value when selective metal ions added at the specific pH value. (**e & f)** showng the negligible absorption change even the presence of Hg^{2+} and Pb^{2+} ions using buffers solution.

The working pH for effectively detecting compound-**4**-**Hg^{2+}**/**Pb^{2+}** and compound-**4c**-**Pb^{2+}** systems was optimized using a range of 7 to 10. The bar chart in **Figure-3.6** shows that a pH range of 7.0-9.0 has an adequate response for both systems. At pH=10 and above, the system's response was negligible due to the formation of mercury and lead hydroxides, as reported in the literature.[16] In this case, a hazy solution also confirmed the formation of insoluble metal hydroxides that displayed a tendency to precipitate. Further studies for compounds **4** and **4c** used a 99% aqueous medium in the pH range of 8.0 to 8.5.

The use of buffers is recommended for the consistent detection of cations. Therefore, different buffers in the basic pH range were explored to observe cations, including Hg^{2+} and Pb^{2+}. As shown in **Figure-3.6 (e** & **f),** no change in the absorption properties of the compound**-4** and **4c** was visible in any buffer. Therefore, the desired pH range was achieved using sodium hydroxide solution in 99 % aqueous medium.

3.5. Spectroscopic studies

Addition of cations (nitrate salts of Ca^{2+}, Mg^{2+}, Mn^{2+}, Fe^{2+}, Co^{2+}, Ni^{2+}, Cu^{2+}, Zn^{2+} , Hg^{2+}, Pb^{2+}, K^{+}, Ag^{+}) in 20 μM of compounds **4** at pH-8 displayed quenching of peak (397 nm) only for Hg^{2+} and Pb^{2+} ions. Changes in the absorption properties of compound **4c** were observed only for the Pb^{2+} cations where a new peak at 302 nm replaced the native peak at 341 nm. No interference was observed for any other cation, while compounds **4** and **4c** selectively detected Hg^{2+} and Pb^{2+} as shown in **Figure-3.7**. Even a ten times excess of the other cation did not change the selectivity of both compounds.

3.5.1. Titration Studies

Successive additions of the Hg^{2+}/ Pb^{2+} ions in a 20 μM solution of compounds **4** and **4c** in each case gave the detection limit. **Figure-3.8 (a)** shows the gradual quenching of the absorption peak for compound-**4** on the sequential addition of Hg^{2+} ions at 397 nm with an isosbestic point at 335 nm. Pb^{2+} ions also gave similar results **Figure-3.8 (c)** with an isosbestic point at 328 nm. Hg^{2+} ions showed no further quenching beyond 20 μM addition, while for Pb^{2+} ions, it extended up to 22 μM, displaying a higher detection limit. The graph between concentration and absorbance gave minimum detection limits of 0.2 μM and 28 μM for Hg^{2+} and Pb^{2+} ions, respectively **Figure-3.8 (b** and **d)**. The use of the IUPAC-approved equation **3σ/k** gave the above results.

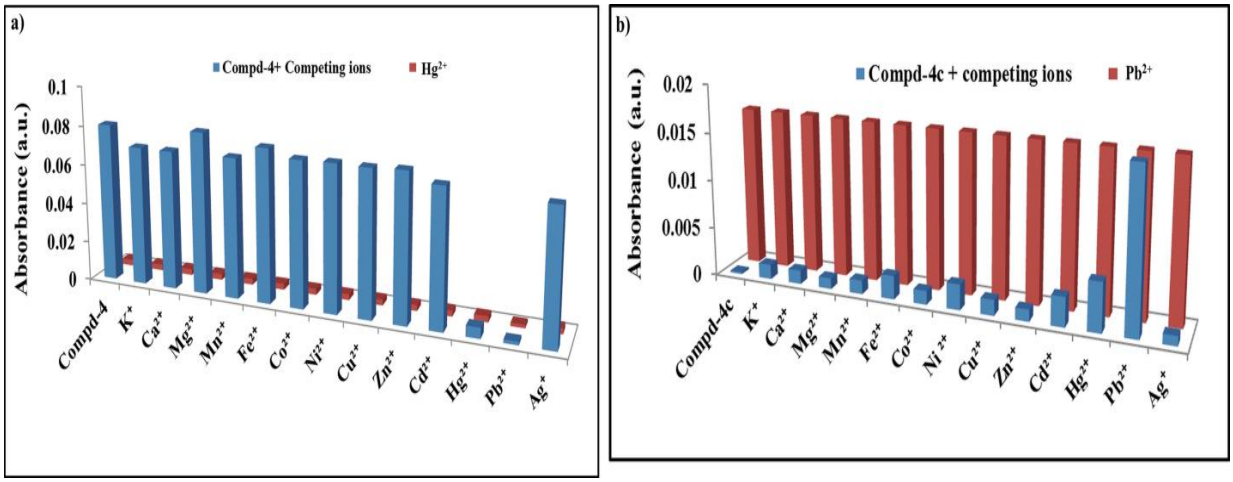

Figure 3.7: Interference studies of the complexes **a)** compound-**4**-Hg^{2+} and **b)** compound-**4c**-Pb^{2+} with various competing ions.

Compound-**4c** also displayed absorbance saturation after the sequential addition of Pb^{2+} ions at 20 μM, having calculated lower limit detection as 1.3 μM **[Figure-3.8 (e & f)].**

3.5.2. Association Constant

Benesi-Hildebrand equations gave stability to the complexes by plotting the reciprocals of difference in absorbance ($1/\Delta A$) and concentration ($1/ [M^{2+}]$). The binding constant for compound-**4**-Hg^{2+} and compound-**4**-Pb^{2+} systems were 0.3×10^5 M^{-1} and 5.3×10^5 $M^{-1,}$ respectively [**Figure-3.9 (a** and **c)]**. Compound-**4c**-Pb^{2+} system gave the constant binding value as 2.5×10^4 M^{-1} **[Figure-3.9 (e)]**. An analysis of the results indicates that Pb^{2+} captured compound-**4** seventeen times more strongly than Hg^{2+} ions. It can be attributed to a higher nuclear charge density for Pb^{2+} ions than Hg^{2+} ions. Compound-**4c**, selective for only Pb^{2+} ions, displayed twenty-one times lower binding capability than its parent compound-**4**. When compared to the literature, compound-**4** and compound-**4c**'s shows comparable binding results, those exhibit 1:1 stiochimetry in **Table-3.1**. Theoretical studies, described later, complimented the above results.

3.5.3. Stoichiometry

Stoichiometry was determined by adding 0.1 to 1.0 equivalents of each metal ion to receptors **4** and **4c** separately, maintaining a total concentration of 20 μM. The above experiment when plotted for change in the absorbance (ΔA) against the mole fraction (Job's Plot), gave maxima at 0.5 equivalents, **[Figure-3.9 (b, d** and **f)]** indicating a stoichiometry of 1: 1 for the metal ions and their corresponding receptors.

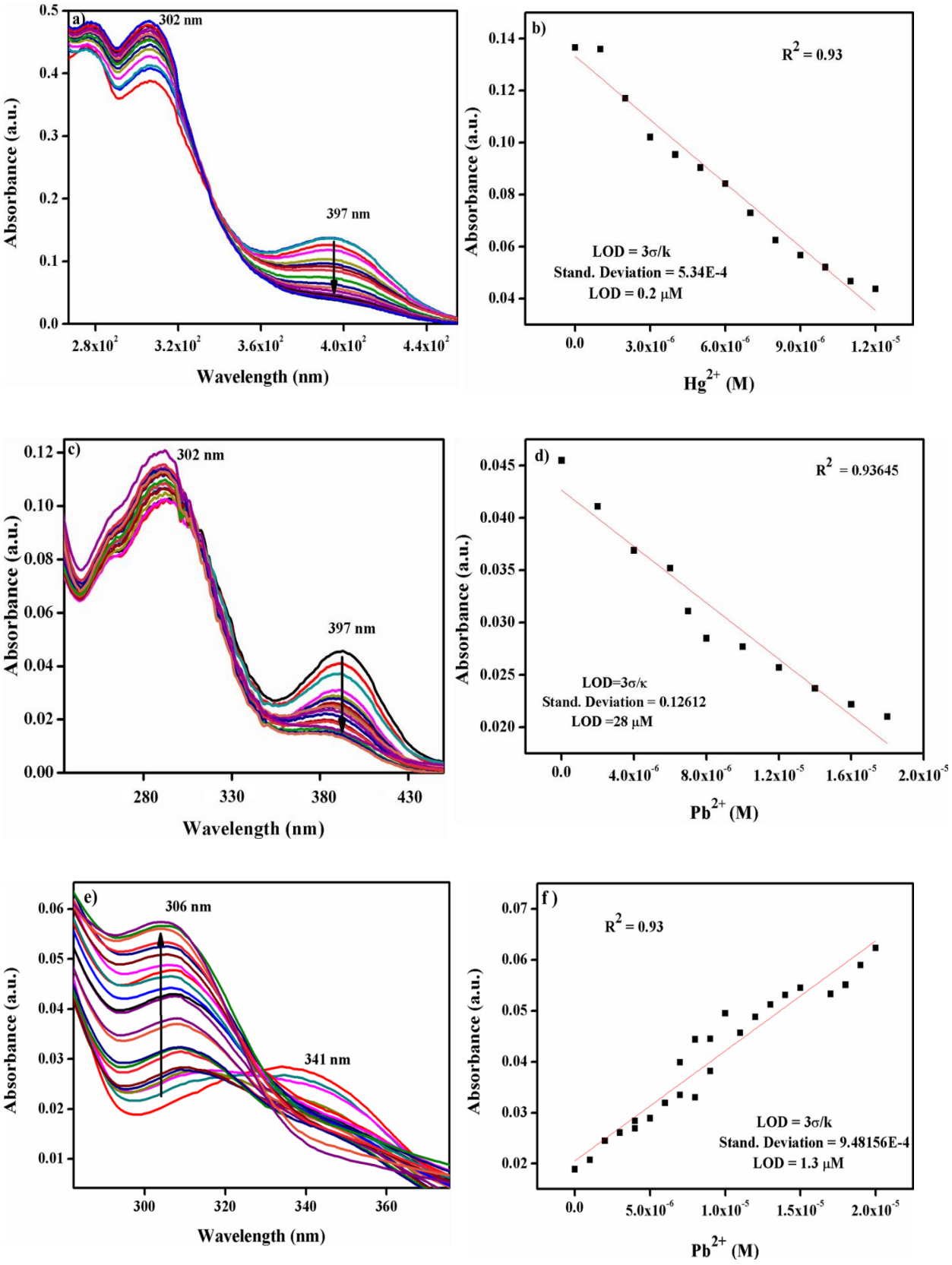

Figure-3.8: Titration spectrum's of compound-**4** and **4c** and their linear plots to quantify the minimum detection limit with the respective metal ions **(a** & **b)** Compound-**4** with Hg^{2+}, **(c** & **d)** Compound-**4** with Pb^{2+} and **(e** & **f)** for Compound-**4c** with Pb^{2+} ions.

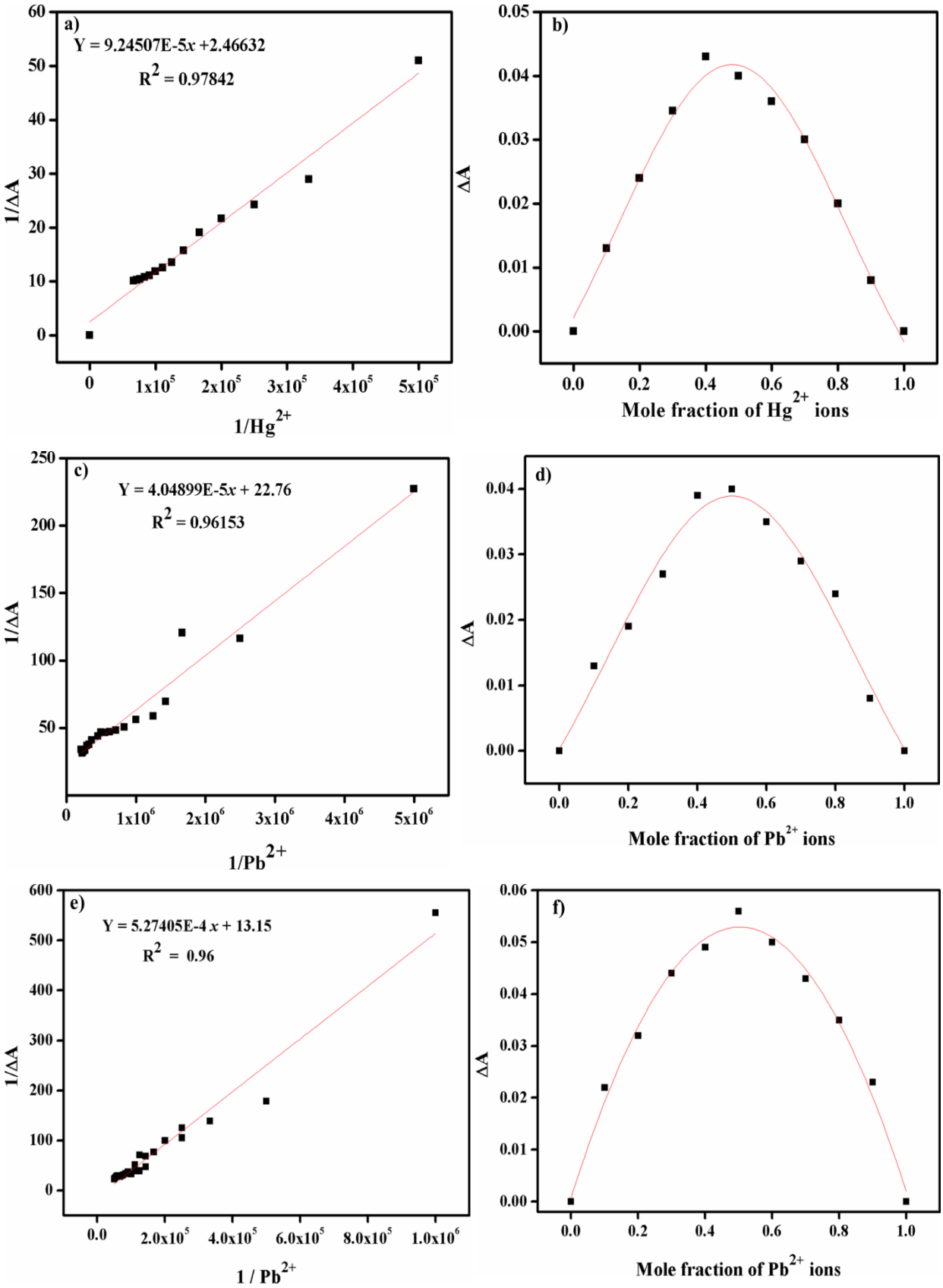

Figure-3.9: Benesi-Hildbrand and job plot's for all the complexes of the compounds **4** and **4c** to identify the binding constant and their stiochiometry **a)** compound-**4**-Hg^{2+}, **b)** compound-**4**-Pb^{2+} and **c)** compound-**4c**-Pb^{2+}.

Overall, of the five synthesized compounds, only two compounds **4** and **4c** displayed the potential due to their 99% aqueous solubility and ability to detect Hg^{2+} and Pb^{2+} ions. Compound **4c** selectivity detected Pb^{2+} ions. This study's only limitation is its inability to respond in the buffer solution despite effectively responding in the pH range of 7.5 to 9.0. The minimum detection limit and the binding constant were 0.2 μM and 0.3 × 10^5 M^{-1} for compound-**4-Hg^{2+}**, 28 μM and 5.2 × 10^5 M^{-1} for compound-**4-Pb^{2+}** and 1.3 μM and 2.5 × 10^4 M^{-1} for compound-**4c-Pb^{2+}** systems.

3.6. Theoretical studies

The computational calculations reasonably estimate the molecules' electron density and their possible interaction with the ions. It is also advantageous in predicting the receptor's stability and frontier molecular orbitals and its complex.[17] Therefore, Gaussian-16 software with the B3LYP method was used for the theoretical calculations in the gas phase. The basis sets were 6-31+g and LANL2MB for the organic molecules and the transition metal ions, respectively.

The optimized conformations of compound-**4** and **4c** *insilico* interacted with Hg^{2+} and Pb^{2+} ions to give the possible interaction site as shown in **Figure-3.10**. Compound-**4** interacted with Hg^{2+} ions using carboxylate group and methoxy ether oxygen, and the Pb^{2+} ion required additional ethereal oxygen to interact. It can be attributed to the latter's small size compared to $Hg^{2+,}$ which facilitated deep penetration in the cavity and further interaction. As discussed above, the seventeen times higher binding constant value for the Pb^{2+} ions (5.3 x10^5 M^{-1}) compared to Hg^{2+} ions (0.3 x10^5 M^{-1}) corroborated with the theoretical studies.

Compound-**4c** selectively interacted with Pb^{2+} ions using two oxygens of the carboxylate group without any contribution from oxygens of its ethers. The carboxylate group's placement away from ethers did not constitute a cavity in this case, as shown in **Figure 3.10 (d)**. Compound-**4**, on the other hand, had a carboxylate group placed appropriately to form the cavity. These results explained the twenty-two times the lower value of the binding constant for the compound-**4c-Pb^{2+}** system compared to the compound-**4c-Pb^{2+}** system.

Calculating the energy difference ($\Delta E_{HOMO\text{-}LUMO}$) for the anionic form of compounds displayed a lowering energy difference upon interaction with the metal ion **(Table-3.2).** It can be attributed to the increased interaction of the metal ions with respective compounds.

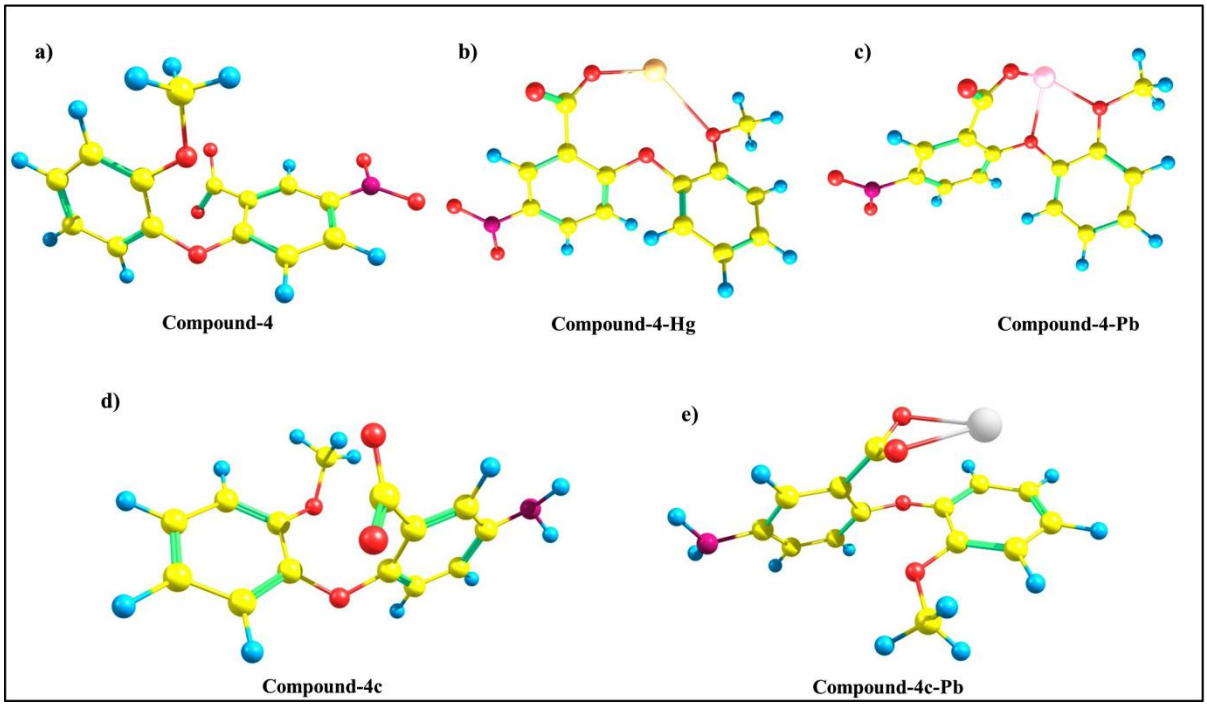

Figure-3.10: Optimized structure using method B3LYP and a basiss set 6-31+g and LANL2MB using Gaussian-16 for **a)** compound-**4**, **b)** compound-**4-Hg**$^{2+}$ **c)** compound-**4-Pb**$^{2+}$, **d)** compound-**4c** and **e)** compound-**4c-Pb**$^{2+}$.

Table-3.2: Representing the energy difference's between HOMO and LUMO orbitals for compounds, **4** and **4c** or with its metal complexes to observe the effective transition between them.

S.No	**Compound**	**Anions - $\Delta E_{HOMO-LUMO}$ kcal/mol**	**$\Delta E_{HOMO-LUMO}$ for complexes (kcal/mol)**		**Difference in ΔE**
1	4	84.28	Hg^{2+}	64.96	19.32
2			Pb^{2+}	76.21	8.07
3	4c	97.19	Pb^{2+}	42.23	54.96

The above theoretical calculations satisfactorily corroborated with the experimental results. However, the predicted interaction of Pb^{2+} with compound-**4c** appeared unfamiliar. Exploration of the literature gave evidence that partially supported the above results. Burt *et al.* have calculated the interaction of Pb^{2+} with deprotonated amino acids in many ways, including the one in this study, as shown in **Figure-3.11 (z)**. The group predicted a similar collaboration between Pb^{2+} ion and amino acids Ala, Val, Leu, Ile, and Pro, validating the theoretical results presented in this work. Lys, the amino acid with NH_2 side chain, also

displayed similar interaction with the metal ion,[18] partially matching our experimental studies on amino acid compound-**4c**.

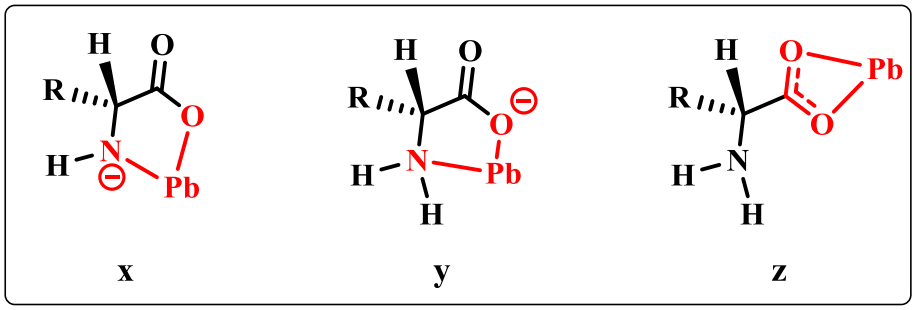

Figure-3.11: Brut et. al. representation of possible interaction of Pb^{2+} ion with different amino acids.

3.7. Conclusion

To conclude,compound-**4** displayed an ability to detect Hg^{2+}, Pb^{2+} ions, and compound **4c** for Pb^{2+} ions selectivity in a 99% aqueous medium. Theoretical calculations collaborated for the predicted site of interaction and the binding constant. The limitation of the molecules to respond only in pH range 7.5 to 9.0 prevented their more comprehensive application for real-life sampling. However, based on the results of pH, solvent and computational studies, the work adds value to the interaction mechanism.

Nonetheless, the work required further improving the working pH range while maintaining same aqueous solubility. Established literature suggests the unique interaction of mercury ions for the thio compounds. It was therefore envisaged to improve the performance of diphenyl ethers for the selective detection of the toxic metal ions by synthesizing their thio derivatives. The next part of the work deals with the studies on thiocarbazole product of diphenyl ether.

References

1. Hollenstein, M.; Hipolito, C.; Lam, C.; Dietrich, D.; Perrin, D. M., *Angew. Chem.* **2008,** *120*, 4418-4422.
2. Zalmi, G. A.; Gawade, V. K.; Nadimetla, D. N.; Bhosale, S. V., *ChemistryOpen* **2021,** *10*, 681-696.
3. Panthi, G.; Park, M., *J.Haz. Mat.* **2022,** *424*, 127565.
4. Megharaj, M., Point Source Pollution. *Encycl. Soil Sci.***2006,** 11, 1324.
5. Das, S.; Raj, R.; Mangwani, N.; Dash, H. R.; Chakraborty, J., *Microbial biodegradation and bioremediation* **2014**, *6*, 23-54.
6. Martinez-Finley, E. J.; Caito, S.; Fretham, S.; Chen, P.; Aschner, M., *Mammalian toxicology* **2015**, *15*, 171-185.
7. F. Edition, Guidelines for drinking-water quality. *WHO chron.***2011**, 38, 104-108.
8. Rawat, K. A.; Bhamore, J. R.; Singhal, R. K.; Kailasa, S. K., *Biosen. Bioelect.* **2017,** *88*, 71-77.
9. McDonagh, C.; Burke, C. S.; MacCraith, B. D., *Chem. Rev.* **2008,** *108*, 400-422.
10. Ma, L.; Li, H.; Wu, Y., *Sens. Actu. B Chem.* **2009**, *143*, 25-29.
11. Zhou, B.; Qin, S.; Chen, B.; Han, Y., *Tetrahedron Letters* **2018**, *59*, 4359-4363.
12. Emandi, G.; Flanagan, K. J.; Senge, M. O., *Photochem. Photobiol. Sci.* **2018,** *17*, 1450-1461.
13. Bahta, M.; Ahmed, N., *J. Photochem. and Photobiol. A Chem.***2019**, *378*, 85-93.
14. Das, S.; Sarkar, A.; Rakshit, A.; Datta, A., *Inorg. Chem.***2018**, *57*, 5273-5281.
15. Liu, D.; Zhu, H.; Shi, J.; Deng, X.; Zhang, T.; Zhao, Y.; Qi, P.; Yang, G.; He, H., *Anal. Methods* **2019**, *11*, 3150-3154.
16. Dimitrova, S.; Mehandgiev, D., *Water Research* **1998**, *32*, 3289-3292.
17. Ziegler, T., *Chem. Rev.***1991**, *91*, 651-667.
18. Burt, M. B.; Decker, S. G.; Atkins, C. G.; *J. Phy. Chem. B* **2011**, *115*, 11506-11518.

Chapter-4

Graphical Abstract:

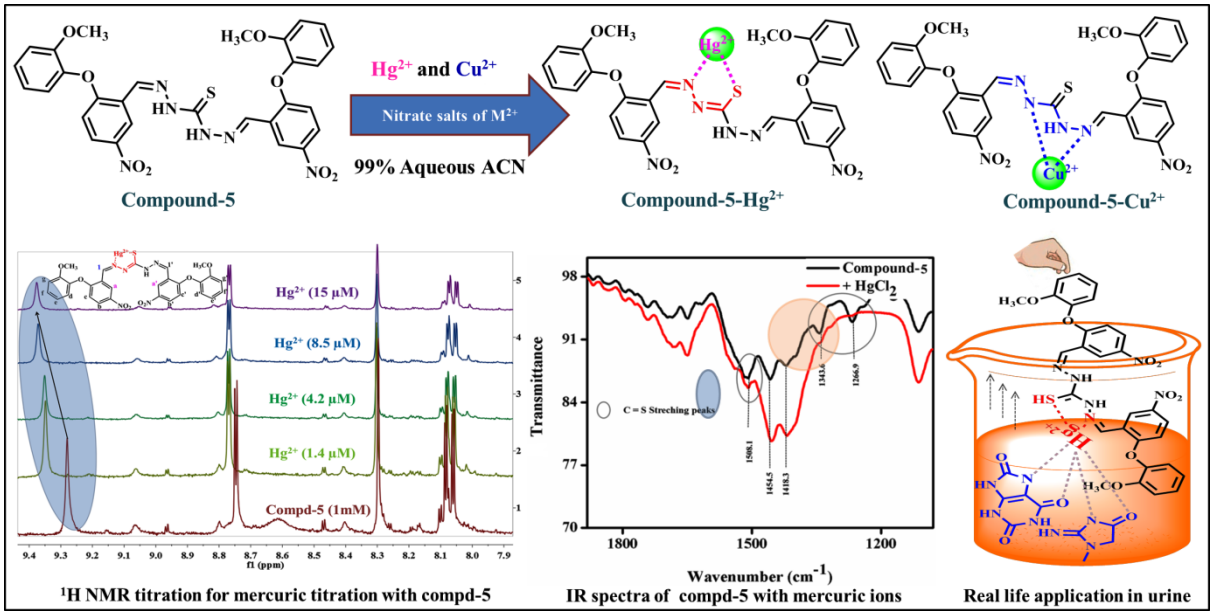

Chapter-4

REFINING THE DETECTION LIMIT OF N',2-BIS(-2-(2-METHOXYPHENOXY)-5-NITROBENZYLIDENE) HYDRAZINE-1-CARBOTHIOHYDRAZIDE (COMPOUNDD-5) FOR MERCURY IONS

4.1. Introduction

Mercury is an extraordinary heavy metal ion that contaminates water due to its presence in the environment by anthropogenic emissions.[1,2] Such hazardous ions ultimately bio-accumulate[3] in water bodies, sea food[4] and soil,[5] causing toxicity and Minamata disease[6]. This medical condition ultimately damages the endocrine glands and the central nervous system.[7-9]

Copper is one of the abundant essential elements in humans, but its concentration is crucial for many significant physiological processes.[10] The alteration of its concentration can cause neurodegenerative diseases like Alzheimer's,[11] Menkes[12] and Wilson.[13] The maximum permissible limit for copper in drinking water and food samples is 1.3 ppm (~20 M).[14] Identifying and quantifying both copper and mercury by convenient methods is therefore essential.

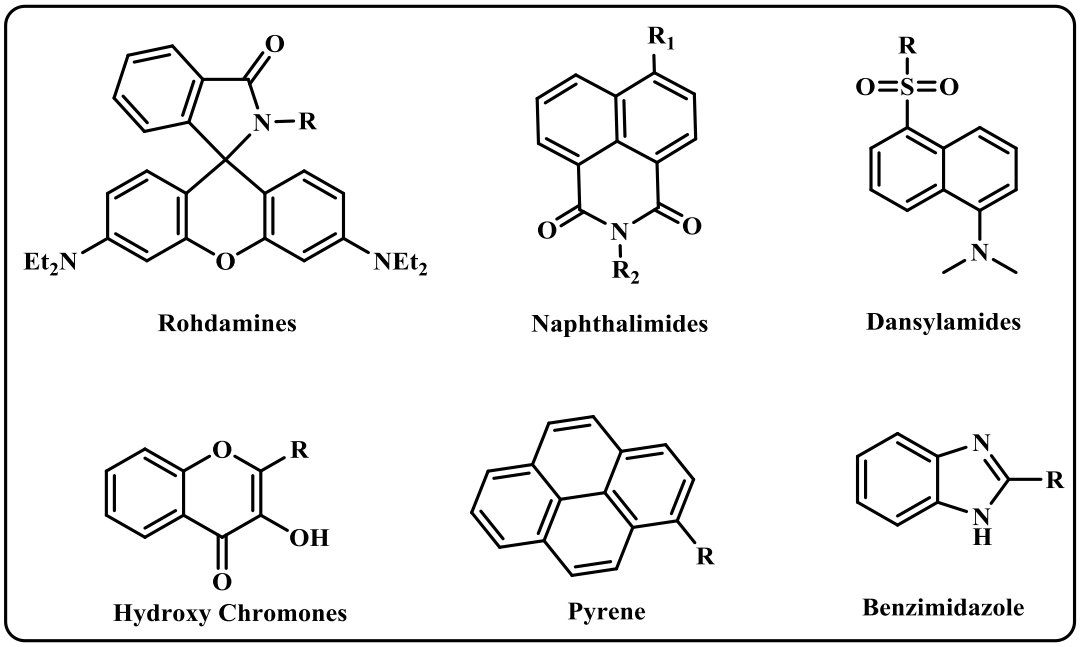

Figure-4.1: Structure of different groups used for sensing Hg^{2+} ions as reported in the literature.

The previous chapter describes the detection of Hg^{2+} and Pb^{2+} ions in an aqueous medium by compound-**4**. However, applying the work for real-life analysis was hard due to its alkaline

working range. The literature was explored to refine further the system for improvising metal ion detection and real-life application. The affinity of Hg^{2+} ions for sulphur-containing compounds is well known.

Table-4.1: Thio-containing organic receptors for metal ion sensing have been identified in the literature.

Receptors	Solvent system	Technique Used	Limit of detection (M)	Reference
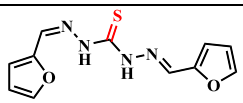	DMSO	UV-Visible	2.72 µM	15
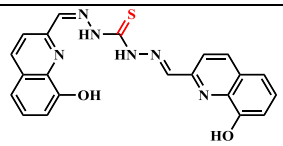	DMF	UV-Visible	0.7 µM	15
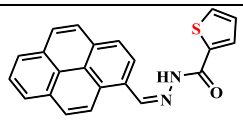	DMSO	UV-Visible and Fluorescence	0.2 µM	16
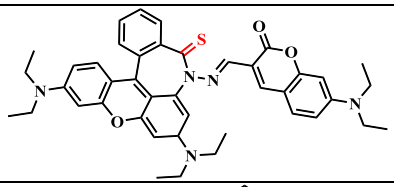	MeOH: H_2O (1:1 v/v)	UV-Visible and Fluorescence	40 nM	17
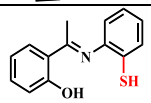	DMSO: H_2O (9.5:0.5 v/v)	UV-Visible	--	18
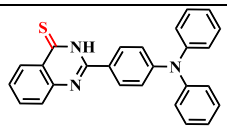	THF	Fluorescence	1.5 µM	19
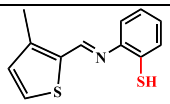	MeOH: H_2O (8:2 v/v)	Fluorescence	20 µM	20
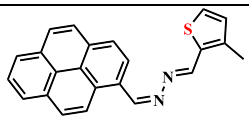	ACN: H_2O (1:1 v/v)	UV-Visible and Fluorescence	30.6 nM	21

Table 4.1 shows the use of organic compounds with thio groups for detecting different cations. The use of rhodamine,[22] naphthalimides,[23] dansylamides,[24] benzimidazole [25] and hydroxyl chromones [26] for sensing Hg^{2+} ions has also been reported (**Figure 4.1)**. These groups utilize the fluorescence advantage to enhance sensitivity and selectivity.

Encouraged by the results of compound-**4** (Previous Chapter) for detecting Hg^{2+} ions, this work preferred using non-fluorescent carbothiohydrazide based derivatives of diphenyl ether.

The work also demonstrates the use of the novel carbothiohydrazide based dimer to determine Hg^{2+} ions in real-life application.

4.2. Synthesis of the Receptor

The Schiff base of compound-**1** with dithiocarbohydrazide under refluxing conditions in a mixture of methanol and water gave compound-**5**, as described in **Chapter-2**. The new dimer molecule gave additional cavities besides the ones formed by native molecule while maintaining the hydrophilicity of its precursor **(Figure-4.2).** According to the HSAB principle, the sulphur-a soft base was preferentially expected to interact with mercury.

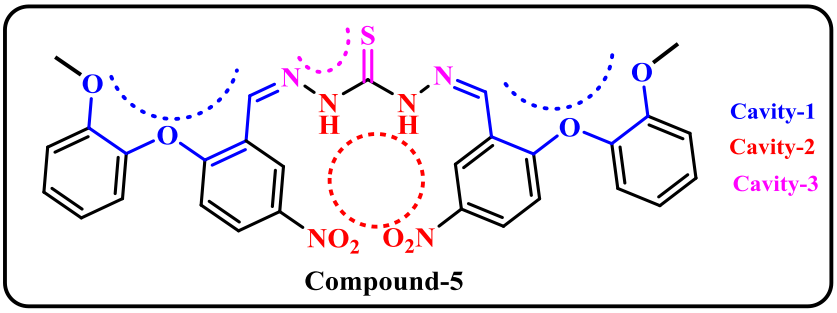

Figure-4.2: Structure of thiocabahydrazide derivative of diphenyl ether. The new dimer molecule gave additional cavity beside the ones formed by the diphenyl ether molecule.

4.3. Spectroscopic Studies

Using a UV-visible spectrophotometer, the photophysical properties of compound-**5** were investigated in a 99% aqueous ACN solution. A 10 µM solution gave an absorption peak at 316 nm (λ_{max}), suggesting π to π* electronic transition due to high absorption intensity **(Figure-4.3a)**. The compound gave no change in absorption properties for any of the anions using respective tert-butyl ammonium salts (CN^-, F^-, Cl^-, I^-, HSO_4^-, HPO_4^-, ClO_4^- and CH_3COO^-).

However, for the cations (nitrates salts of K^+, Ca^{2+}, Mg^{2+}, Mn^{2+}, Fe^{2+}, Co^{2+}, Ni^{2+}, Cu^{2+}, Zn^{2+}, Hg^{2+} and Pb^{2+}), quenching of maxima at 316 nm was observed only for Hg^{2+} and Cu^{2+} in a 10 µM aqueous solution using 3mM HEPES buffer **[Figure-4.3 (a)]**. Mercury nitrate required dissolution in an acidic medium to make an aqueous solution. Therefore the quenching with Hg^{2+} ions required further verification using another counter ion. The use of mercury chloride salt gave no change in Hg^{2+} ions quenching, indicating consistent results with either of the counter ions **[Figure-4.3 (b)]**.

Further, **Figure-4.3 (a)** shows that quenching by Hg^{2+} accompanied a blue shift of 20 nm while for Cu^{2+} ions, there was no significant shift. Interference due to other competing ions having a 10 times excess was not observed as shown in **Figure-4.3 (c)**.

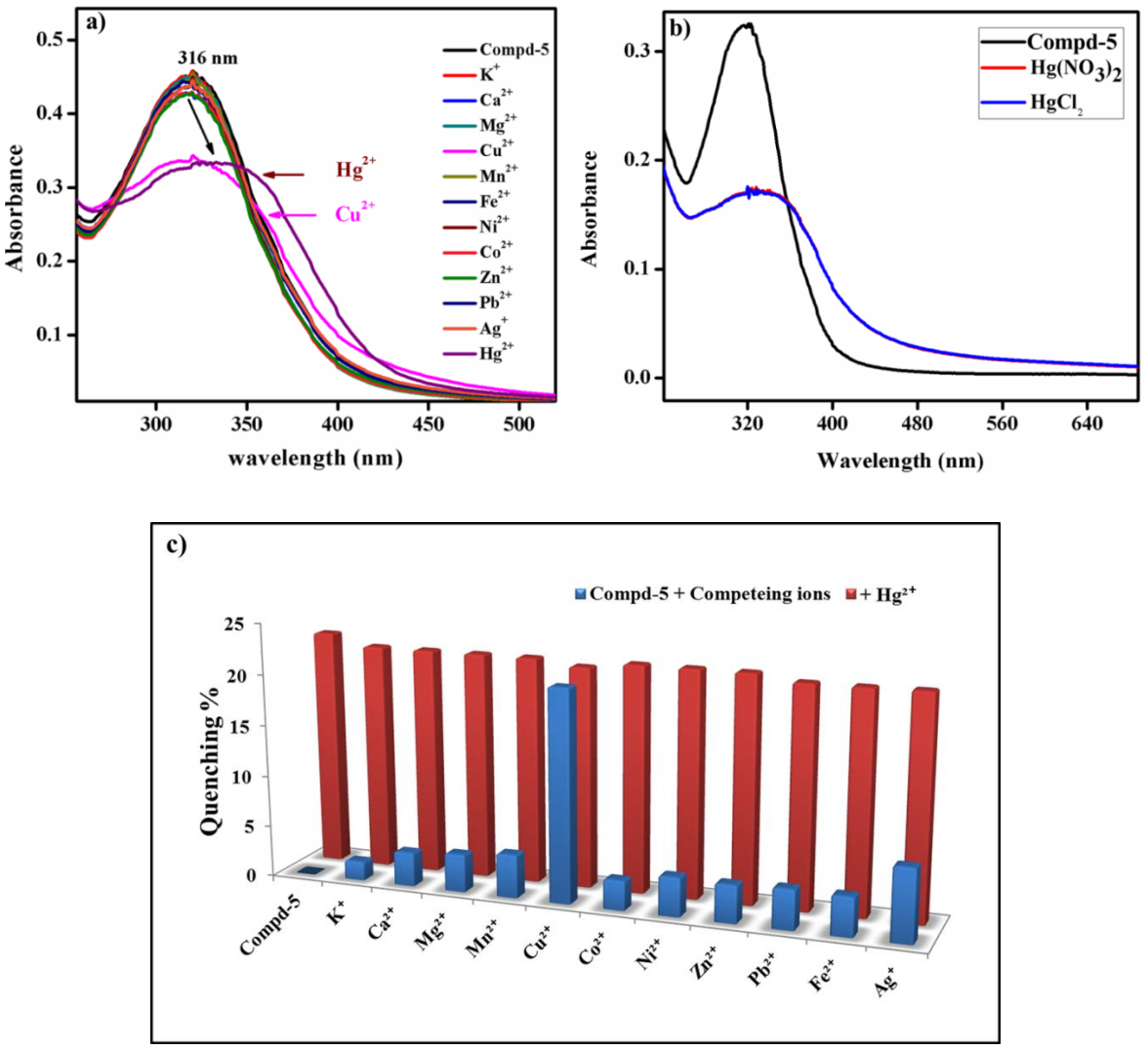

Figure-4.3: (a) Absorption spectrum of Compound **-5** with nitrate salt of various metal ions in aqueous HEPES buffer (3mM) /acetonitrile (99:1, v/v). **(b)** Quenching of compound-**5** with nitrate and chloride salts of Hg^{2+} was same in UV-Visible spectra. **(c)** Interference studies of compound-**5** for Hg^{2+} in the presence of different competing ions calculated using quenching percentage.

4.4. Titration Studies

The minimum detection limit and binding constant were determined using the titration of compound-**5** with Hg^{2+} and Cu^{2+} ions separately. Sequential additions of the ions were carried out in 99% aqueous ACN solution of compound-**5** (10 μM) until a plateau was observed for both Hg^{2+} and Cu^{2+} ions, as shown in **Figure 4.4 (a & b),** respectively. Thus, a minimum detection limit was calculated as 27 nM and 160 nM for Hg^{2+} and Cu^{2+} ions, respectively, using 3σ/K expressions **Figure-4.4 (c & d)**. Using the Benesi Hildebrand equation, the association constant of Cu^{2+} or Hg^{2+} ions with compound-**5** was found to be 9.1×10^{5} M^{-1} and 1.2×10^{5} $M^{-1,}$ respectively **[Figure-4.4 (e & f)]**. These results revealed that the binding of Cu^{2+} ions with compound-**5** was seven times more than with Hg^{2+} ions.

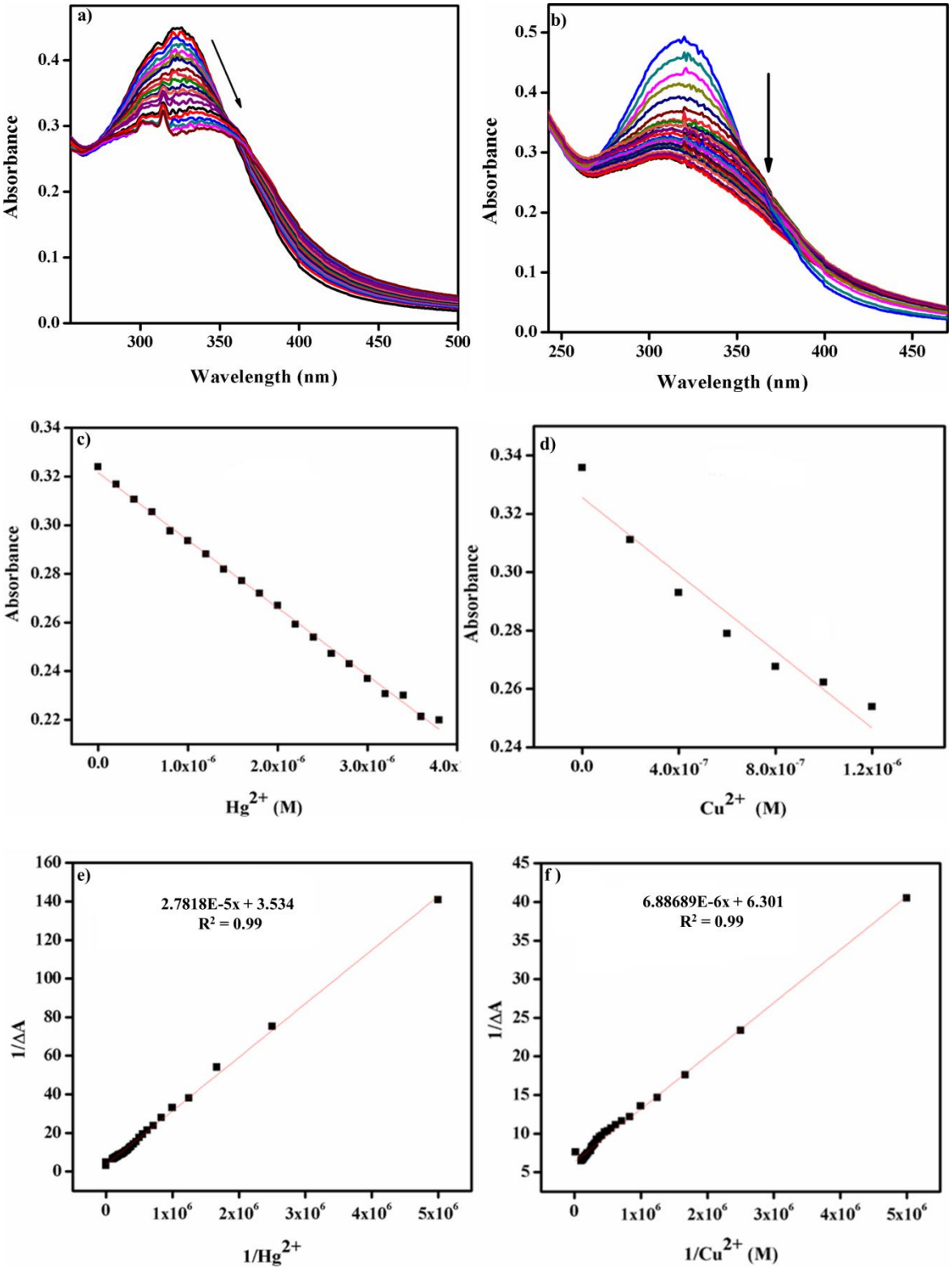

Figure-4.4: Titration spectra of compound-**5** (10 × 10^{-6} M) with **(a)** Hg^{2+} & **(b)** Cu^{2+} ions between the concentration 0.1 µM to 30 µM. **(c** & **d)** Linear graph plotted to calculate the detection limit for Hg^{2+} & Cu^{2+}. **(e** & **f)** Benesi Hildebrand linear plot for compound-**5** with different concentration of **(a)** Hg^{2+} and **(b)** Cu^{2+} ions.

Further, to determine the stoichiometric ratio, varying equivalents (0.1 to 0.9) of receptor (Compound-**5**) and ions (Cu^{2+} and Hg^{2+}) were added in the 99% aqueous ACN and observed

for a change in the absorption. The graphs in **Figure-4.5** show the plot between ΔA versus mole fraction for Cu^{2+} and Hg^{2+} ions separately. In both cases, maxima at 0.5 displayed 1: 1 stoichiometry **[Figure-4.5 (a & b)]**. The theoretical calculations in the following paragraphs (Section-4.7) complemented these results and the strong binding constant for Cu^{2+} ions compared to Hg^{2+} ions.

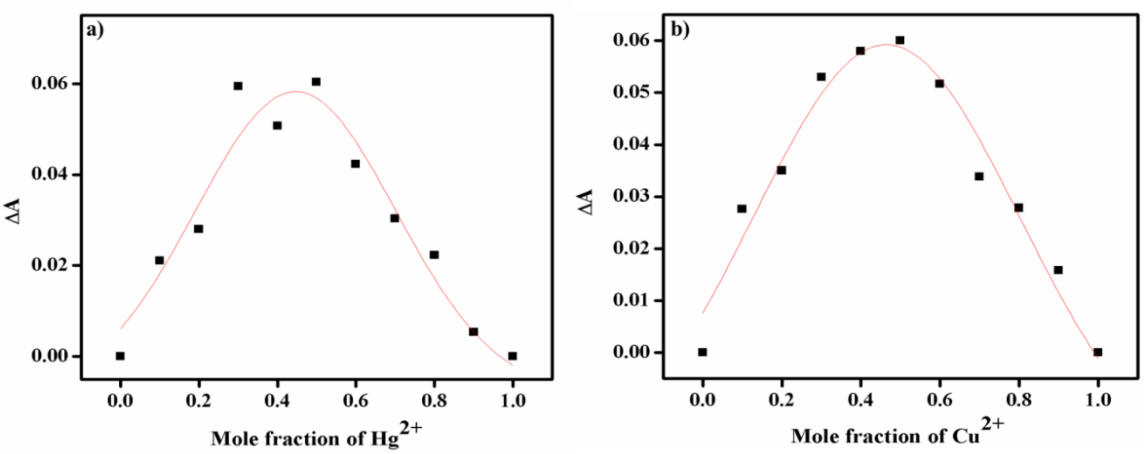

Figure 4.5: Job's plots for compound-**5** with (a) Hg^{2+} and (b) Cu^{2+} ions shows 1:1 stoichiometry.

4.5. NMR Titrations

It was possible to observe the interaction of Hg^{2+} ions with compound-**5** using NMR experiments. However, for the paramagentic Cu^{2+} ions, broad peaks did not yield conclusive results. ^{1}H NMR of compound-**5** displayed two signals at δ9.30 and δ8.31 ppm, corresponding to protons numbered 1 and 1', respectively **(Figure-4.7)**. Despite being symmetrical protons, a significant shift in the δ value is attributed to its helical structure as determined by the theoretical calculations. **Figure-4.6** shows that one of the two shielded protons appears at δ 8.31 ppm due to shielding by the nitro group as a result of special influence compared to other proton (δ 9.30 ppm) that orients itself outside the helix.

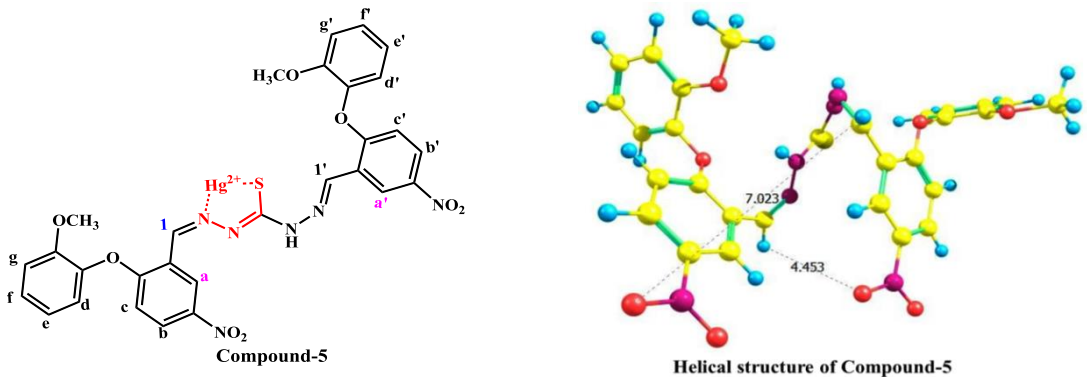

Figure-4.6: Optimized structure of Compound-**5**, showing the unsymmetrical Schiff base proton's 1 and 1'.

The step-wise addition of Hg^{2+} in 1mM of compound-**5** shifted the signal of proton appearing at δ9.30 ppm further downfield as shown in **Figure-4.7.** It was due to the influence of the cation's interaction with nitrogen of Schiff's base and sulphur of the thiocarbazole.

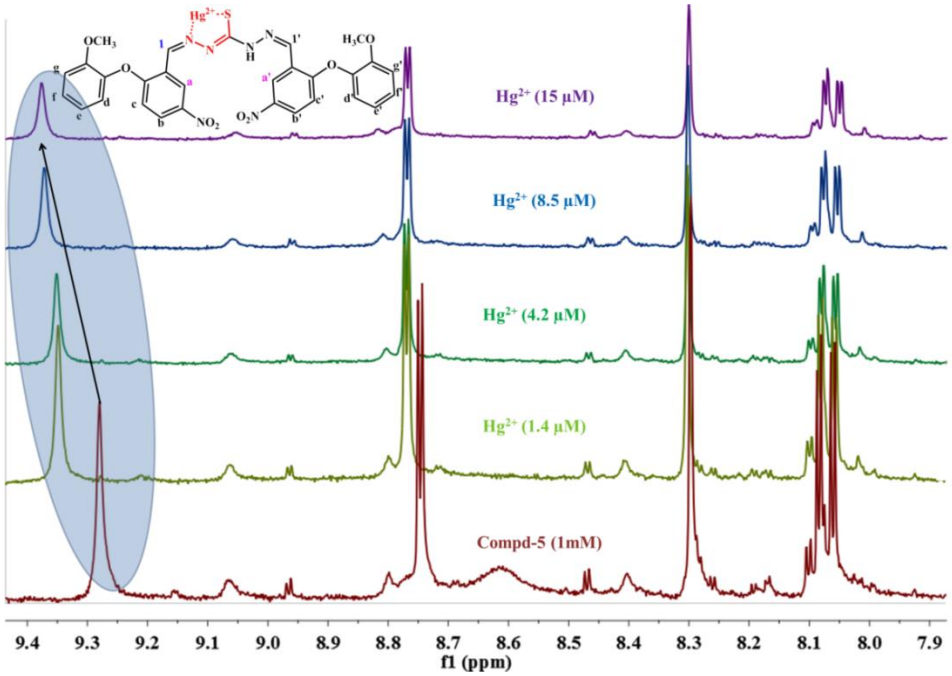

Figure-4.7: ^{1}H NMR titration spectra of compound-**5** (10^{-3}M) with different concentration of Hg^{2+} ions (1.4, 4.2, 8.5, 15µM) using $CDCl_3$.

The aromatic proton (a and a') also showed cascade effect of downfield shift for its position on addition of Hg^{2+} ions. However, no significant change was observed in their δ values for the other protons **(Figure-4.7)**. Above studies are in line with 1:1 stoichiometry of Job's plot and Gaussian calculations showing single binding site with thiocarbazole. ^{1}H NMR studies with compound-**5-Cu^{2+}** system gave inconclusive broadening of the peaks. The engagement of only one cation despite the presence of two cavities has been discussed with IR evidence in the next section.

4.6. IR Spectra

In order to further anaylze the interaction mechanism of Hg^{2+} ions with the receptor, IR spectrum for compound-**5** and compound-**5-Hg^{2+}** complex were compared.

The interaction specific peaks for compound-**5** appeared at $\nu_{(C=S)}$ 1508 cm^{-1}, 1344 cm^{-1} and 1267 cm^{-1} as shown in **Figure 4.8**. On addition of 1 equivalent of Hg^{2+} ions in compound-**5** the peaks due to **$R_2C=S$** stretch at 1344 cm^{-1} and 1267 cm^{-1} disappeared while one at 1508 cm^{-1} quenched. The disappearance of the carbon sulphur double bond peak confirmed the

formation of $\mathbf{R_2C\text{-}S\text{---}Hg^{2+}}$ complex formation. No change was observed in the other peaks appearing due to $\nu_{(C=N),}$ $\nu_{(N-H),}$ $\nu_{(C-H)}$ methoxy or imine groups.

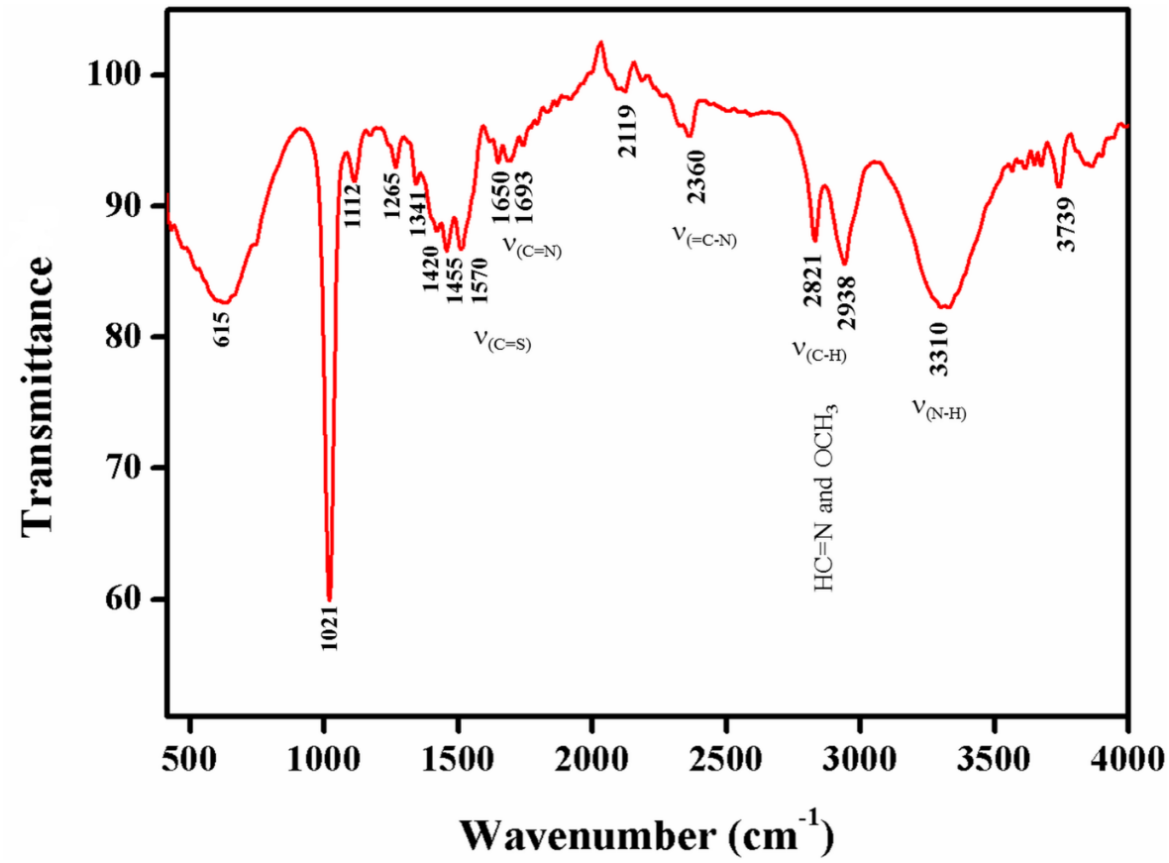

Figure-4.8: Confirmation of compound-**5** synthesis via appearing a stretching peaks due to $\nu_{C=O}$, $\nu_{C=N,}$ ν_{C-N}, ν_{C-H} and ν_{N-H} in IR spectra.

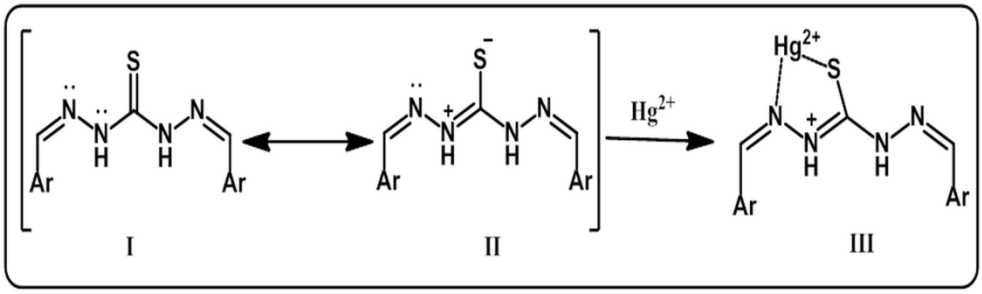

Scheme-4.1: Proposed mechanism of Hg^{2+} detection due formation of five membered ring with stable resonating thiolate ion of compound-**5**.[27]

Theoretical calculations, discussed in the next section, and the literature reports citing five membered Hg^{2+} containing cyclic rings **(III) Scheme- 1** having a resonating structure **(II)** with imine's thiolate ion [27] with nitrogen atom confirmed the proposed interactions.

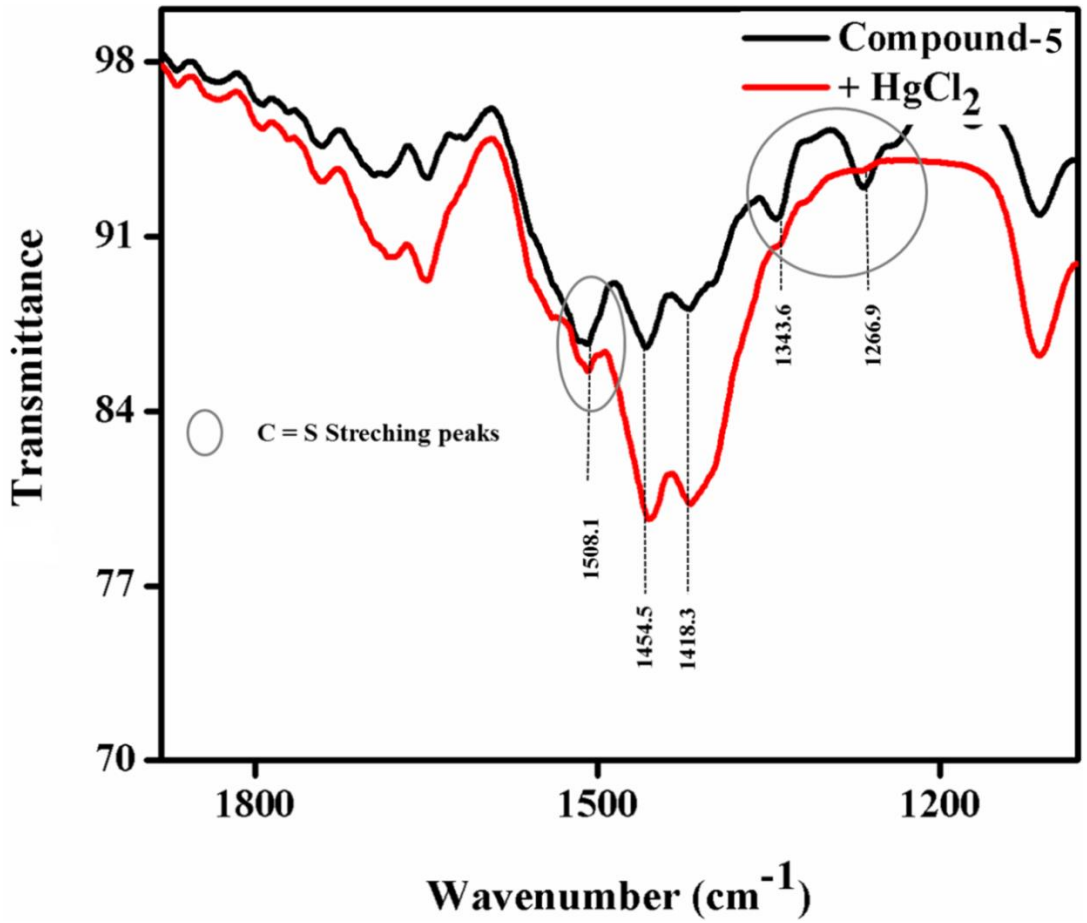

Figure-4.9: IR spectra of compound-**5** shows C=S stretching peaks at 1508 cm^{-1}, 1344 cm^{-1} and 1267 cm^{-1} **(Black)** was disappeared on the addition of Hg^{2+} ions.**(red).**

4.7. Theoretical Calculations

Theoretical studies of compound-**5** for its interaction with Hg^{2+} and Cu^{2+} ions using Gaussian 16.0 software were done using B3LYP (Becke 3 Lee-Yang and Parr) method.[28] Regular helical structure of compound-**5 [Figure-4.10 (a)]** after interacting with Hg^{2+} via central sulphur and nitrogen (N-2') of Schiff's base brings both A and A' aromatic rings in one plane where rings B and B' are perpendicular to the plane but in opposite directions **[Figure-4.10 (b)]**. The planarity of rings A and A' is attributed to hydrogen bonding interactions between NH-1 and NH-1' with corresponding ethereal oxygen of diphenyl ethers. However as shown in **Figure-4.10 (c)**, Cu^{2+} interacts with N-1 nitrogen on one side and N-2' nitrogen of Schiff base on the other side to partially disrupt the helical structure of compound-**5**. The results obtained here are in line with the Job's plot calculations for the 1:1 stoichiometry.

Red shift in the UV-Vis spectra for compound-**5-Hg^{2+}** system from 316 nm to 342nm is attributed to conformational change of compound-**5** from helical to the planar structure. However, in the case of compound-**5-Cu^{2+}** system, only quenching of the 316 nm peak is

observed without any shift as the helical structure remains intact. Quenching in both the cases is due to the interactions of compound-**5** with corresponding cations.

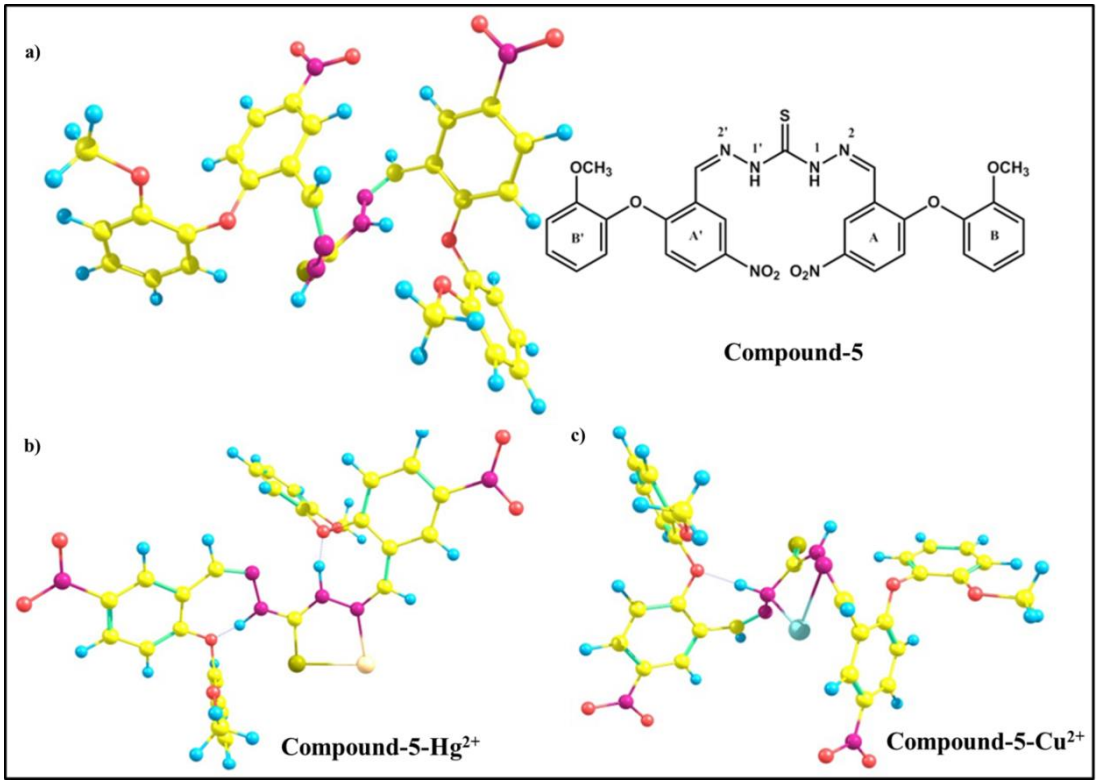

Figure 4.10: a) Helical structure of Compound-**5** optimized using Gaussian 16.0 software **b)** Ring A and A' lie in the same plane after interaction with Hg^{2+} ion **c)** Helical structure of Compound-5 gets partially disrupted after interaction with Cu^{2+} ion.

Energy minimization calculations of the compound-5 bound to Hg^{2+} and Cu^{2+}, in gaseous phase, displayed decrease in the energy difference between Highest occupied molecular orbital (HOMO) and Lowest Occupied molecular orbital (LUMO) for the compound-**5-Hg^{2+}** and compound-**5-Cu^{2+}** systems as compared to native compound-**5 (Table 4.2** and **Figure-4.11)**.

HOMO and LUMO energy levels of compound-**5**, as shown by frontier molecular orbitals, highlight the maximum electron density in the thiocarbazole region **[Figure-4.11 (a)]**. This suggests the functional group's maximum possibility of interaction with the cations. The electron density upon interaction with Hg^{2+} ion gets shifted to electron withdrawing aromatic nitro group for compound-**5-Hg^{2+}** system **[Figure-4.11 (b)]**. In case of compound-**5-Cu^{2+}** system, however, thiocarbazole region retains maximum electron density besides shifting partial electron cloud to aromatic ring containing non-interacting N-2 Schiff's base as shown in [**Figure-4.11 (c)]**.

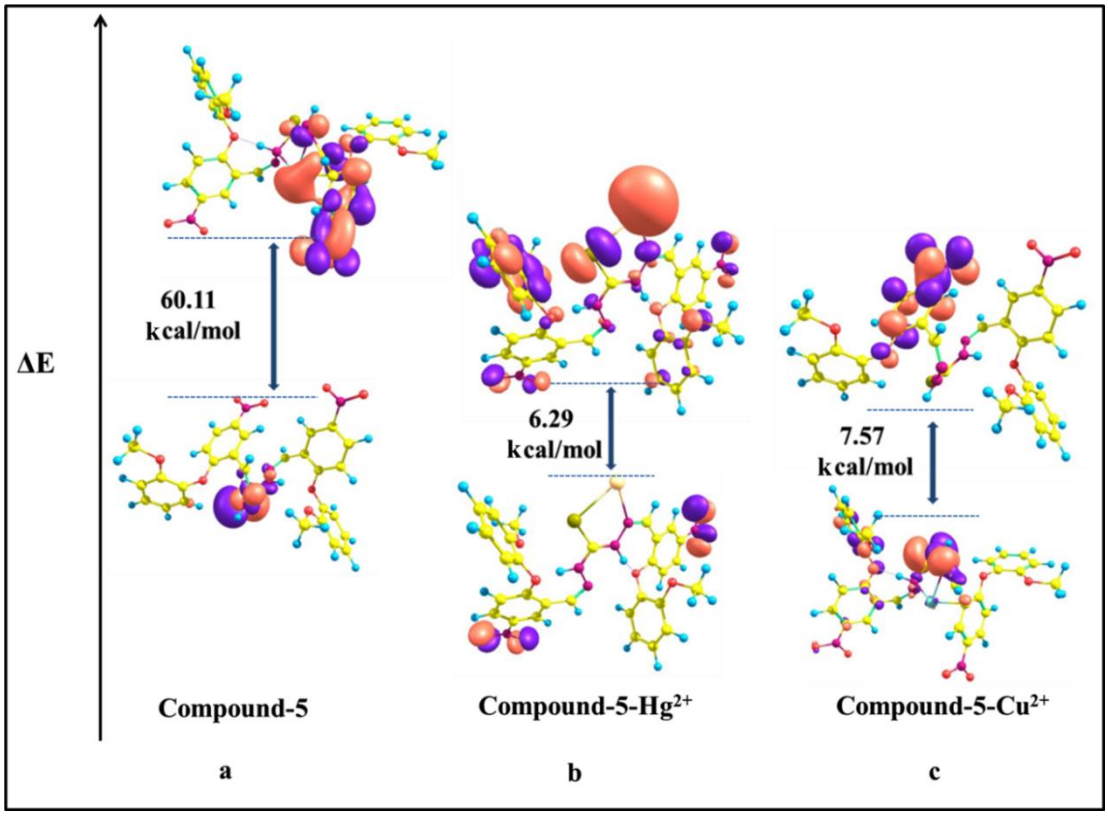

Figure-4.11: Optimized frontier HOMO-LUMO orbitals of compound-**5** along with their energy differences.

Table-4.2: Energy difference calculated from E_{HOMO} and E_{LUMO} for systems in gas phase using Gaussian 16.0 software by B3LYP method

S. No.	System	E_{HOMO} (kcal/mol)	E_{LUMO} (kcal/mol)	ΔE (kcal/mol)
1.	**Compound-5**	-135.54	-75.43	60.11
2.	**Compound-5-Hg^{2+}**	-217.11	-210.81	6.29
3.	**Compound-5-Cu^{2+}**	-265.68	-258.11	7.57

4.8. Application of Compound-5 for the detection of Hg^{2+} ions in Urine Sample

Ability of compound-**5** to detect nano molar concentration of Hg^{2+} ions in aqueous medium encouraged us to develop a method for detection of the cation in the biological fluids. Hair, blood serum and urine are the indicators of exposure to mercury for humans.[29] Urine was the fluid of choice due to its comparatively easy and non-invasive sampling method.[30] However, the presence of uric acid and cretanine not only interfeared in neat urine in the same UV range but also competed with compound-**5** for binding the Hg^{2+} ions. Therefore, to avoid such interferences a dilute urine sample was used for the studies.[31] This resulted in increase the potency of compound-5 to detect Hg^{2+} ions from nano molar range to micro molar range.

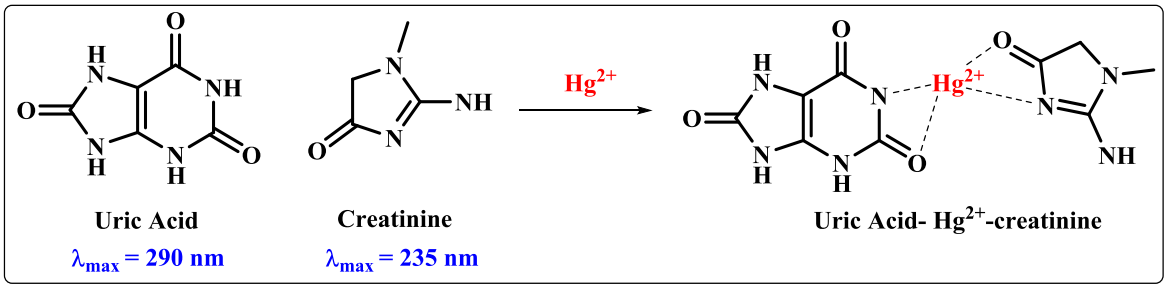

Figure-4.12: Structure of biomolecules present in the urine sample that interefere in the detection of mercuric ions.

To estimate the Hg^{2+} binding efficiency of the uric acid and cretanine as compared to compound-**5**, two initial sets of titrations were performed. In the first case, compound-**5** when added to a mixture of 0.3% urine and Hg^{2+} **[Figure-4.13 (a)]** displayed increase in the intensity of uric acid (293 nm) with simultaneous appearance of peak due to compound-**5-Hg^{2+}** complex (341 nm). This suggested capture of Hg^{2+} ions by compound-**5** from uric acid-Hg^{2+} complex and release of free uric acid. In second titration **[Figure-4.13 (b)]** no change in compound-**5-Hg^{2+}** complex was observed, when increasing quantity of urine was added, thus indicating inability of uric acid in the urine to bind with Hg^{2+} ions in presence of compound-**5.** This suggested stronger binding of compound-**5** with the cation as compared to components present in urine.

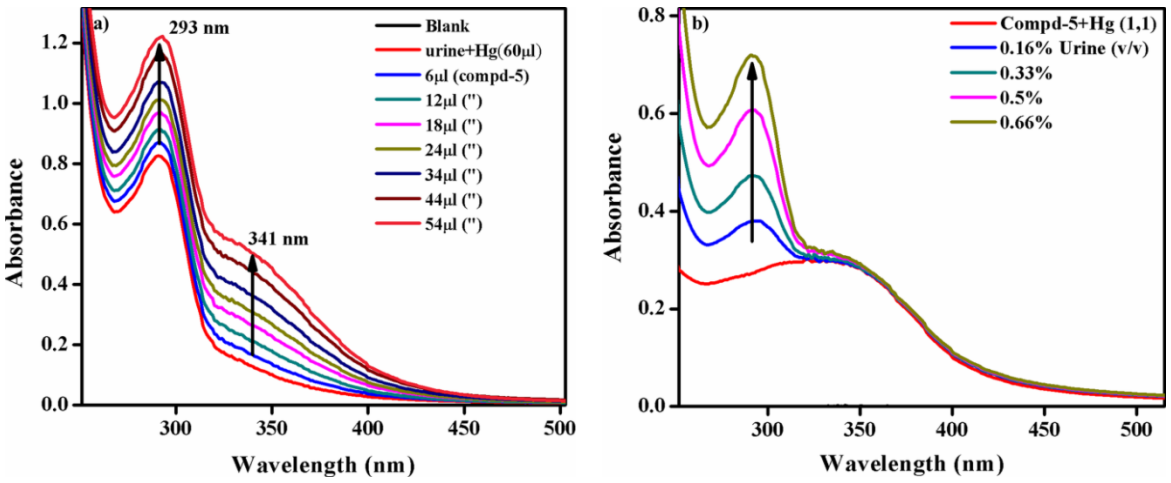

Figure-4.13: (a) Titration of compound-**5** with 0.3% v/v urine sample in presence of Hg^{2+} ion **(b)** Titration of urine sample with compound-**5-Hg^{2+}** system.

Further a calibration curve for quenching of compound-**5** was plotted using different concentrations of Hg^{2+} (0.1, 0.3, 0.6, 1.3, 2.3, 3.3 µM) as shown in **Figure-4.14**. From the graph 68 nM was calculated as the limit of detection for Hg^{2+} ion in 0.3% urine sample.

When scaled to the original concentration of Hg^{2+} ions in native urine sample it gave the original limit of detection as 22 μM.

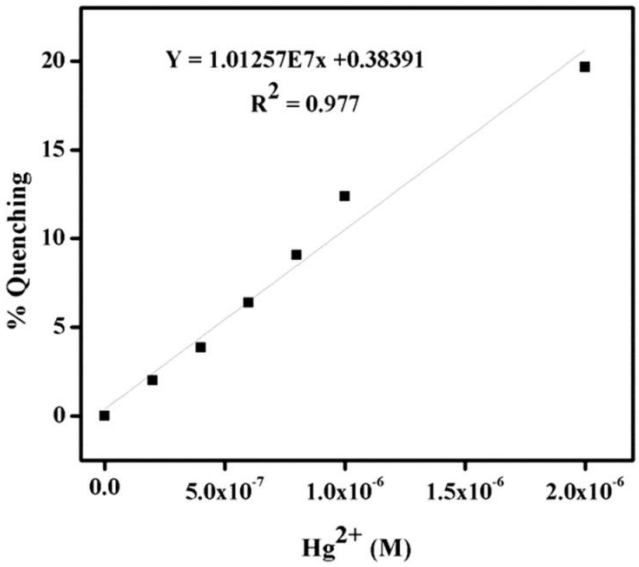

Figure-4.14: Calibration curve for the quenching of Compound-**5** when urine with different concentrations of Hg^{2+} (0.1, 0.3, 0.6, 1.3, 2.3, 3.3 μM) is added.

This methodology was extended further to detect lower concentration of Hg^{2+} ions (nM) in urine by standard addition method. The urine sample containing Hg^{2+} ions (3 μM) was spiked by adding known concentration of Hg^{2+} ions and diluted with distilled water to reach nano-molar range. **(Annexure-1)** From the calibration curve **(Figure-4.14)** total cation concentration was determined. Finally the difference of total cation concentration and spiked quantity initially added gave the concentration of Hg^{2+} ions originally present in the urine. The results were complemented and thus validated by mercury analyzer. **(Annexure-2)** the calculations used to calculate the original concentration of mercury in urine before spiking was briefly described in **Annexure-2 of Section-I and II**.

4.9. Conclusion

The work presented here shows the synthesis of a diphenyl ether tagged thiocarbohydrazide-based receptor (Compound-**5**) that selectively detects Hg^{2+} and Cu^{2+} ions in ninety-nine per cent aqueous medium with a detection limit of 27 nM and 0.16 μM respectively. Photophysical studies, NMR and IR spectroscopies displayed a 1:1 stoichiometry for both the cations. Theoretical studies further revealed different binding sites for the Hg^{2+} and Cu^{2+} ions. Compound-**5** was additionally utilized to detect mercuric ions in the dilute human urine sample to mitigate the challenge of the interferences from the UV active compounds in the concentrated urine sample. However, the dilution factor compromised the detection limit

from nM to μM. Nonetheless, the work forms the basis for designing and exploring molecules as sensors for Hg^{2+} and Cu^{2+} ions in environmental and other biological samples.

Annexure-1

Calculation for the Determining of [Hg^{2+}] in Urine Sample Using Compd-5

Step wise Procedure after Optimization

Step-1: Taken urine sample with unknown amount of Hg^{2+} ions **(Spl-I)**.

It actually contained 3 μM of Hg^{2+} ions as per analysis of Mercury analyzer. (Figure –S11 and Annexure-II)

*(This sample after diluting with distilled water to 2.7% **(Spl-II)** reduces the concentration of Hg^{2+} ions to 80 × 10^{-9} M which is beyond the detectable range with this method. Therefore there is need to spike it with known concentration of Hg^{2+} ions to reach the detectable range.)*

Step-2: Spiked above sample with 10 × 10^{-6} M of Hg^{2+} ions and then diluted with distilled water to 2.7% v/v to reach the detectable range. Thus,

$$\textbf{Total } Hg^{2+}(x) = \textbf{Unknown} + 2.62\times10^{-7}\ \textbf{M} \quad \text{------- (Eq-1)}$$

Following steps show

Step-3: Initial absorbance at 10 × 10^{-6}M Compd-**5** : $A_0 = 0.3631$

Step-4: Absorbance of Compd-**5** with spiked urine sample prepared in Step-2 above ensuring that concentration of Compd-**5** is 10 × 10^{-6} M : $A = 0.3491$

Calculations

Calculation of percentage quenching using equation (Shown for one of the triplicate experiment)

$$\textbf{Q\% (Y)} = 100-\{(A/A_0) \times 100\} \quad \text{------- (Eq-2)}$$

Replacing A_0 and A from Step-3 and Step-4 above

$$\textbf{Q\% (Y)} = 100-\{(0.3491/0.3631) \times 100\} = 3.9 \pm 0.6$$

From **Figure-6.16**

$$Y = (1.01257\ E\ 7\ x) + 0.38391$$

Replacing Y from above $3.9 = (1.01257E7\ x) + 0.38391$

$$x = (3.9 - 0.38391) / 1.01257E7 = (3.5 \pm 0.2) \times 10^{-7}\ M$$

Using Eq-1 Total $Hg^{2+}(x)$ = Unknown + 2.6×10^{-7} M

3.47×10^{-7} = Unknown + 2.6×10^{-7} M

Unknown = 3.5×10^{-7} M - 2.6×10^{-7} M = 0.9×10^{-7} M

Multiplying introducing dilution factor to get original concentration of Hg^{2+} ions in Urine

$$(10 \times 10^{-6} / 2.6 \times 10^{-7})\ 0.9 \times 10^{-7} = \textbf{(3.4 ± 0.8) × } 10^{-6}\ \textbf{M}$$

Annexure-2

Validation [Hg^{2+}] in Urine Sample by Mercury Analyzer

Step-1: Taken **Spl-1** (Annexure-1) containing 3 μM of Hg^{2+} ions.

Step-2: Using $M_1V_1=M_2V_2$ diluted **Spl-1** with distilled water so as to have [Hg^{2+}]=17.8 $\times 10^{-9}$ M
[3×10^{-6} M × 0.00596 (dilution factor obtained from $M_1V_1=M_2V_2$) = 17.8×10^{-9} M]
Step-3: Submitted for analysis of [Hg^{2+}] using Mercury Analyzer
(The dilution was required as the instrument "M*ercury Analyzer" used has maximum detection range of 40 ppb*)

Result obtained from Analysis report (**Fig-S11 below**) = [Hg^{2+}] = 3.03 ppb

Finding molarity from the Concentration using equation
ppb = **[(**Molarity × Mol. Wt.) /1000] × 10^{-9}

Molarity = (3.03 × 200.59) / 10^{-6} = **15.1** × $\mathbf{10^{-9}}$ **M**

Result: Using dilution factor 0.00596 to find [Hg^{2+}] in **Spl-1** = 15.1 × 10^{-9} M / 0.00596
= 2.5 × 10^{-6} M

Above results calculated by Mercury Analyzer lies in the statistical range (3.4 ± 0.8) × 10^{-6} M of the result calculated using Compd-**5** using Absorption method.

References

1. Raj, D.; Maiti, S. K., *Environ. Monit. Assess.* **2019**, *191*, 566.
2. Xun, Y.; Feng, L.; Li, Y.; Dong, H., *Chemosphere* **2017**, *189*, 161.
3. Xinmin, Z.; Kunli, L.; Jian'an,; Yilun, L., *Sci. Total Environ.* **2006**, *368*, 713.
4. Matsuyama, A.; Yano, S.; Taninaka, T.; Kindaichi, M.; Sonoda, I.; Tada, A.; Akagi, H., *Mar. Pollut. Bull.* **2018**, *129*, 503.
5. Mergler, D.; Anderson, H. A.; Chan, L. H. M.; Mahaffey, K. R.; Murray, M.; Sakamoto, M.; Stern, A. H., *AMBIO: J. Hum. Environ.* **2007**, *36*, 3.
6. a) Boening, D. W., *Chemosphere* **2000**, *40*, 1335; b) Mutter, J.; Naumann, J.; Schneider, R.; Walach, H.; Haley, B. *Neuro Endocrino. Lett.* **2005**, *26*, 439.
7. Zhang, Y.; Zeng, G. M.; Tang, L.; Zhu, Y.; He, X. X.; He, Y., *Anal. chem.* **2015**, *87*, 989.
8. Leopold, K.; Harwardt, L.; Schuster, M.; Schlemmer, G., *Talanta* **2008**, *76*, 382.
9. Hu, B.; Hu, L.L.; Chen, M. L.; Wang, J. H., *Biosens. Bioelectron.* **2013**, *49*, 499.
10. Kim, K. B.; Kim, H.; Song, E. J.; Kim, S.; Noh, I.; Kim, C., *Dalton Transactions* **2013**, *42*, 16569.
11. Shiono, Y.; Hayashi, H.; Wakusawa, S.; Yano, M., *Med. EM* **2001**, *34*, 54.
12. Milhavet, O.; Lehmann, S., *Brain Res. Rev.* **2002**, *38*, 328.
13. Peters, D. G.; Connor, J. R.; Meadowcroft, M. D.; *Neurobiol. Dis.* **2015**, *81*, 49.
14. Georgopoulos, A. R. G.; Yonone-Lioy, M. J.; Opiekun, R. E.; Lioy, P. J., *J. Toxicol. Environ. Health, B* **2001**, *4*, 341.
15. Momidi, B. K.; Tekuri, V.; Trivedi, D. R., *Spectrochim. Acta A Mol. Biomol. Spectrosc.* **2017**, *180*, 175.
16. Tekuri, V.; Sahoo, S. K.; Trivedi, D. R., *Spectrochim. Acta A Mol. Biomol. Spectrosc.* **2019**, *218*, 19.
17. Ma, Q.-J.; Zhang, X.-B.; Jin, Z.; Mao, G.-J.; Shen, G.-L.; Yu, R.-Q., Anal. *Chim. Acta* **2010**, *663*, 85.
18. Alizadeh, K.; Parooi, R.; Hashemi, P.; Rezaei, B.; Ganjali, M. R., *J. Hazard. Mater.* **2011**, *186*, 1794.
19. Mei, Q.; Wang, L.; Tian, B.; Yan, F.; Zhang, B.; Huang, W.; Tong, B., *New J. Chem.* **2012**, *36*, 1879.
20. Singhal, D.; Gupta, N.; Singh, A. K., *RSC advance* **2015**, *5*, 65731.
21. Sarkar, S.; Roy, S.; Saha, R.; Panja, S. S., *J. Fluoresc.* **2018**, *28*, 427.
22. Ko, S. K.; Yang, Y. K.; Tae, J.; Shin, I., *J. Am. Chem. Soc.* **2006,** *128* , 14150.
23. Y. G. Shi, Y. L. Duan, J. H. Chen, X. H. Wu, Y. Zhou, J. F. Zhang, *Bull. Korean Chem. Soc.* **2013**, *34*, 63.
24. Tharmaraj, V.; Pitchumani, K., *Anal. Chim. Acta* **2012**, *751*, 171.
25. Satapathy, R.; Wu, Y. H.; Lin, H. C., *Org. lett.* **2012**, *14*, 2564.
26. Svechkarev, D.; Dereka, B.; Doroshenko, A., *J. Phys. Chem. A* **2011**, *115*, 4223.
27. Chae, M. Y.; Czarnik, A. W., *J. Am. Chem. Soc.* **1992**, *114*, 9704.
28. Tang, X.; Zhu, Z.; Liu, R.; Ni, L.; Qiu, Y.; Han, J.; Wang, Y., *Spectrochim. Acta, Part A* **2019**, *211*, 299-305.
29. Ruggieri, F.; Majorani, C.; Domanico, F.; Alimonti, A., *Int. J. Environ. Res.* **2017**, *14*, 519.
30. Eskandarian, A., *Iran. J. parasitol.* **2013**, *8*, 177.
31. Du, J.; Zhu, B.; Chen, X., *Small* **2013**, *9*, 4104.

Section-III

Anion Detections

Chapter-5

Graphical Abstract:

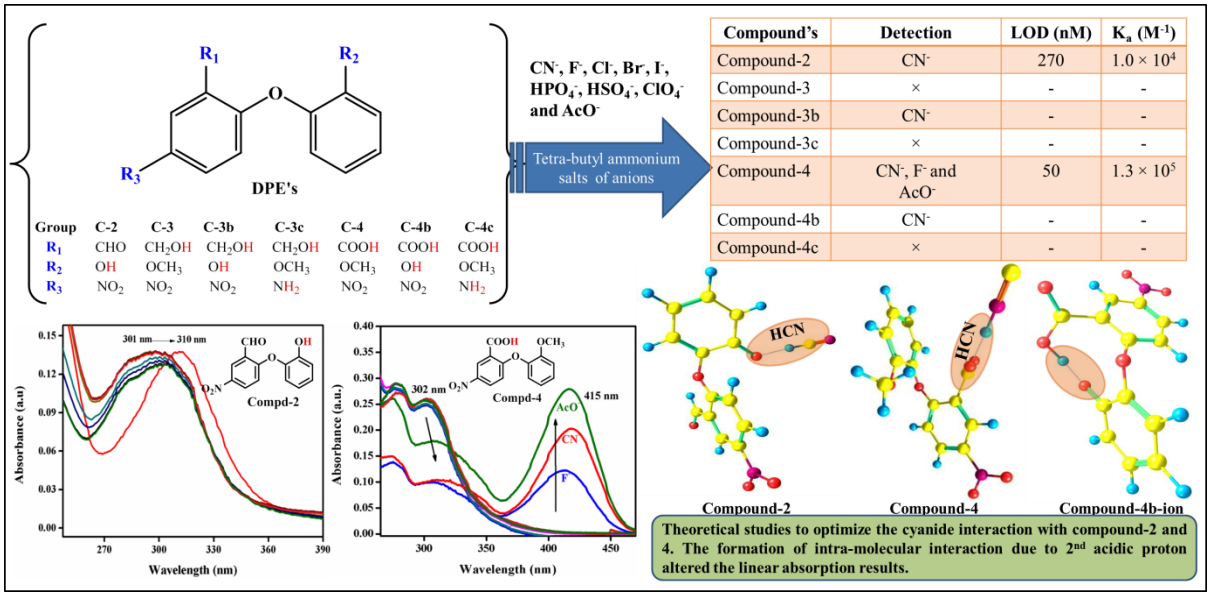

Chapter-5

DETECTION OF ANIONS WITH VARIOUS DIPHENYL ETHER DERIVATIVES

5.1. Introduction

The advances in chemical and biological sciences have witnessed tremendous progress in anion sensing and their vital role in chemical, industrial, environmental and biological processes.[1,2] Fluoride, cyanide, sulphite, acetate and superoxide ions are some of the elementary anions. These anions play a critical role in dental health, osteoporosis,[3,4] electroplating, gold mining, production of organic chemicals,[5] industrial preservatives,[6] antibodies, enzyme mechanism,[7] metabolism, cell growth[8,9] and many more. However, untreated release, overexposure or overdose of these anions is harmful leading to soil salinity, [10] long-term toxicity or fatal pathological disorders.[11] Thus, qualitative and quantitative detection of these ions is crucial in monitoring environmental and human exposure. The development of simple, low-cost, and readily available sensors to monitor anions' concentration, location, and function is an important and active area to explore.[12,13] A reliable sensor should comply with the photophysical requirements, such as absorbing the desired wavelength range and detection using inexpensive optics.

Broadly, three approaches for sensing anions are well known.[14] One of the early approaches included an anion-binding site designed using hydrogen bond donors arranged close to the 'reporter' group (**Table-5.1**). The anions bind to the hydrogen bond donor group, changing the receptors electronic or photophysical properties and allowing their detection using electrochemical or optical techniques.[15] The second approach uses the chemical reaction of a specific anion on a small molecule to generate a new species with different optical properties for its selective detection. The receptor molecule, in this case, is called chemodosimeters.[16] This methodology is well-known for the sensing of fluoride and cyanide ions. A third approach involves disrupting an indicator-receptor complex by a specific anion, thereby changing the indicator's electronic properties for convenient detection.

Phenyl ethers have recently been shown to possess the above features.[12] Their ability to absorb from 275-360 nm due to π to π^* transitions and the ease of modifying the aromatic ring to fine-tune their properties make them a potential candidate to explore their properties for anion sensing. This chapter focuses on the absorption studies of the synthesized diphenyl ethers, tuned using different substituents on the rigid planer phenyl rings, to explore their

Table-5.1: Receptors serve as an anion-binding group for hydrogen bond donors.

Receptors	**Solvent system**	**Technique Used**	**Limit of detection (M)**	**Refer.**
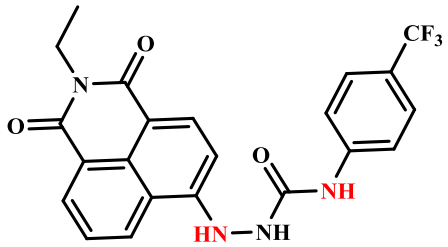	DMSO	UV-Visible & Fluorescence	1×10^{-6}	17
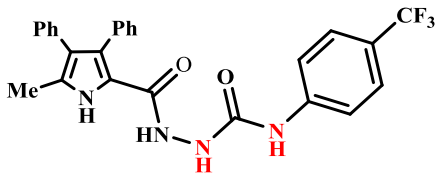	DMSO	UV-Visible	NA	18
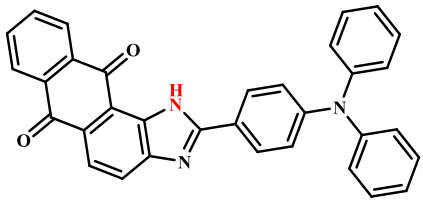	DMSO	UV-Visible & Fluorescence	5.9×10^{-7}	19
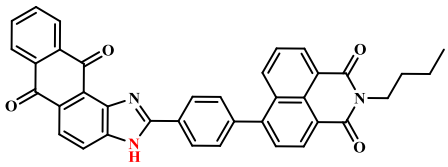	EtOH: H_2O (9:1)	UV-Visible & Fluorescence	1.59×10^{-9}	20
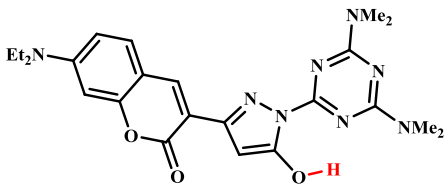	DMSO	UV-Visible & Fluorescence	0.1×10^{-6}	21
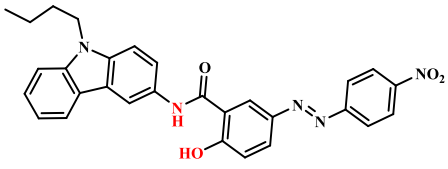	ACN: Acetone (9:1)	UV-Visible & Fluorescence	NA	22

interaction, selectivity and *in-silico* studies to sense anions and understand the mechanism of interaction.

5.2. Selection of the Receptor Molecules

Chapter-2 describes the synthesis of ten diphenyl ether molecules **(Schemes- 2.1 to 2.3)**. Seven of these molecules **(Figure-5.1)** possessed a proton attached to either nitrogen or oxygen, a possible anion-binding site as the hydrogen bond donors. It was envisaged to explore the potential of these molecules for the selective detection of anions. The hydrogen bond donors attached to the diphenyl ether skeleton of these molecules included phenolic **(**compounds **2, 3b, 4b)**, carboxylic **(**compounds **4, 4b** and **4c)**, benzyl alcohol **(**compounds **3, 3b** and **3c)** and amino groups (compound **3c, 4c)**. Four of the seven molecules **(**compounds **3b, 3c, 4b** and **4c)** held two hydrogen bond donor groups. Consequently, the variety of the functional groups attached to the motif presented differential donor capability for each molecule.

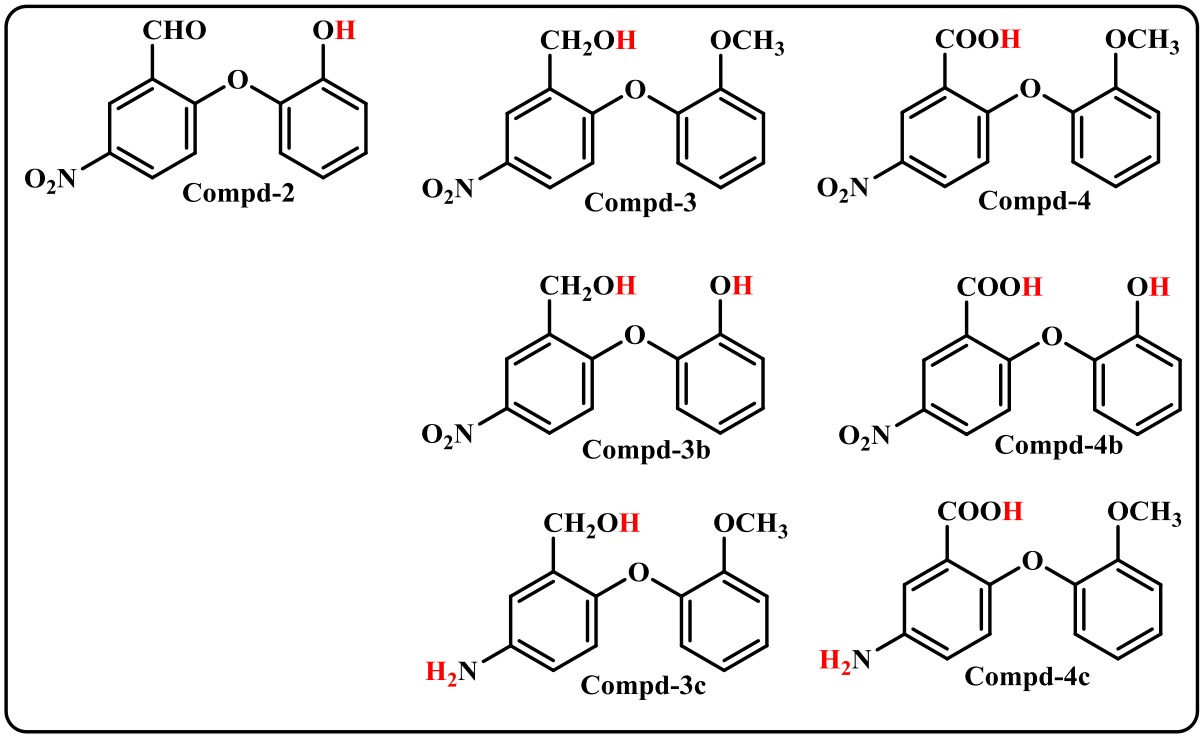

Figure-5.1: Structures of shortlisted diphenyl ether molecules with protons attached to either nitrogen or oxygen presented a possible anion-binding site due to the availability of the hydrogen bond donors.

5.3. Absorption Studies

5.3.1. Absorption Spectra and Addition of Anions: The absorption studies of the synthesized diphenyl ethers **(Figure-5.1)** gave their λ_{max} in the expected wavelength range. **Figure-5.2** shows that compounds **2, 3, 4, 3b** and **4b** are absorbed with their λ_{max} in the 301-310 nm range, and compounds **3c** and **4c** between 340- 350 nm. The presence of the lone pair on amino groups for compounds **3c** and **4c (Figure-3.2 (g & h)** resulted in the extended

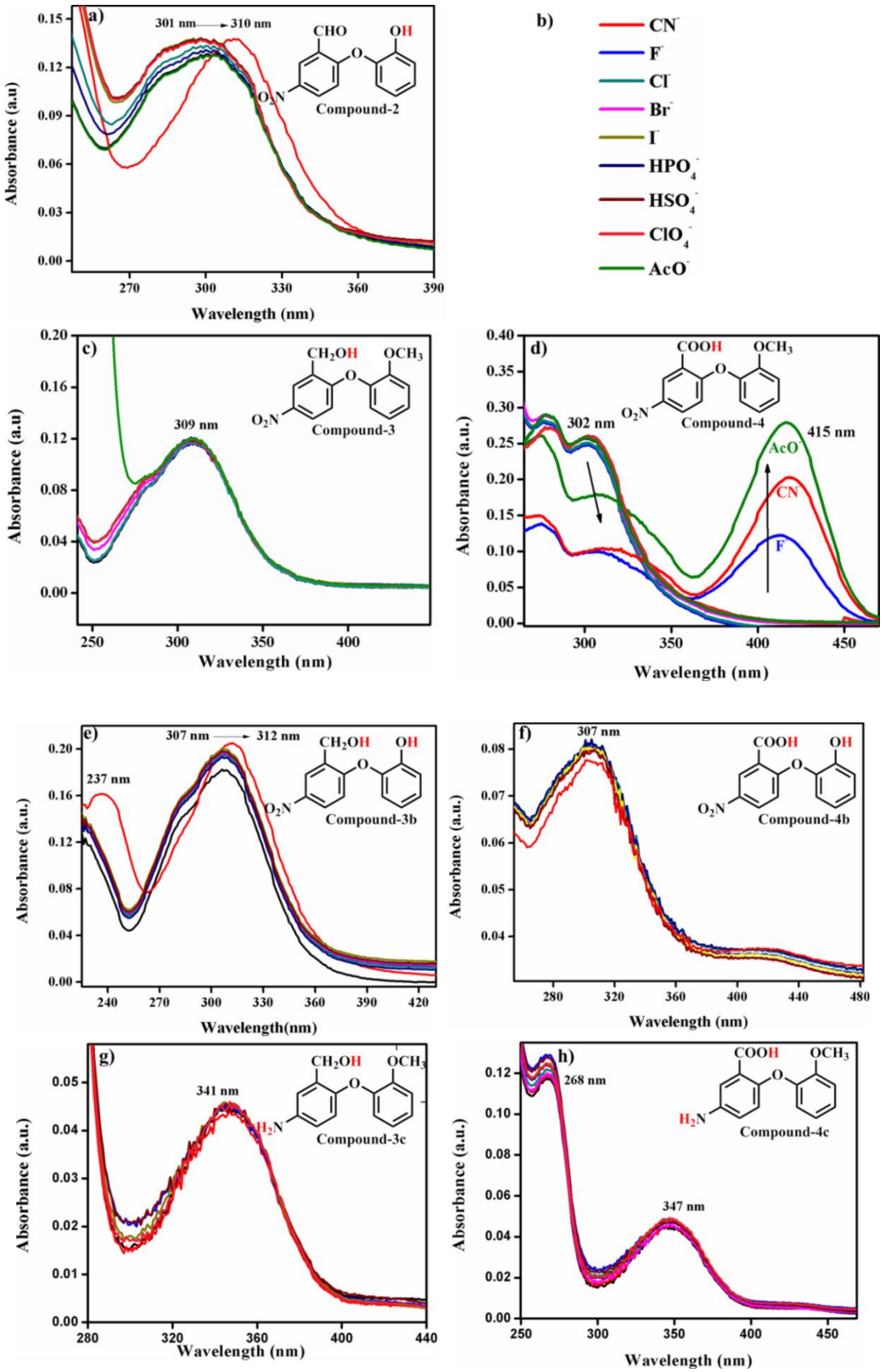

Figure-5.2: Change in the absorption properties of the synthesized molecules (0.1M stock in ACN) after adding ten times excess of different anions.

Conjugation, thereby subsequent redshift to 340- 350 nm as compared to compounds **2**, **3**, **4**, **3b** and **4b (Figures-3.2 (a, c-f)**.

All the compounds were evaluated to detect anions by observing a change in their λ_{max} on adding ten times excess of F^-, Cl^-, Br^-, I^-, $CN.^-$, AcO^-, HPO_4^-, HSO_4^-, ClO_4^- ions. To maintain uniformity, all the anions used were tetra-butyl ammonium salt.

5.3.2. Compounds **2** and **4**: **Figure-5.2** displays a significant change in the absorption properties of compounds **2 [Figure-5.2 (a)]** and **4 [Figure-5.2 (d)]**. Compound-**2** shows a redshift from 301 nm to 310 nm selectively for the cyanide ions. Compound-**4** shows the decreased intensity at 302 nm with the simultaneous appearance of three new peaks around 423 nm for the fluoride, cyanide and acetate ions. The hydrogen bond donor capability of the phenolic and carboxylate groups for compounds **2** and **4** resulted in the increased conjugation **(Figure-5.3)** upon adding anions. Thus, there was a change in the absorption properties of both the molecules, as shown in **Figure 5.2** (**a & d)**.

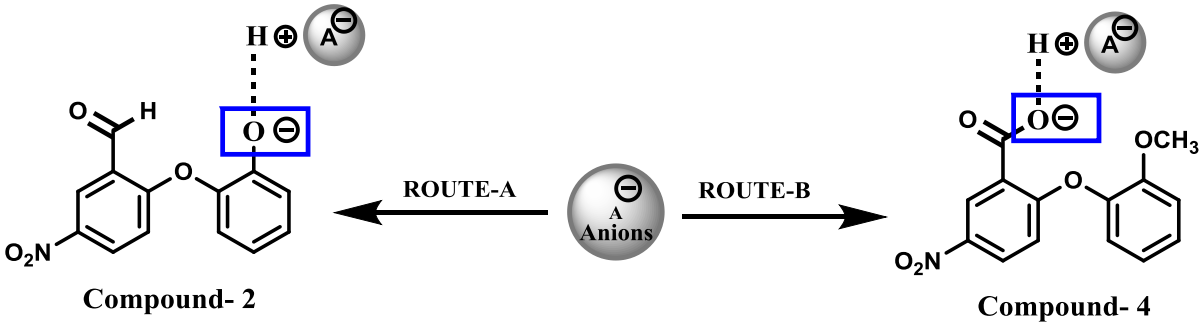

Figure-5.3: Increased conjugation on the phenoxy **(**compound-**2)** and carboxylic acid **(**compound-**4)** groups due to interaction of the anions with the acidic protons resulted in the corresponding redshift.

5.3.3. Compounds **3b** and **4b**: Compared to compounds **2** and **4**, compounds **3b [Figure-5.2 (e)]** and **4b [Figure-5.2 (f)]** displayed a marginal redshift of 5-6 nm only on the addition of excess cyanide ions. No change was observed for the F^-, Cl^-, Br^-, I^-, AcO^-, HPO_4^-, HSO_4^-, and ClO_4^- ions. Both compounds contained more than one hydrogen bond donor groups. Compound **3b** carried phenoxy and benzyl alcohol groups, and 4b appended phenolic and carboxylate groups. Despite two hydrogen bond donor groups, the change in optical properties was marginal for both compounds on adding the cyanide ions. It can be hypothesized that although the basicity of the cyanide ion abstracted the acidic protons from compounds-**3b** and **4b**, the presence of a second hydrogen bond donor group compensates for the abstracted proton through intramolecular hydrogen bonding, as shown in **Figure 5.4**. [23]

5.3.4. Compounds **3** and **3c**: Compounds **3 [Figure-5.2 (c)]** and **3c [Figure-5.2 (g)]** did not show any change in the absorption properties on adding anions. As discussed above, these results indicated the absence of sufficient hydrogen bond donor capability or any reactive site in the two compounds. The results also pointed to the lack of desired basicity of anions to abstract a proton or nucleophilicity to change their $\lambda_{max.}$ The benzyl protons in compounds **3** and **3c** lacked the hydrogen bond donation capability to be abstracted by any of the anions.

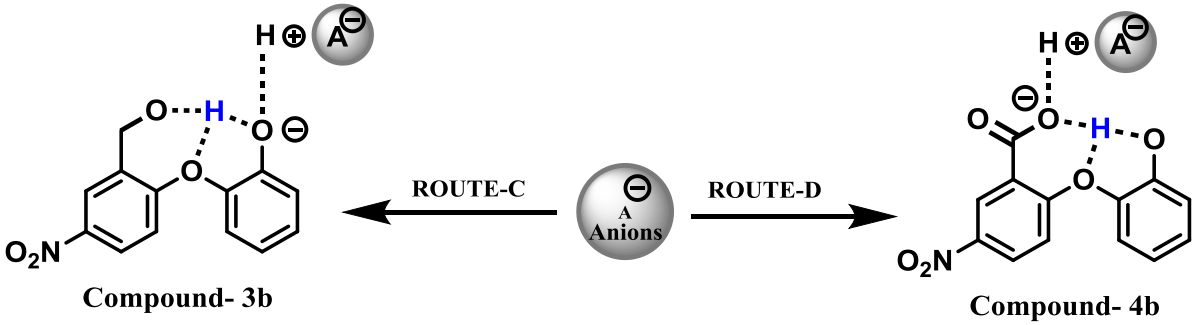

Figure-5.4: The presence of a second hydrogen bond donor group diminishes the precise detection of the cyanide ions. Benzyl alcohol group in case of compound **3b** and phenolic group in case of compound **4b** compensates for the abstracted proton through intramolecular hydrogen bonding.

5.3.5. Compound **4c**: The natural tendency of compound **4c [Figure-5.2 (h)]** to exist in the zwitterionic form **[Figure-5.5, (4c1)]** and the resulting interionic interactions **(4c2)** prevented the exchange of anions.

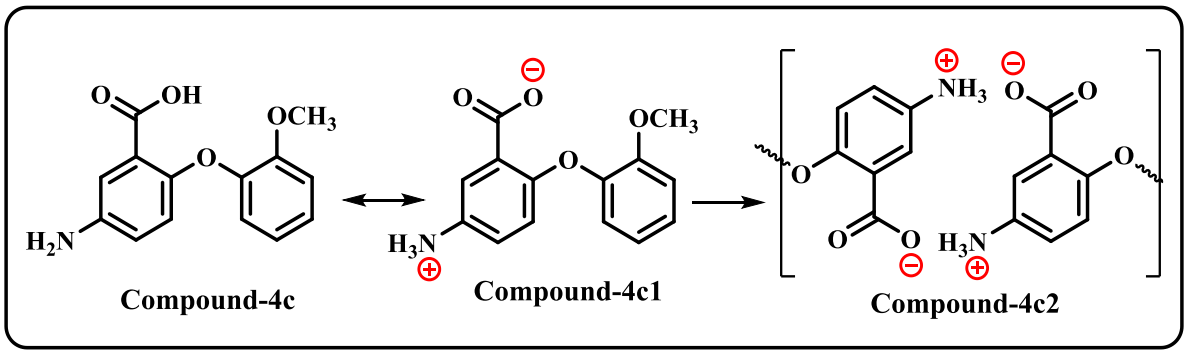

Figure-5.5: Tendency of compound-**4c** to exist in the zwitterionic form (compound-**4c1**) and the resulting interionic interactions (compound-**4c2**) prevented to exchange the anions.

It has been reported that solvents having a high dielectric constant facilitate the self-assembly of aromatic amino acids into rigid supramolecular.[24] Recently, Ehud Gazit's group established the self-assembly mechanism for the aromatic amino acids, phenylalanine (Phe) and tryptophan (Trp), for the amyloid-like structure formation.[25] Therefore, an acetonitrile medium with a dielectric constant of 37.5 can be hypothesized to facilitate interionic interactions for compound-**4c2.** The hypothesis is based on the report by R. Sharma's group

that carried self-assembly formation for L-phenyl alanine in a solvent system having a dielectric constant of 31.5.[24]

5.4. Titration Studies

As discussed above, the preliminary studies suggested the potential of compound-**2** to detect cyanide ions selectively and for compound-**4** to detect cyanide, fluoride and acetate ions in the acetonitrile medium. Thus, titration studies were carried out for both compounds to calculate the detection and binding constants limit.

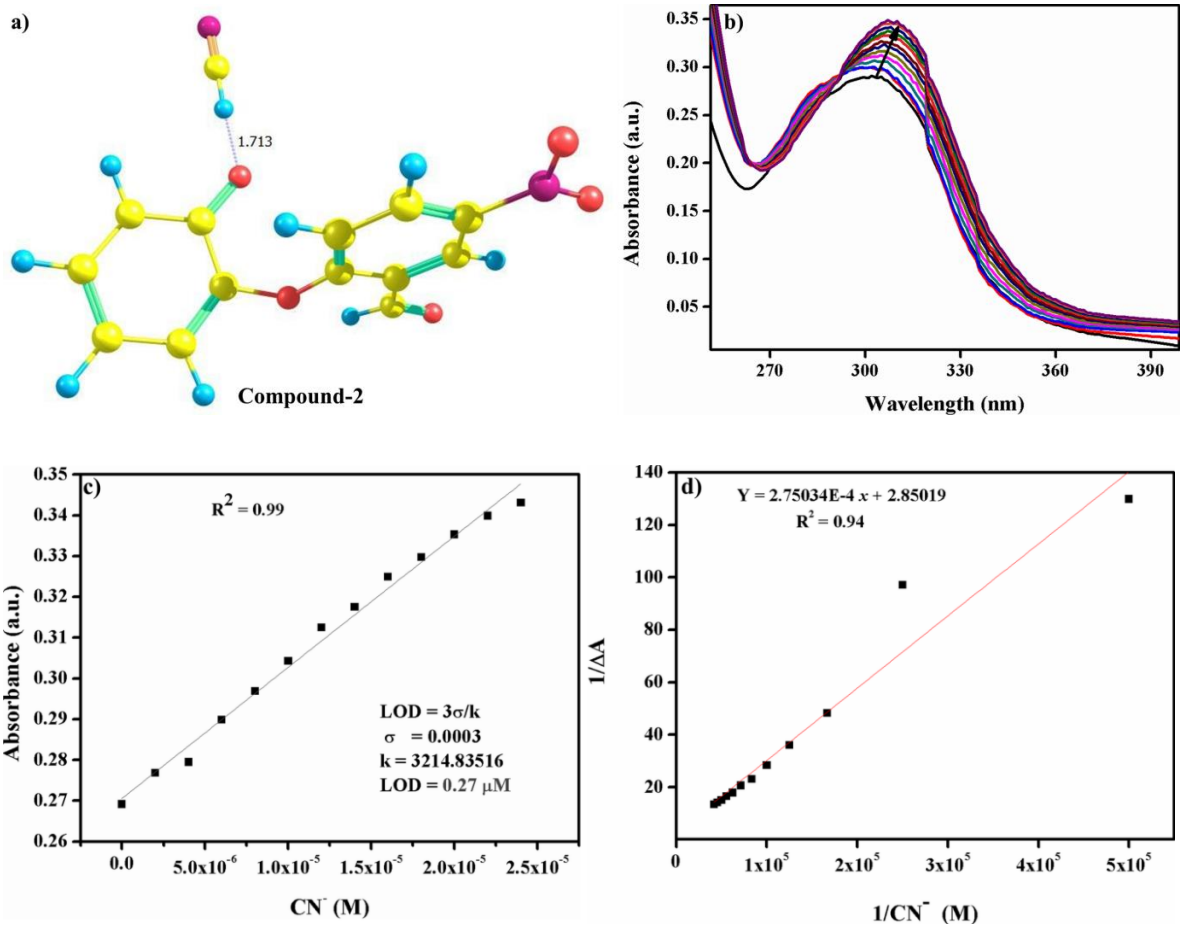

Figure-5.6: Theoretical and experimental findings for compound-**2** with CN^- ion. a) Compound-**2** optimized conformer with CN^- ion, b) Titration absorption data, c) Linear plot to compute the minimal detection limit, and d) Benesi-Hildebrand plot.

5.4.1. Compound-**2:** Gas-phase theoretical studies (Gaussian 16) for the compound-**2** and the cyanide ion displayed an increased length of the phenolic O-H bond from 0.96 Å to 1.71 Å upon interacting with the anion **[Figure 5.6 (a)]**, indicating the association of the cyanide ion with the phenolic proton. The incremental addition of cyanide ions to a 20 µM solution of compound-**2** in an acetonitrile medium gave a titration curve with an isosbestic point at 291 nm. The saturation for the cyanide ions was obtained at 1.2 time's excess, as shown in

[Figure-5.6 (b)]. The absorbance vs. anion concentration graph **[Figure-5.6 (c)]** displayed a linear response for the receptor on adding the anion. The binding constant of the system was determined to be 1.0×10^{4} M^{-1} using the Benesi-Hildebrand equation from the graph of reciprocals of anion concentration and change in absorbance.

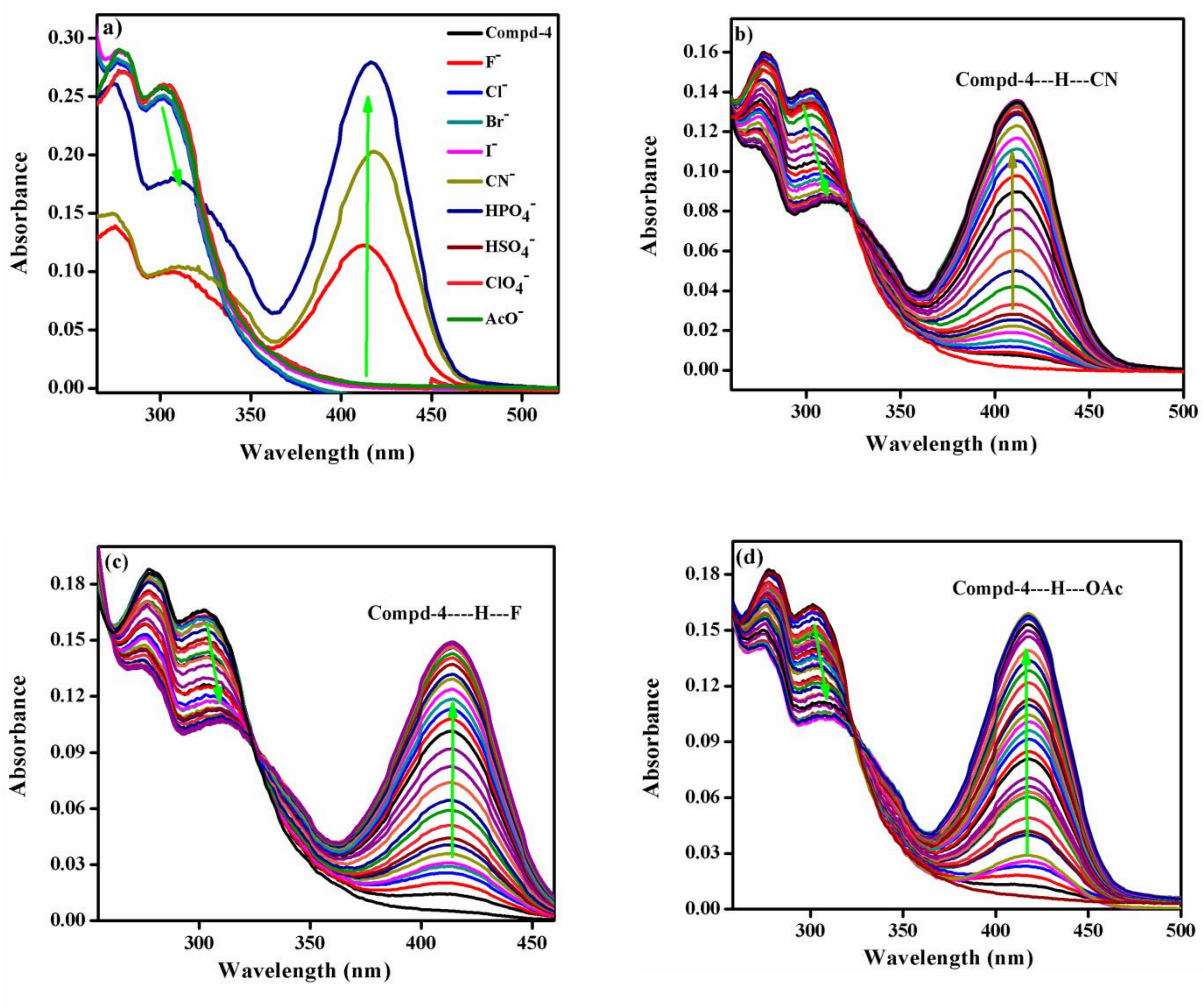

Figure-5.7: (a) UV-Vis spectra of compound-**4** (20 µM) with 10 times excess of all the anions. **(b)**Titration spectra of compound-**4** (20 µM) shows sequential quenching with CN^- **(c)** F^- and **(d)** AcO^- ions in ACN medium.

The slope of the plot gave the detection limit of cyanide ions as 0.27 µM, which was much lower than the maximum permissible limit of the cyanide ions (1.9 µM) in drinking water set by the World Health Organization (WHO). [26]

5.4.2. Compound-**4:** The high absorptivity (ϵ = 12472 mol^{-1} L cm^{-1}) for compound-**4** suggested the transition from π to -π^* orbitals. Further, titration studies were carried out to determine the minimum detection limit of compound-**4** for the CN^-, F^- and AcO^- anions. **Figure 5.7** shows the peaks at 276 nm and 302 nm being quenched when CN^- **[Figure-5.7 (b)],** F^- **[Figure-5.7 (c)]** and AcO^- **[Figure-5.7 (b-d)]** ions were sequentially added in a 20

μM of compound-**4** in each case. The quenching accompanied enhancement in the peak intensity at 415 nm.

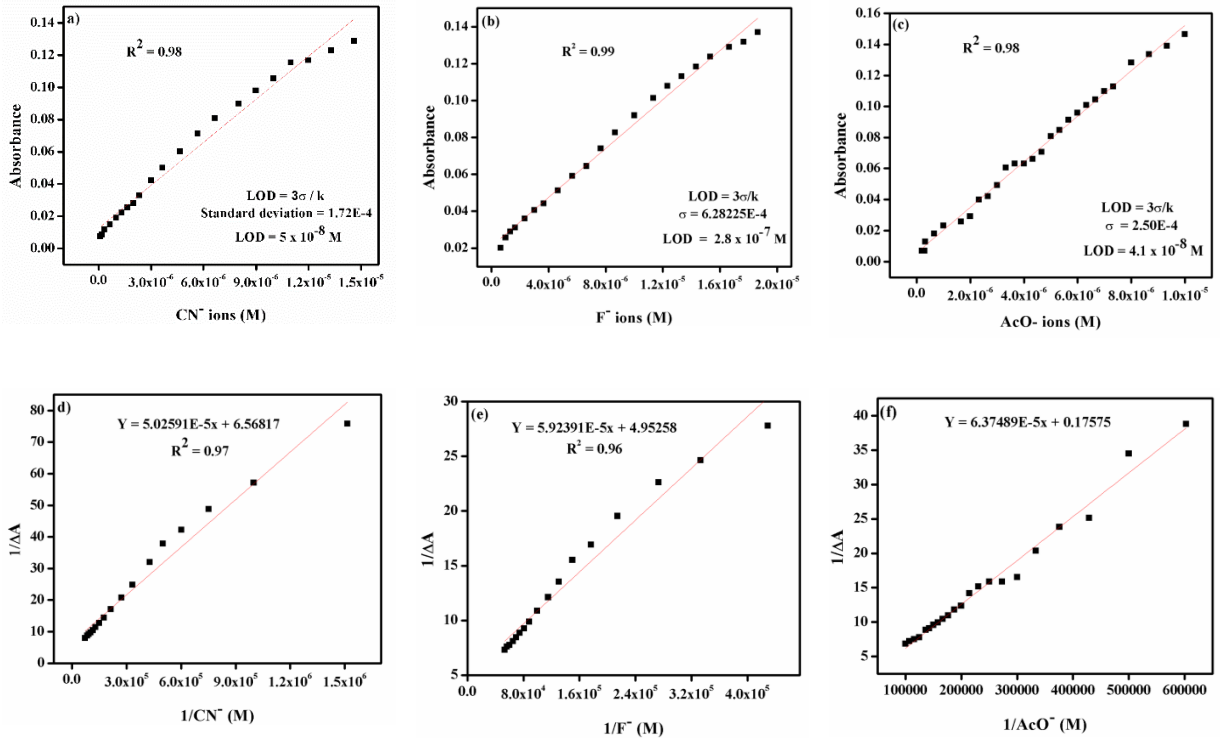

Figure-5.8: Linear plot for the absorbance of **compound-4** at 415 nm with respect to the concentration of **(a)** CN^- ions, **(b)** F^- ions and (**c**) AcO^- ions to calculate the minimum detection limit as 50 nM, 280 nM and 41 nM respectively in ACN medium. Binding constant of anions using Bensi-hildbrand plot between absorbance differences of **compound-4** at 415 nm verses the concentration of **(d)** CN^- (1.3 x 10^5 M^{-1}) **(e)** F^- (0.8 x 10^5 M^{-1}) and **(f)** AcO^- ions (2.0 x 10^3 M^{-1}) in ACN medium.

The detection limit was calculated using the linear slope and the standard deviation in the absorbance obtained for the peak at 415 nm (IUPAC approved **3σ/k**). The lowest detection limit for the C.N.$^-$, F^- and AcO^- ions was found to be 50 nM, 280 nM and 41 nM, respectively **[Figure-3.8 (a-c)]**. Likewise**,** the binding constant of the anions using the Benesi -Hildebrand equation for the CN^-, F^- and AcO^- ions were 1.3 x 10^5 M^{-1}, 0.8 x 10^5 M^{-1} and 2.0 x 10^3 M^{-1}, respectively **[Figure-3.8 (d-f)]**.

Compound-**4** displayed a hundred times stronger interaction with the CN^- and F^- ions (10^5 M^{-1}) than the AcO^- ions (10^3 M^{-1}). Compared to the other two anions, the weak interaction of the acetate ions can be attributed to the bipolar nature and its large size.

5.5. Theoretical studies

Experimental results were corroborated by theoretical studies in the gas phase with Gaussian 16 software using the B3LYP method and 631+G(d) as a basis set. Compounds **2**, **4**, **3b** and

4b were evaluated for their interactions with the cyanide ions to explore and justify the mechanism. **Table-5.2** shows the zero-point energy (threshold energy) of all the native molecules after initial calculations in gas phase. Compound-**4** displayed maximum stability compared to the other three molecules, as evident from the native state zero-point energy comparison.

Table-5.2: Minimum energies of the responsive compounds in the native and after interaction with the CN^- anion.

Compound	Native State	Compound + CN^- ions	δE	Binding Constant
	Hartree			M^{-1}
2	-1006.62	-1024.30	17.68	1.0×10^4
4	**-1045.91**	**-1138.67**	**92.76**	1.3×10^5
3b	-932.56	-1025.48	**92.92**	Not determined
4b	-931.38	-1006.14	74.76	Not determined

The interaction with the cyanide ions further reduced the zero-point energy for all four molecules. **Table-5.2** shows comparable stabilization for compounds **4** (δE =92.76) and **3b** (δE =92.92) upon interaction with the cyanide ions. Compared to compounds **2** and **4b**, the stability in the case of the compounds **4** and **3b** was more significant **(Table-5.2)**.

The above results corroborated with the experimental results where the binding constant for compound-**4** was ten times more than compound-**2**. As discussed above, the plot of titrations in compounds **3b** and **4b** did not yield a linear plot; therefore, the binding constant in both cases could not be calculated.

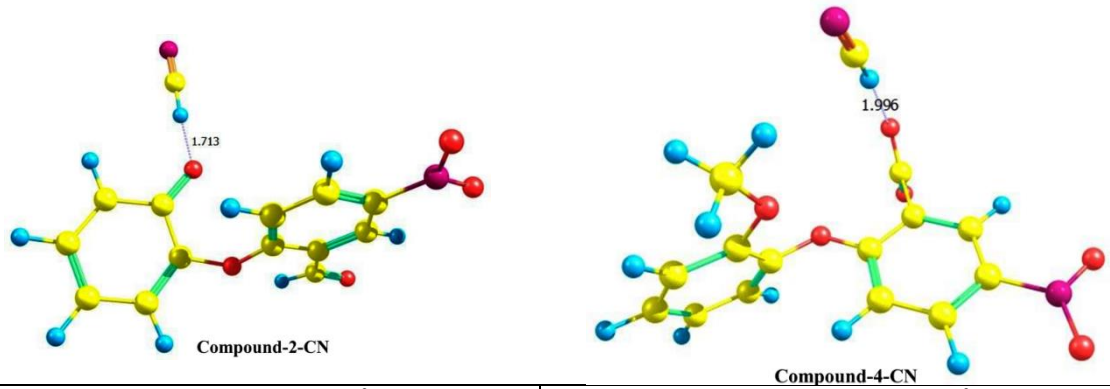

O-H Bond Length (Å)		O-H Bond Length (Å)	
Compound-2	0.969	**Compound-4**	0.979
Compound-2-CN	1.713	**Compound-4-CN**	1.996

Figure-5.9: In-silico modelling to optimize the best conformers of compound-**2** and compound-**4** with CN^- ion and differentiate the (O-H) bond length of native compounds.

5.5.1. Interactions: Further exploration of the theoretical results was done for compounds **2** and **4** in the absence and presence of the cyanide ion. The optimized structure of compounds **2** and **4** displayed an increased length of the OH bonds from 0.9691 **Å** and 0.9791 **Å** to 1.7131

Å and 1.9961 Å, respectively **(Figure-5.9)**. This supported the proposed binding of the hydrogen bond donor group in compounds **2** and **4** with the cyanide ion.

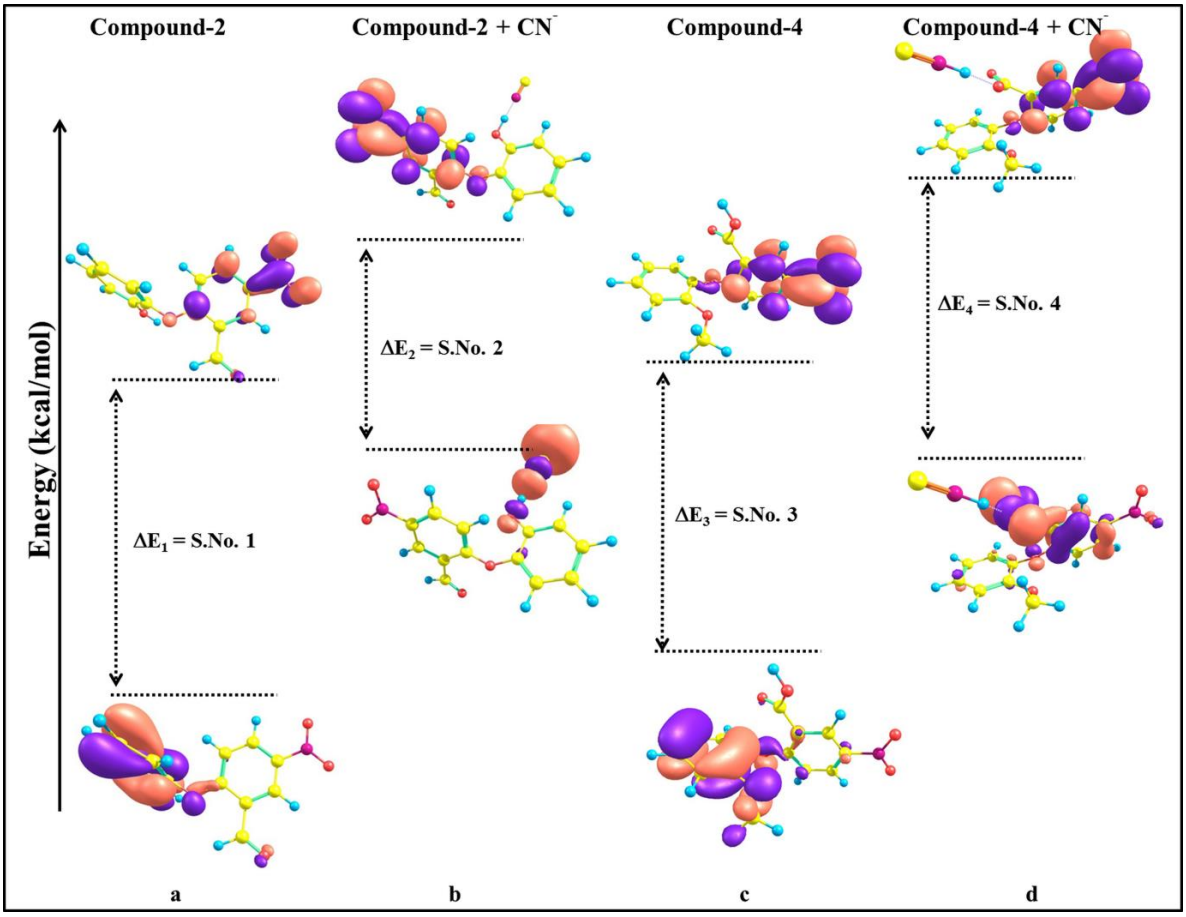

S.No	Compounds	E_{HOMO}	E_{LUMO}	ΔE
		(kcal/mol)		
1	**2**	-161.11	-71.10	90.07
2	**2+CN**	-75.06	-17.42	57.64
3	**4**	-150.50	-65.72	84.78
4	**4+CN**	-78.62	-3.20	74.36

Figure-5.10: Representation of frontier molecular orbitals for both the native compounds (Compound-**2** and compound-**4**) and its conformers with cyanide ions. Table shows the energies of HOMO and LUMO orbital's for the respective compounds and their energy differences in terms of ΔE's.

Figures **5.2 (a & d)** show that both compounds **2** and **4** displayed a minor red shift upon interaction with the cyanide ion. This can be attributed to the intramolecular charge transfer. Therefore, HOMO and LUMO orbitals for both the compounds were compared with their corresponding cyanide complexes. **Figure-5.10 (a)** shows that electron density for the HOMO of compound-**2** is mainly located over the phenolic unit, whereas for the LUMO orbital, it is distributed over the nitro group of the benzaldehyde unit. Upon interaction with the cyanide ions, the HOMO electron density shifted towards the cyanide ion and the LUMO electron density over the aromatic ring of the benzaldehyde unit **Figure-5.10 (b)**. This

suggested the intramolecular charge transfer mechanism for compound-**2** upon interaction with the cyanide ions. Similarly, HOMO in the case of compound-**4 [Figure-5.10 (d)]** had electron density distributed over the anisole unit that shifted to the carboxylic acid upon interaction with the cyanide ions **Figure-5.10 (c),** again suggesting the intramolecular charge transfer mechanism for compound-**4** as well.

Further, the decreased band gap ΔE (ΔE = E_{LUMO}-E_{HOMO}) for compound-**2** from 90.07 kcal/mol to 57.64 kcal/mol and compound-**4** from 84.78 kcal/mol to 75.36 kcal/mol signifies increased interaction for both the compounds with the cyanide ions.

5.5.2. Compounds **3b** and **4b**: Compounds **3b** and **4b** contained two hydrogen bond donor groups. Besides the common phenolic in each case, these were benzyl **(3b)** and carboxylic **(4b)** groups. The theoretical calculations for compounds **3b** and **4b** with the cyanide ions displayed abstraction of the phenolic protons **[Figure-5.11 (a)** and **(b)]**. However, the experimental results indicated a very small redshift (5nm) for compound-**3b** and no change in the absorption properties for compound-**4b**, as shown in **Figure-5.2**.

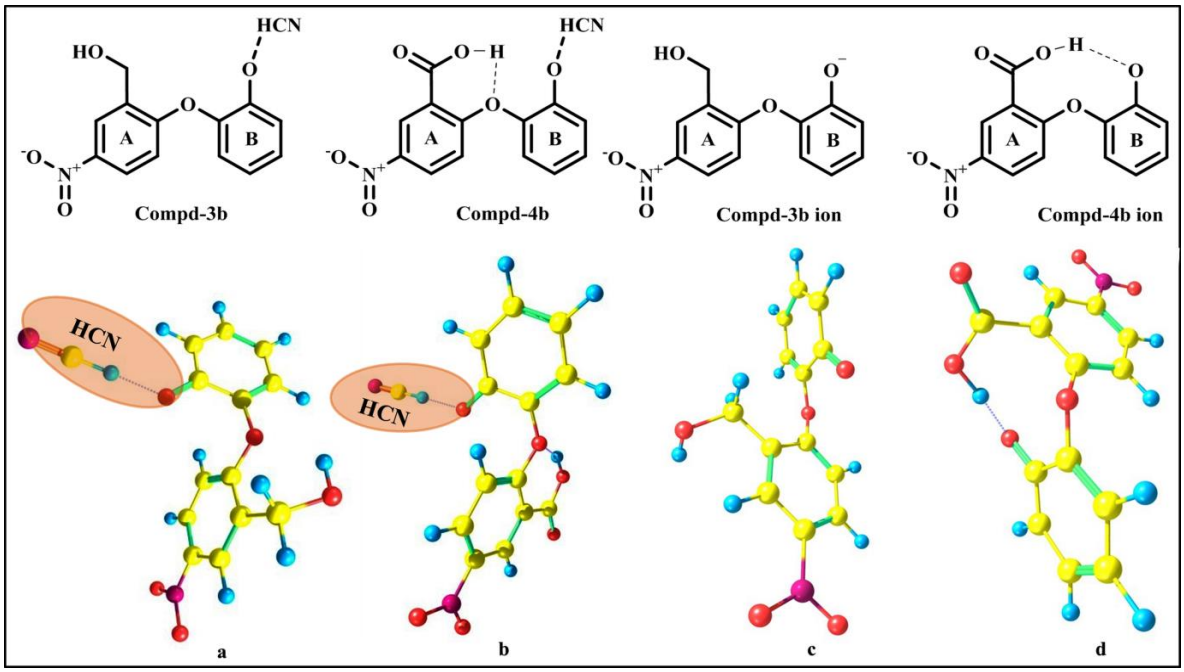

Figure-5.11: Structure optimization of compound-**3b** and **4b** with cyanide ion and its conjugate ions formed while the acidic proton was abstracted.

Therefore, it was hypothesized that the abstraction of the hydrogen bond donor groups by the cyanide ion leads to the neutralization of the delocalization by the other acidic protons present in the molecules, as shown in **Figure-5.4**. Therefore, the role of other active hydrogen bond donor groups was explored using theoretical calculations. Optimizing the anions corresponding to compounds-**3b** and **4b** displayed the neutralization of the delocalization for

compound-**4b** only, as shown in **Figure-5.11 (c)**. Compound-**3b**, however, did not display any contribution from the benzyl proton to stabilize the anion, as shown in **Figure-5.11 (d)**.

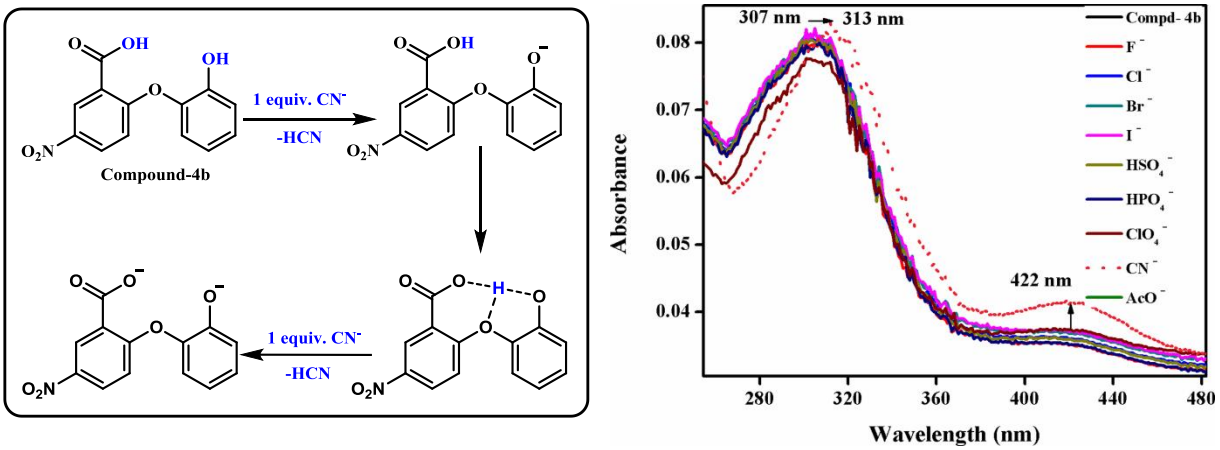

Figure-5.12: Proposed interaction of compound-4b with 1 & 2 equivalent of cyanide ions, b) absorption change were observed only when 2- equiv. of cyanide was used.

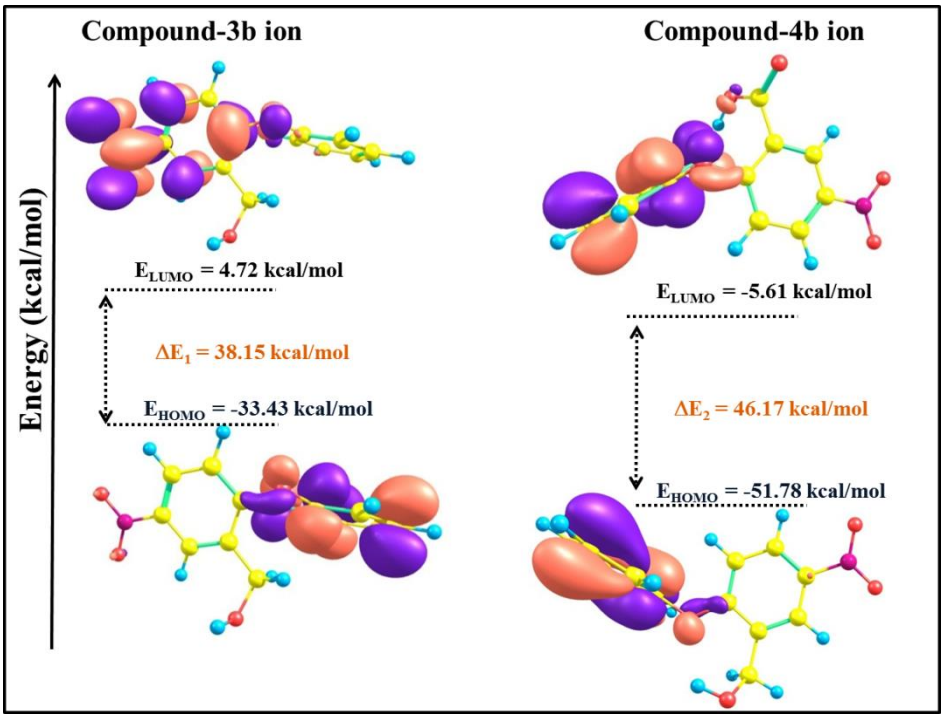

Figure-5.13: HOMO-LUMO energy orbital diagrams for the conjugate anions of compound-**3b** and **4b**.

The above observation was complemented by adding an excess of the cyanide ions, which gave a new peak corresponding to carboxylate anion, as for the compound-**4** above, at 422 nm. Thus, it can be concluded that the excess of the cyanide ions in **4b** abstracted the other acidic proton of the carboxylic acid to form carboxylate species that absorb at 422 nm **(Figure-5.12)**.

Further, the calculation of the energies for the HOMO and LUMO for the conjugate anions corresponding to **compounds 3b** and **4b** predicted a stable anion in the latter case **(Figure-5.12)**. The E_{HOMO} for the **4b** anion was minimum at -51.78 kcal/mol compared to **3b** at -33.43 kcal/mol. Moreover, the ΔE ($\Delta E = E_{LUMO}-E_{HOMO}$) value for **anion 4b** was high compared to compound-**3b**, accounting for no change in the absorption spectra compared to its native compound-**4b** on the addition of one equivalent of the cyanide ions.

The above calculations supported the experimental results indicating a small redshift for compound-**3b** and no change in the absorption properties for compound-**4b** under normal circumstances.

5.6. Conclusion

Seven diphenyl ethers containing one or two acidic protons were considered for the selective detection of the anions. The highlight of the study was the confirmed proton abstraction mechanism for compounds-**2** and **4** by the cyanide ions. Theoretical studies complemented the experimental results, as shown in **Figures 5.9** and **5.10**.

Compound-**2** was selective for the cyanide ions. The theoretical studies displayed a decrease in the energy difference of the HOMO and LUMO from 90.07 kcal/mol to 57.64 kcal /mol, complimenting the results. Titration studies gave the binding constant and detection limit $1.0 \times 10^4\ M^{-1}$ and 270 nM for compound-**2**.

Compound-**4**, however, responded to the presence of fluoride and acetate ions besides cyanide ions. Of all the three anions, the cyanide ion gave the best binding constant ($1.3\times10^5\ M^{-1}$) for compound-**4**. The detection limit of the cyanide ion (50 nM) was found to be comparable with the acetate (41nM) ions. The energy difference between HOMO and LUMO decreased by 10.42 kcal/mol upon binding with the cyanide ions. Both compounds detected the cyanide ions at a much lower limit than the WHO's permissible limit (1.9 μM).

Compounds-**3b** and **4b**, containing two acidic protons each, although responded to the cyanide ions' exclusive presence but did not give the required results upon titration with the anion for the quantitative estimation. It was hypothesized that the presence of other acidic proton's interference upon the conjugate anion's formation. Theoretical studies confirmed the above hypothesis in the case of compound-**4b**, but no evidence was available for compound-**3b**. Theoretical studies' results were further complimented by the addition of the excess cyanide ions in the solution of compound-**4b**, which gave an absorption peak in the carboxylate region, confirming the hypothesis of the interference due to other acidic protons.

Compound-**3c** did not detect any anion due to the absence of the hydrogen bond donor capability. At the same time, compound-**4c**, an amino acid, existed as a self-interacting zwitterionic species resisting interaction with any anion.

Overall, the above studies gave a detailed insight into the proton abstraction mechanism for the diphenyl ether derivatives by the anions in the presence of a single acidic proton, two acidic protons and quaternizable protons.

References

1. Evans, N. H.; Beer, P. D., *Angew. Chem. Int. Ed.* **2014**, *53*, 11716-11754.
2. Prabodh, A.; Sinn, S.; Biedermann, F., *Chem. Rev.* **2022,** *122*, 3459-3636.
3. Pitt, P.; Berry, H., *Postgrad. Med. J.* **1991**, *67*, 323.
4. Zheng, X.; Zhu, W.; Liu, D.; Ai, H.; Huang, Y.; Lu, Z., *ACS Appl. Mater. interfaces* **2014**, *6*, 7996-8000.
5. Xu, Z.; Chen, X.; Kim, H. N.; Yoon, J., *Chem. Soc. Rev.* **2010**, *39*, 127-137.
6. De Azevedo, L. C.; Reis, M. M.; Motta, L. F.; Rocha, G. O. d.; Silva, L. A.; de Andrade, J. B., *J. Agric. Food Chem.* **2007**, *55*, 8670-8680.
7. Liu, X.; Cooper, D. E.; Cluntun, A. A.; Warmoes, M. O.; Zhao, S.; Reid, M. A.; Liu, J.; Lund, P. J.; Lopes, M.; Garcia, B. A., *Cell* **2018**, *175*, 502-513.
8. Hayyan, M.; Hashim, M. A.; AlNashef, I. M., *Chem. Rev.* **2016**, *116*, 3029-3085.
9. Sauer, H.; Wartenberg, M.; Hescheler, J., *Cell. Physiol. Biochem.* **2001**, *11*, 173-186.
10. Rhoades, J.; Kandiah, A.; Mashali, A., *FAO, Rome* **1992**, *18*, 133-151.
11. Jones, J. E., *J. Exp. Biol.* **1941**, *18*, 170-181.
12. Kumar, A.; Chhibber, M., *ChemistrySelect* **2022**, *7*, e202104386.
13. Sharma, R.; Mittal, S. K.; Chhibber, M., *J. Electrochem. Soc.* **2015,** *162*, B248-B256.
14. Gale, P. A.; Busschaert, N.; Haynes, C. J.; Karagiannidis, L. E.; Kirby, I. L., *Chem. Soc. Rev.* **2014**, *43*, 205-241.
15. Beer, P. D.; Gale, P. A., *Angew. Chem. Int. Ed.* **2001**, *40*, 486-516.
16. Gale, P. A.; Quesada, R., *Coord. Chem. Rev.* **2006**, *250*, 3219-3244.
17. Ali, D. P.; Kruger, P. E.; Gunnlaugsson, T., *New J. Chem.* **2008**, *32*, 1153-1161.
18. Evans, L. S.; Gale, A.; Light, M. E.; Quesada, R., *Chem. Comm.* **2006**, *9*, 965-967.
19. Sharma, B. K.; Singh, P. S.; Kamble, R., *Progress in Chemical and Biochemical Research* **2020**, *3*, 296-318.
20. Kim, M.; Mergu, N.; Son, Y.-A., *J. Lumin.* **2018**, *204*, 244-252.
21. Yalçın, E. Seferoğlu, N. Seferoğlu, Z., *J. Mol. Struct.* **2018**, *1155*, 573-581.
22. Tummachote, J.; Punyain, W.; Sirikulkajorn, A.; Tomapatanaget, B., *Spectrochim. Acta A Mol. Biomol. Spectrosc.* **2019**, *214*, 384-392.
23. Chen, W.-H.; Pang, Y., *Tetrahedron Lett.* **2010**, *51*, 1914-1918.
24. Singh, P.; Brar, S. K.; Bajaj, M.; Narang, N.; Mithu, V. S.; Katare, O. P.; Wangoo, N.; Sharma, R. K., *Mater. Sci. Eng. C* **2017,** *72*, 590-600.
25. era, S. ue, . ehak, . acoby, . i, W. Shimon, L. . eck, . r l, P.; Cao, Y.; Gazit, E., *ACS nano.* **2020,** *14*, 1694-1706.
26. F. Edition, Guidelines for drinking-water quality. *WHO chron.* **2011**, *38*, 104-108.

Chapter-6

Graphical Abstract:

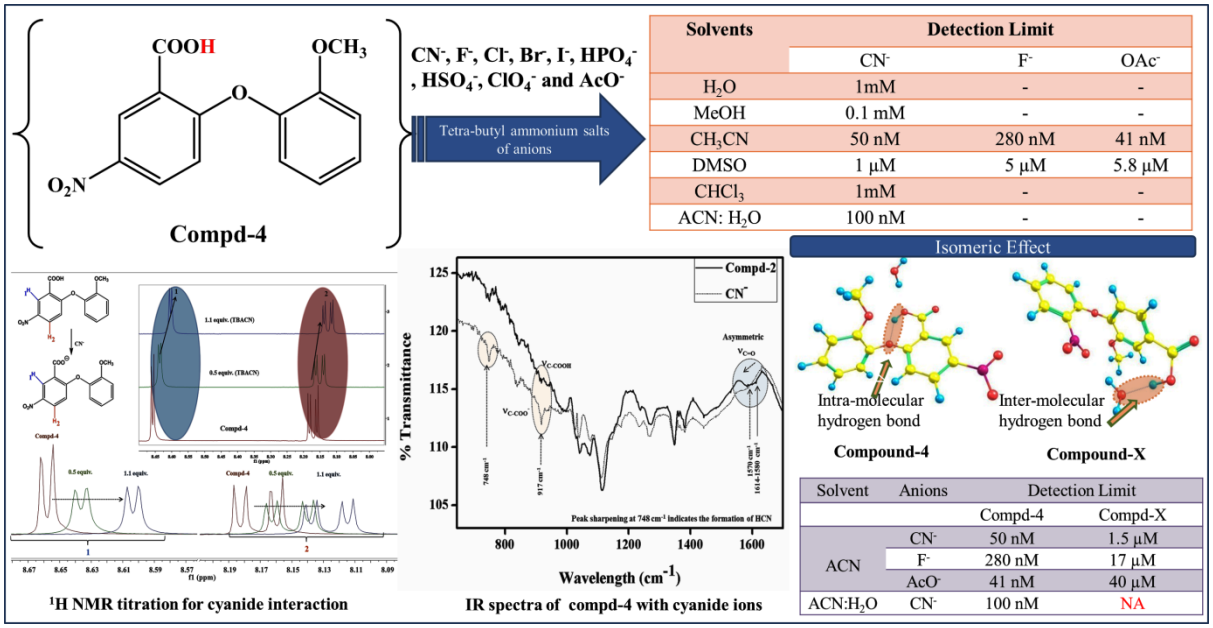

Chapter-6

OPTIMIZING 2-(2-METHOXY PHENOXY)-5-NITROBENZOIC ACID (COMPOUND-4) FOR THE SELECTIVE DETECTION OF THE CYANIDE IONS IN NEUTRAL SEMI-AQUEOUS MEDIUM

6.1. Introduction

The physical and chemical properties of the cyanide ion have made it an important species due to its incredible application in environment, life, synthesis and industry.[1] The use of compounds containing cyanide ions is prevalent in fertilizer, pesticide, pharmaceutical, electroplating, mining, plastic and many more industries.[2] The discharge of this ion from these units in the effluent and its accumulation in water, soil and air is a cause of concern due to cyanide induced toxic effects in both health and environment.[3] As mentioned in the previous chapter, the permissible limit for cyanide ions in drinking water is 1.9 μM.[4] The cyanide ions are known to damage the lungs, gastrointestinal tract and skin in humans.[5] This is evident from the reports where the interaction of the cyanide ions with the heme-proteins and the cytochrome a_3 affects many cellular processes of mammals.[6, 7] Therefore, there is a need to develop an efficient methods for the detection of cyanide anions.

Many organic ligands are known to respond to cyanide ions' presence by using optical, electrochemical and other spectroscopic techniques (NMR, IR, GC-MS, and HRMS etc.).[8] However, the poor solubility of most organic ligands in water and the solvation of the cyanide ions in an aqueous medium limit their development as sensors. Yet, many sensors have been developed to detect cyanide ions in an aqueous medium. **Table-6.1** below shows the structure, solvent system, detection limit and method used to detect cyanide ions.

Phenyl ether-based molecules are not very popular for detecting ions despite their ability to act as chromophores and a convenient synthesis route. As discussed in Chapter-2, despite the diphenyl ether skeleton offering unique advantages, few research groups have explored the use of diphenyl ethers to detect ions.[9]

The previous chapter highlighted the detection of anions by 2-(2-hydroxy phenoxy)-5-nitrobenzaldehyde **(**compound-**2)** and 2-(2-methoxy phenoxy)-5-nitrobenzoic acid **(**compound-**4)**.

Table-6.1: Comparison of organic receptors for CN^- ions detection in different solvents.

Receptors	Solvent system	Technique Used	Limit of detection (M)	Reference
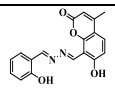 Azine 7-hydroxy-8-((*E*)-(((*E*)-2-hydroxybenzylidene) hydrazono)methyl)-4-methyl-2*H*-chromen-2-one	DMSO:H_2O (7:3)	UV-Visible & Fluorescence	1.69×10^{-7}	10
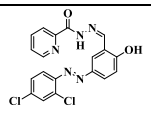 Azo *N*'-((*Z*)-5-((*E*)-(2,4-dichlorophenyl)diazenyl)-2-hydroxybenzylidene)picolinohydrazide	DMSO:H_2O (6:4)	UV-Visible	6.4×10^{-6}	11
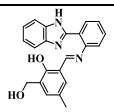 Benzaimidazole (*E*)-2-(((2-(1*H*-benzo[*d*]imidazol-2-yl)phenyl) imino)methyl)-6-(hydroxymethyl)-4-methylphenol	ACN: H_2O (9:1)	Fluorescence	37×10^{-9}	12
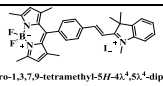 Bodify (*E*)-2-(4-(5,5-difluoro-1,3,7,9-tetramethyl-5*H*-4λ^4,5λ^4-dipyrrolo[1,2-*c*:2',1'-*f*] [1,3,2]diazaborinin-10-yl)styryl)-1,3,3-trimethyl-3*H*-indol-1-ium iodide	EtOH: H_2O (9:1)	UV-Visible & Fluorescence	1.59×10^{-9}	13
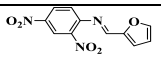 Imine (*E*)-*N*-(2,4-dinitrophenyl)-1-(furan-2-yl)methanimine	ACN	UV-Visible	4.12×10^{-6}	14
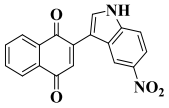 Indole 2-(5-nitro-1*H*-indol-3-yl)naphthalene-1,4-dione	DMF: H_2O (1:1)	UV-Visible & Fluorescence	2.1×10^{-9}	15
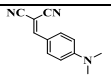 Malononitrile 2-(4-(dimethylamino)benzylidene)malononitrile	H_2O	UV-Visible	6.17×10^{-7}	16
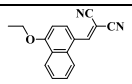 Napthalene 2-((4-ethoxynaphthalen-1-yl)methylene)malononitrile	THF: H_2O (9:1)	UV-Visible & Fluorescence	1.1×10^{-6}	17
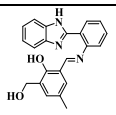 Napthalimide (*E*)-2-(((2-(1*H*-benzo[*d*]imidazol-2-yl)phenyl)imino)methyl)-6-(hydroxymethyl)-4-methylphenol	ACN: H_2O (9:1)	UV-Visible	1.45×10^{-6}	12
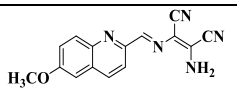 Quinoline 2-amino-3-(((*E*)-(6-methoxyquinolin-2-yl)methylene)amino)maleonitrile	DMSO:H_2O (2:1)	UV-Visible	5.3×10^{-6}	18
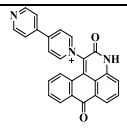 1-(2,7-dioxo-2,7-dihydro-3*H*-naphtho[1,2,3-*de*] quinolin-1-yl)-[4,4'-bipyridin]-1-ium	ACN	Voltameter	28×10^{-6}	19
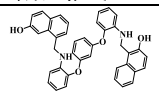 8-(((2-(3-(2-(((2-hydroxynaphthalen-1-yl)methyl)amino)phenoxy)phenoxy)phenyl)amino)methyl)naphthalen-2-ol	ACN: H_2O (9.9:0.1)	Voltameter	0.4×10^{-6}	20
Diphenyl ether 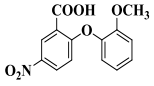 2-(2-methoxyphenoxy)-5-nitrobenzoic acid	ACN	UV-Visible	50×10^{-9}	21
	ACN: H_2O (9.5:0.5)		100×10^{-9}	

The former selectively detected the cyanide ions while later could detect fluoride and acetate ions besides cyanide ions. It was envisaged to optimize both the compounds for detection in the aqueous medium for broader applications.

Preliminary studies for the aqueous solubility with 10 μM of compound-**2** did not give any encouraging results due to the precipitate formation. On the other hand, 20 μM of compound-**4** gave a clear aqueous solution with an absorption pattern similar to the one obtained in the acetonitrile medium, as shown in **Figure-6.1**.

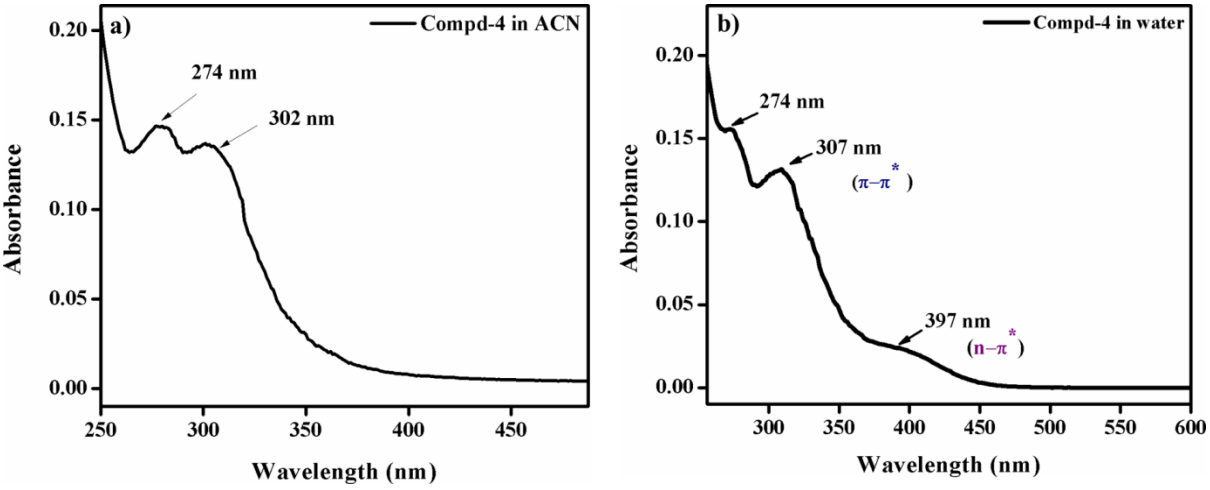

Figure-6.1: Absorption spectrum of compound-**4** in acetonitrile and 99% aqueous medium.

This chapter describes the optimization of compound-**4** for the selective detection of cyanide ions in the aqueous medium.

6.2. Preliminary Spectroscopic Studies

Studies with compound-**4** to explore the selectivity for any of the three anions were initiated using absorption studies at different pH.

6.2.1. <u>Effect of pH</u>: Compound-**4** displayed an absorption band at 274 and 307 nm in the aqueous medium with a small hump at 397 nm **[Figure-6.2 (a)]** in the UV-Visible absorption studies. This required exploration under different pH conditions to understand its behaviour. In the alkaline solution (pH 8.0 to 10.0), the hump at 397 nm displayed an increase in its intensity, while no change was observed in the case of acidic pH as shown in **Figure-6.2 (b)** (pH 6.1& 4.0). The increased intensity at 397 nm in the alkaline medium can be attributed to the formation of the carboxylate anion **[Figure-6.2 (c)]** as a result of the abstracted proton from the carboxylic acid. Studies in the presence of HEPES buffer in pH 7.0 to 8.5 showed no absorption change while anions were added. Thus, compound-**4** in the normal pH range

(7.0 to 8.0) displays a tendency to show a new band in the range of 395-415 nm in the presence of a specific anion that can abstract a proton.

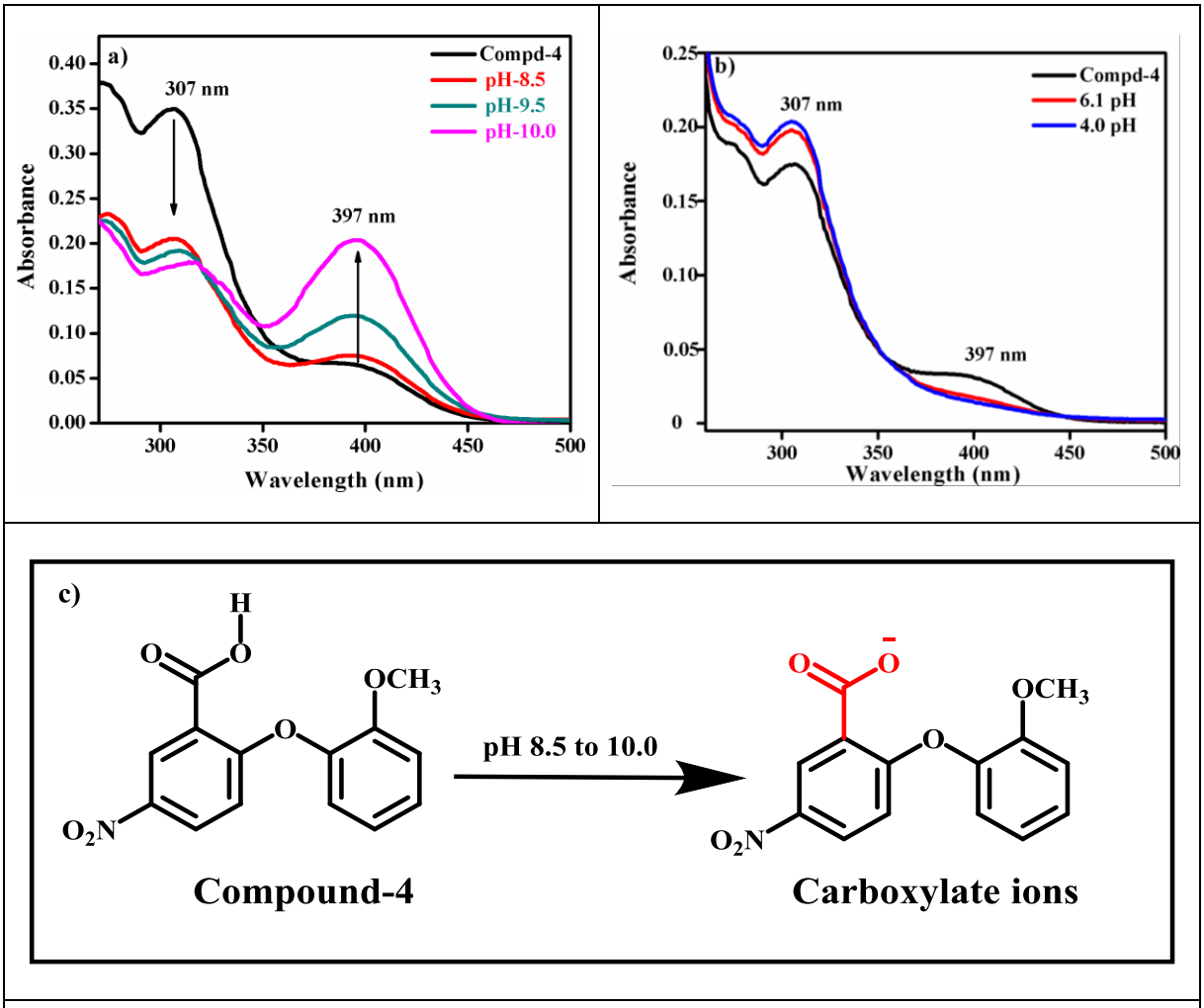

Figure-6.2: Absorption behavior of compound-**4** at **a)** alkaline and **b)** Acidic pH. **c)** Formation of the carboxylate anion of compound-**4** in alkaline medium.

The above studies concluded compound-**4** might have broader applicability for detecting anions in the neutral pH range of 7.0 to 8.0.

6.2.2. <u>Effect of Solvents</u>: The optimization required to study compound-**4** in different solvents. The absorption properties of compound-**4** in the commonly used protic and aprotic solvents were analyzed to explore selectivity for the anions. **Figure-6.3** shows the selectivity detection of the cyanide ions in the presence of protic solvents methanol, water and chloroform. In contrast, DMSO, an aprotic solvent, gave no selectivity as reported earlier in the ACN medium.

Table-6.2 shows the minimum quantity of any anion required to reflect a change in absorption properties of compound-**4**. The detection of three ions (F^-, CN^- and AcO^-) in

aprotic solvents can be due to the polarization of the carboxylic group. This facilitates less solvated anions to conveniently abstract the proton from compound-**4** to form **species x (Scheme-6.1)**. Interestingly, the higher polarization of compound-**4** (not shown in Table-6.2) in DMSO can detect phosphate ions at 0.1 mM concentrations **[Figure-6.4 (a)]**. On the other side, higher solvation of F^- and AcO^- ions in protic solvents (water, methanol and chloroform) restrict proton abstraction from compound-**4** as compared to less solvated CN^- ions. The results align with the studies carried out by Pliego and Riveros who have reported that $\Delta G^\circ_{solvation}$ for fluoride, cyanide and acetate anions is comparatively lower in aprotic than in protic solvents.[22]

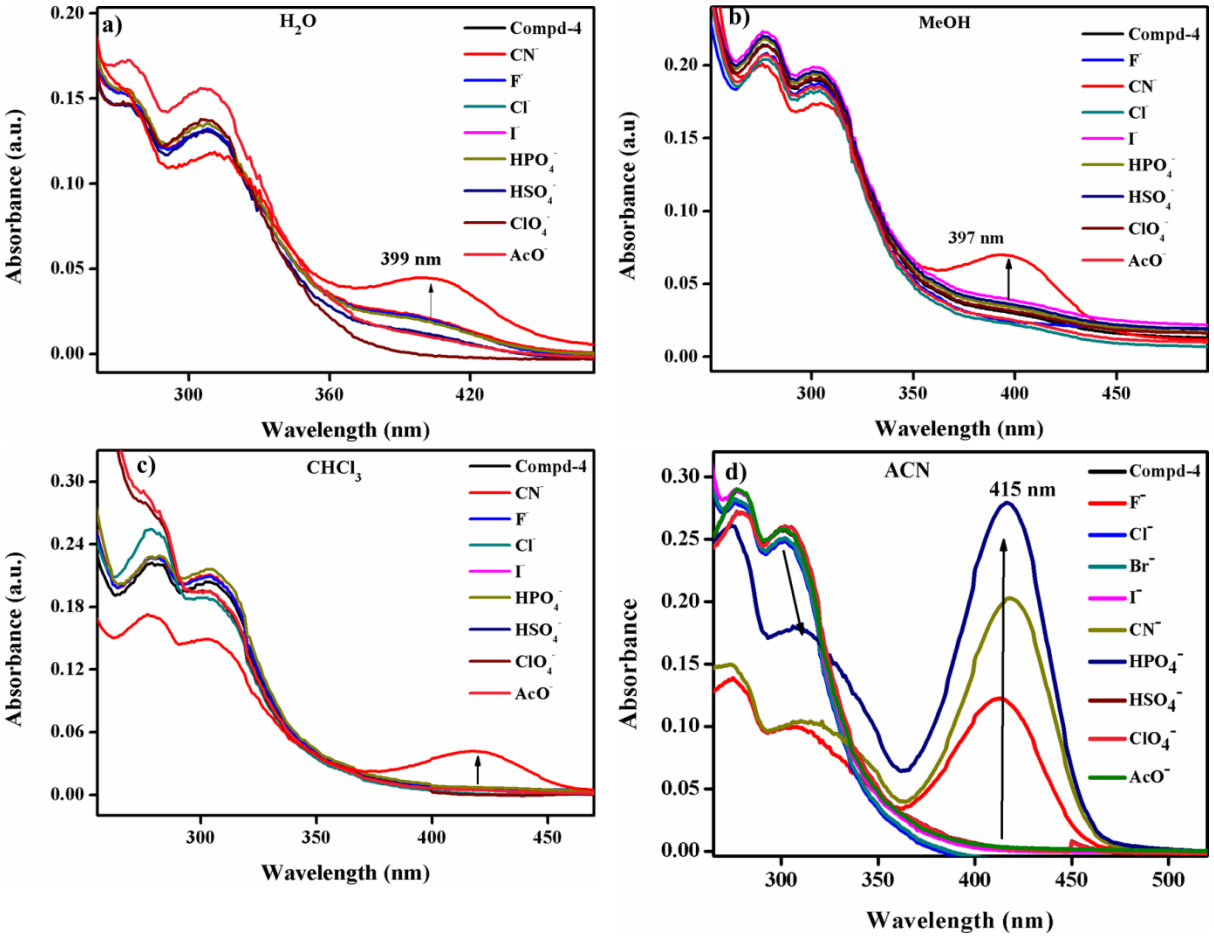

Figure-6.3: Absorption spectra of compound-**4** with Tetrabutylammonium salts of anions in different solvent systems **a)** H_2O **b)** MeOH, **c)** $CHCl_3$ **d)** ACN.

The selective detection of ions in an aqueous medium is always advantageous. However, Compound-**4** selectively detects cyanide ions in a 100% aqueous medium was insignificant due to the millimolar detection level **(Table-6.2)**.

Table 6.2: Comparative results for the minimum detection limit of compound-**4** for CN^-, F^- and AcO^- ions in different solvents.

S. No.	Solvents	Detection Limit (nM)		
		CN^-	F^-	OAc^-
1	H_2O	1×10^6	-	-
2	MeOH	1×10^5	-	-
3	**CH_3CN**	**50**	**280**	**41**
4	DMSO	1×10^4	5×10^4	5.8×10^4
5	$CHCl_3$	1×10^6	-	-
6	**ACN: H_2O (95:5)**	**1×10^2**	-	-

However, this did not discourage us from developing a solvent system for detecting cyanide ions with an optimal detection range. Initial experiments with different ratios of ACN:Water (95:5, 90:10 and 80:20) gave a notable detection of up to 100 nM for the cyanide ions in the 95:5 system **[Figure-6.4 (b, c & d)]**. Thus, further studies were carried out in the optimized solvent system described in the following paragraphs.

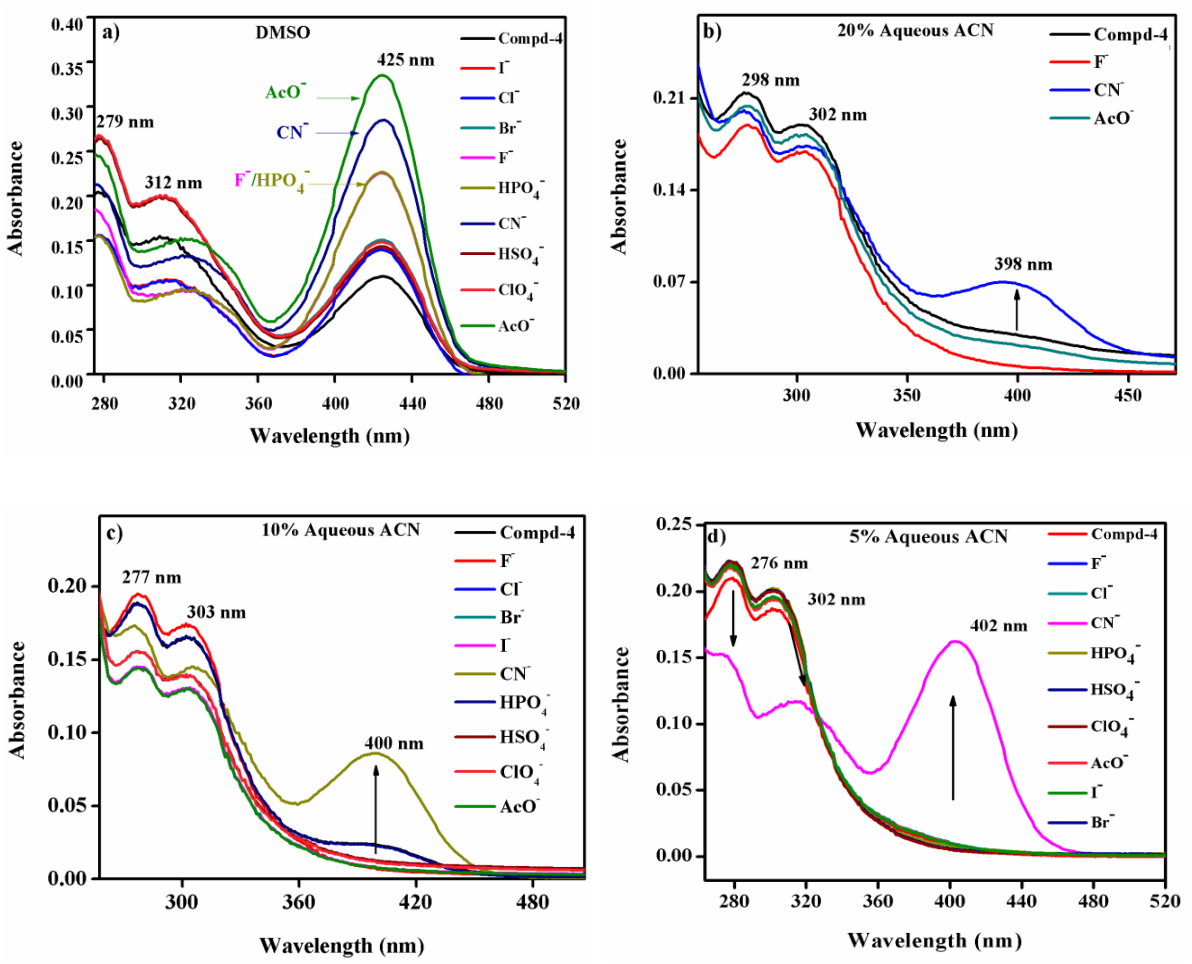

Figure-6.4: Absorption spectrum of compound-**4** with Tetrabutylammonium salts of anions using different solvent system **(a)** in DMSO, **(b)** in 20% Aqueous ACN, **(c)** in 10%Aqueous ACN, **(d)** in 5%Aqueous ACN.

6.3. Photo-physical Studies in an Aqueous Medium

Absorption studies with 33 equivalents of tertiary butyl ammonium salts of different anions (F^-, Cl^-, Br^-, I^-, CN^-, OAc^-, HPO_4^-, HSO_4^- and ClO_4^-) using 20 µM of compound-**4,** were carried out in 5% aqueous ACN **[Figure-6.4 (d)]**. Quenching of the native peaks at 276 nm and 302 nm was observed with the simultaneous appearance of a new peak at 402 nm in the presence of cyanide ions. Comparing **Figure-6.3 (d)** and **Figure-6.4 (d)**, no change in the absorption pattern is visible except a blue shift of 13 nm for a 415 nm peak when the 5% aqueous ACN solvent system is switched over from the ACN system discussed in chapter-3.

Interference studies were carried out to explore the detection of cyanide by compound-**4** in the presence of other competing ions (10 equivalents). As shown in **Figure-6.5**, no interference was observed with any of the anions except in case of sulphate. This was due to the highly acidic proton of the sulphate that could replace the abstracted proton from carboxylic acid as discussed above in **Figure-6.2 (b)**. Interestingly, the phosphate anion did not interfere due to its less acidic proton and thus were unable to replace the abstracted proton of the carboxylate in the aqueous medium.

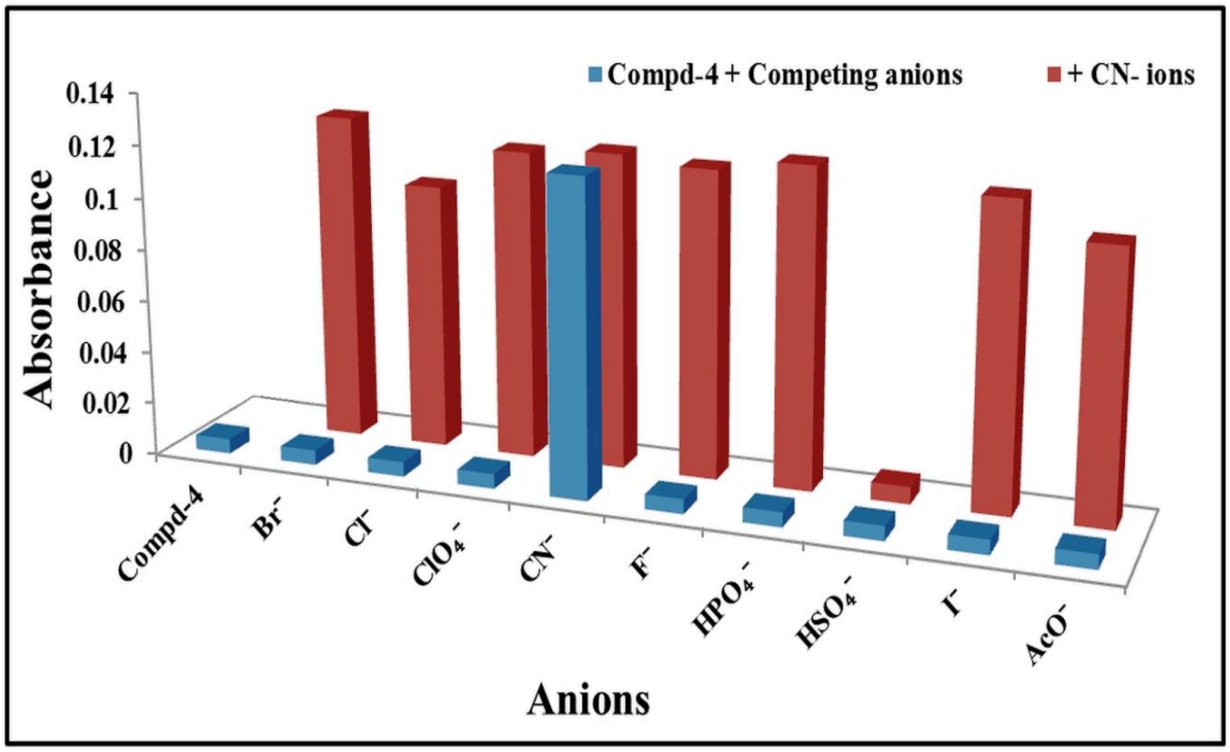

Figure-6.5: Interference studies with competing anions. The blue bars represent the absorption intensity of compound-**4** at 402 nm with 10 equiv of competing anions. The red bar represents the absorption intensity of compound-**4** after the addition of 1 equiv. of CN^- ion in **[**Compound-**4-competing ion]** solution.

6.3.1. Titration studies

Titration studies to quantify the minimum detection limit, were carried out using the sequential addition of cyanide ions in 20 µM of compound-**4** in the optimized solvent system (ACN: H_2O = 95:5 v/v). **Figure-6.6 (a)** shows an isosbestic point at 319 nm as quenching at 276 nm and 306 nm was observed with the consecutive appearance of a new peak at 402 nm. No further change in the absorption spectrum was observed beyond 33 µM (1.65 equivalents) addition of the cyanide ions until saturation point. A minimum detection limit at 0.1 µM using an IUPAC-approved equation was obtained from the linear plot between the change in absorbance (at 415 nm) vs concentration of cyanide ions as shown in **Figure-6.6 (b).**

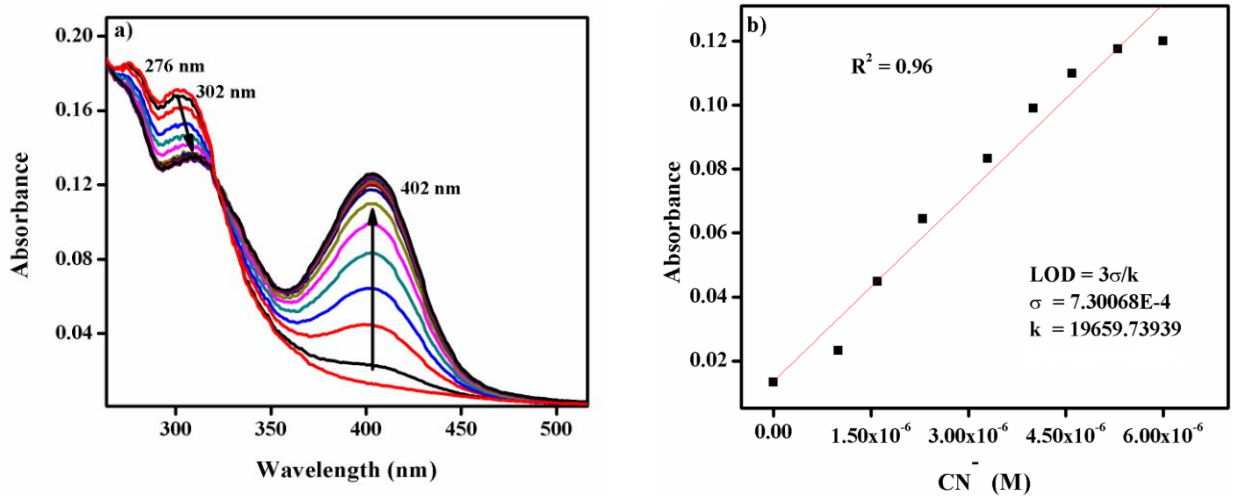

Figure-6.6: a) Titration of **compound-4** (20 µM) with the sequential addition of cyanide ions in 5% aqueous ACN. b) Linear plot for the [CN^-] at 402 nm to determine minimum detection limit for cyanide ions with **compound-4**.

6.3.2. Binding Behaviour and Stoichiometry

The use of the Benesi-Hildebrand equation gave the binding affinity of the cyanide ions as 0.5×10^5 M^{-1} **[Figure-6.7 (a)]** in the 5% aqueous ACN medium. Overall, the aqueous medium enhanced the selectivity of compound-**4** with a little compromise on its binding affinity. The affinity was reduced by half compared with the pure acetonitrile medium, as reported in the previous chapter (1.3×10^5 M^{-1}). The reduced binding affinity can be attributed to the more significant solvation of compound-**4** and the cyanide ions on changing the medium from pure ACN to the 5% aqueous ACN. This is also reflected in lowering the detection limit from 50 nM to 100 nM when the medium was replaced as shown in **Table–4.2** above. Stoichiometry studies using Job's plot **[Figure-6.7 (b)]** method gave maxima at 0.5 equivalents indicating 1:1 stoichiometry for the cyanide ion and compound-**4**.

6.4. Emission Studies

An emission study of compound-**4** was performed to distinguish the interaction of anions. As evident from the Y-axis in **Figure-6.8 (a)**, a weak emission was observed at 381nm on excitation at 305 nm. As compared to 20 µM in the absorption studies, emission studies required a higher concentration (60 µM) in the aqueous ACN medium. The selectivity of compound-**4** for the cyanide ions corroborated with a significant blue shift of 22 nm (381nm to 359 nm) along with a new peak at 448 nm in the emission spectrum. Further, excitation around 415 nm did not reveal emission properties for the **[**compound-**4**-CN^- **ion]** system. Constrained by the low-intensity emission of compound-**4,** limited studies were performed (titration) to calculate the minimum detection limit and their association constant. Sustainable quenching was observed in the fluorescence intensity of compound-**4** (60 µM) on the sequential addition of cyanide ions **[Figure-6.8 (b)]**. As calculated from the linear graph, the Detection limit and the association constant for CN^- ions were 1.5 µM and 0.2 × 10^5 M^{-1}, respectively **[Figure-6.8 (c &d)]**.

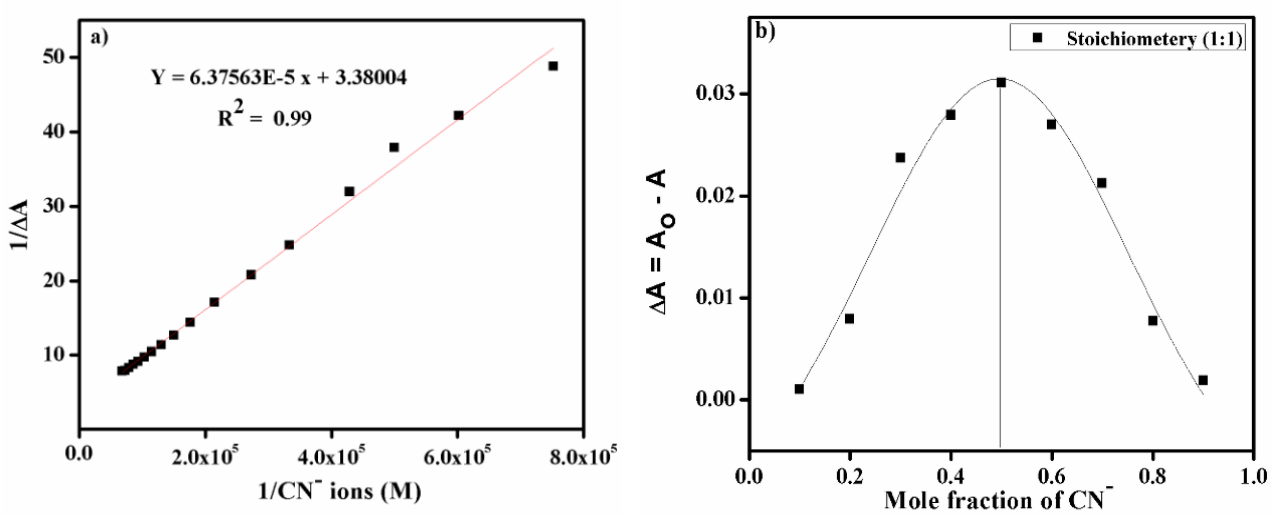

Figure-6.7: a) The binding constant of the cyanide ions with **compound-4** was found to be 0.5 × 10^5 M^{-1} using the Benesi-Hildebrand plot. **b)** Job's plot gave maxima at 0.5 equivalents indicating 1:1 stoichiometry for the cyanide ion and **compound-4**. Studies were done in 5% aqueous ACN.

Emission studies were considered insignificant and not taken up further due to the low response of **compound-4,** which gave ten times the lower value for the binding constant and the detection limit.

6.5. Mechanism of Interaction

As discussed in the previous chapter, a proton abstraction mechanism is also proposed in this case. To authenticate the hypothesis, the methyl ester of compound-**4,** compound-**4a,** was

synthesized **(Chapter-2),** which did not respond to any of the anions due to the absence of acidic proton, as shown in **Scheme–6.1**.

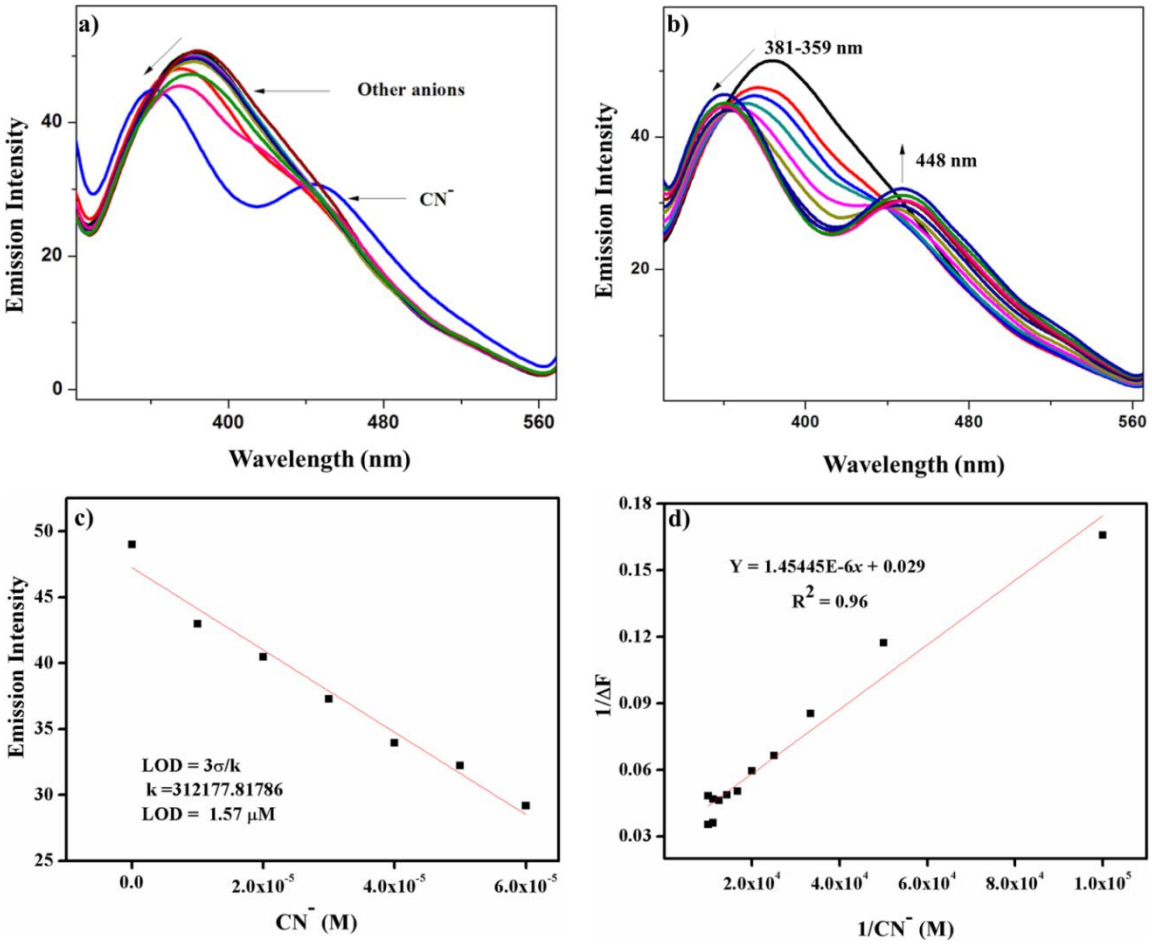

Figure-6.8: a). Fluorescence interaction studies of anions with compond-**4** (60 μM). **(b)** Titration spectrum of compound-2 with the sequential addition of cyanide anions in 5% aqueous ACN. **(c)** Linear plot between the intensity versus the concentration of CN^- ions at 359 nm to determine minimum detection limit. **(d)** The binding constant of the cyanide ions with compound-**4** was found to be $0.2 \times 10^5 M^{-1}$ using fluorescence.

We further hypothesized that the optimum nucleophilicity due to the presence of the nitro group facilitated the abstraction of a proton from the carboxylic group in compound-**4.** Therefore compound-**X,** a positional isomer of compound-**4**, was synthesized carrying the carboxylic acid group on the diphenyl ether ring that did not hold a nitro group. However, in a 5% aqueous ACN medium, no detection for any of the anions was observed. Compared to compound-**4**, the absence of intramolecular hydrogen bonding between ethereal oxygen and carboxylic acid proton, confirmed later by theoretical studies, prevented compound-**X** from responding in the aqueous medium. Interestingly, compound-**X** was selective for the same three anions (CN^-, F^- and AcO^-) as compound-**4** was when explored in the presence of anions (F^-, Cl^-, Br^-, I^-, CN^-, OAc^-, HPO_4^-, HSO_4^-, ClO_4^-) under similar conditions.

Scheme-4.2

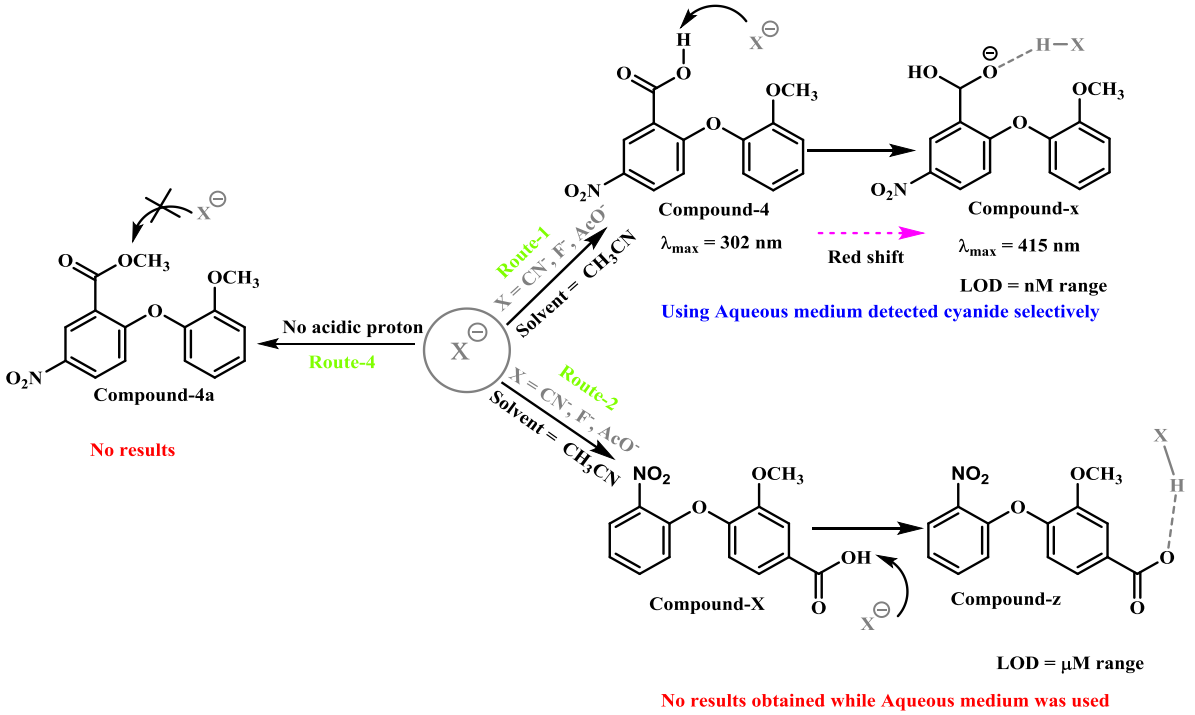

Scheme-6.1: Representation of diphenyl ether derivatives for anion sensing and cause of their anionic interaction.

However, the detection limit was one thousand times lower than compound-**4 (Table-6.3).** Thus, it can be concluded that the carboxylic proton in compound-**4** is more selective than one in compound-**X**. It can be attributed to the presence of the nitro group on the same ring as carboxylic acid in compound-**4**. For compound-**X**, on the other hand, the nitro group exerts an electron-withdrawing effect remotely through the nitro phenyl group on the carboxylic acid proton due to its presence on another aromatic ring.

Table-6.3: Minimum detecton limit for compound-**4** and **4c** with cyanide, fluoride and acetate ions in acetonitrile medium.

Anions	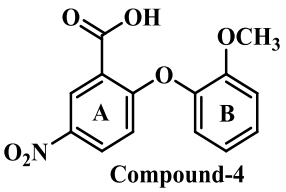 Compound-4	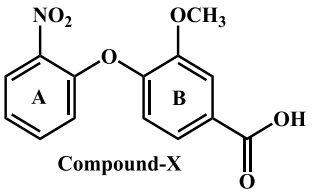 Compound-X
	Detection Limit in ACN medium	
	(nM)	**(µM)**
CN^-	50 nM	1.5 µM
F^-	280 nM	17 µM
AcO^-	41 nM	40 µM

6.6. NMR Titration

Further, to establish the proton abstraction mechanism, as discussed in the previous chapter, the ^{1}H NMR spectroscopic titration of compound-**4** with cyanide ions was performed.

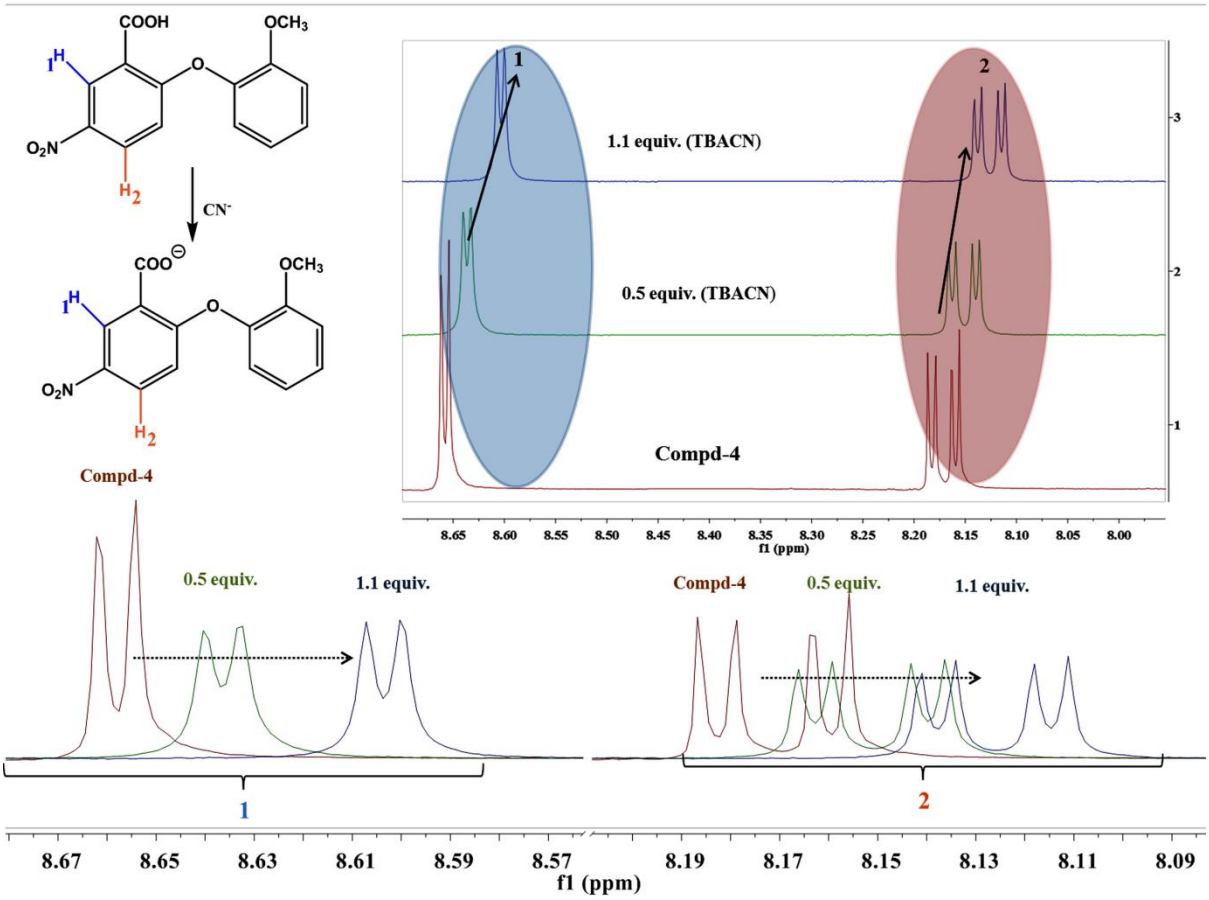

Figure-6.9: ^{1}H NMR titration of **compound-4** with 0.5 and 1.1 equivalent of the cyanide ions shows an up field shift due to the formation of the carboxylate ion.

Figure-6.9 displays major aromatic peaks that showed an up-field shift due to the formation of carboxylate ions by adding 0.5 and 1.1 equivalents of the cyanide ions. Peaks at 8.67 and 8.17 ppm corresponding to protons-1 and 2 **(Figure-6.9)** drifted up-field to 8.60 and 8.13 ppm. It can be attributed to the formation of the carboxylate anion and hence enhanced electron density. These results justified the UV-Vis spectroscopic studies for the formation of a new peak at 397 nm at pH 8.0 to 10.0 [**Figure-6.2 (a)]** and at 415 nm in the presence of the cyanide ions. Carboxylic proton appearing at 11.16 ppm were not observed in the titration studies **(Figure-6.10)**. Although proton-1 and proton-2 displayed significant up-field drift due to the formation of the carboxylate ion, other aromatic peaks in ring-A also drifted slight up-

field, as evident from the complete scan of the NMR spectrum (**Figure-6.10)**. The shifting of the peaks in ring B was negligible.

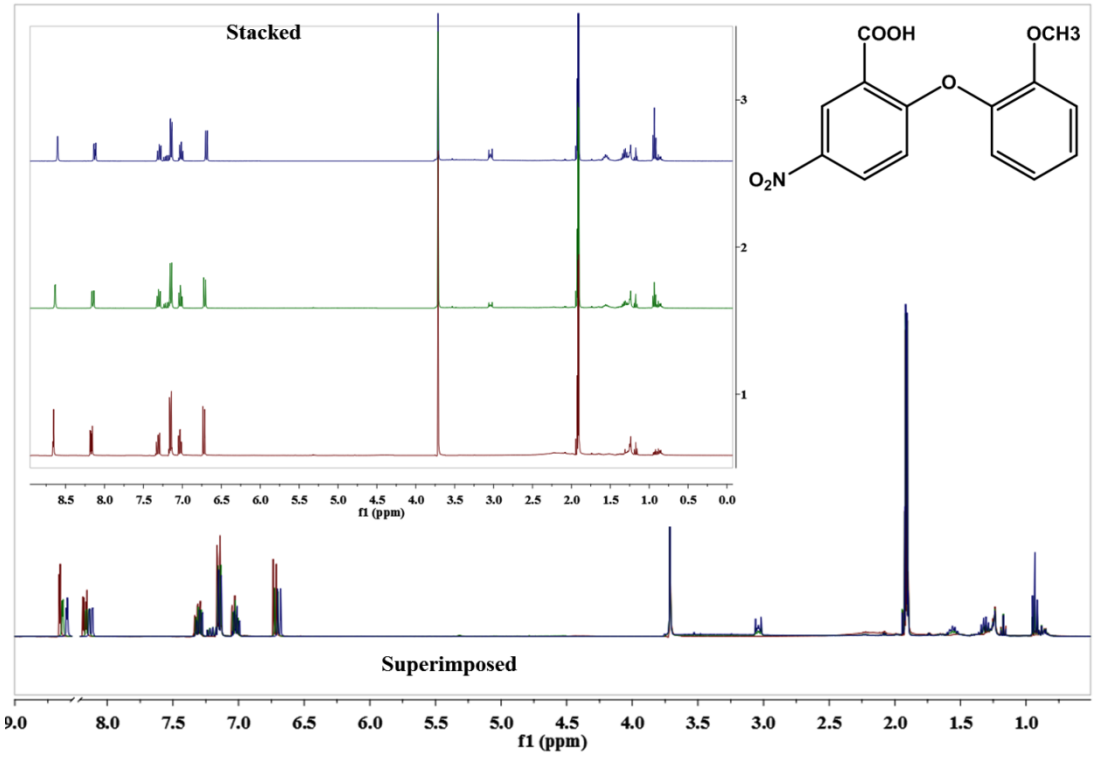

Figure-6.10: Representation of Full ^{1}H NMR titration spectra of compound-**4** with 0.5 and 1.1 equivalent of terta-butylammonium cyanide in superimposed and stacked form.

Acid-base titration studies were observed using ^{1}H NMR spectra to confirm the proton abstraction mechanism further. It was envisioned that if the above hypothesis is correct, the abstraction of the carboxylic proton in compound-**4** by a strong base, sodium hydroxide, will give a similar pattern as the above. The aromatic protons titrating in CD_3CN solution of compound-**4** with OH^- ions (NaOH) gave a similar graph as shown in **Figure-6.11,** confirming proton abstraction. The larger shift in the case of OH^- ions (0.4 ppm to 0.04 ppm) than the CN^- ions (0.02 ppm) at 0.5 equivalent concentrations of the anions can be attributed to the exceptional acidic proton abstraction capability of the OH^- ions as compared to the CN^- ions. It also suggests relatively partial abstraction in the case of the CN^- ions.

6.7. IR Studies

Infrared spectroscopy further corroborated the proposed mechanism. The dotted line in **Figure-6.12** represents adding 1 equivalent of the cyanide ions in a diethyl ether solution of compound-**4** compared with native its IR spectra (Continuous line). A new peak for the HCN

emerged with the addition of the cyanide ions at 748 cm^{-1}.[23] The intensity of the (Ar)**C-COOH** stretch increased at 917 cm^{-1} on adding the cyanide ions.

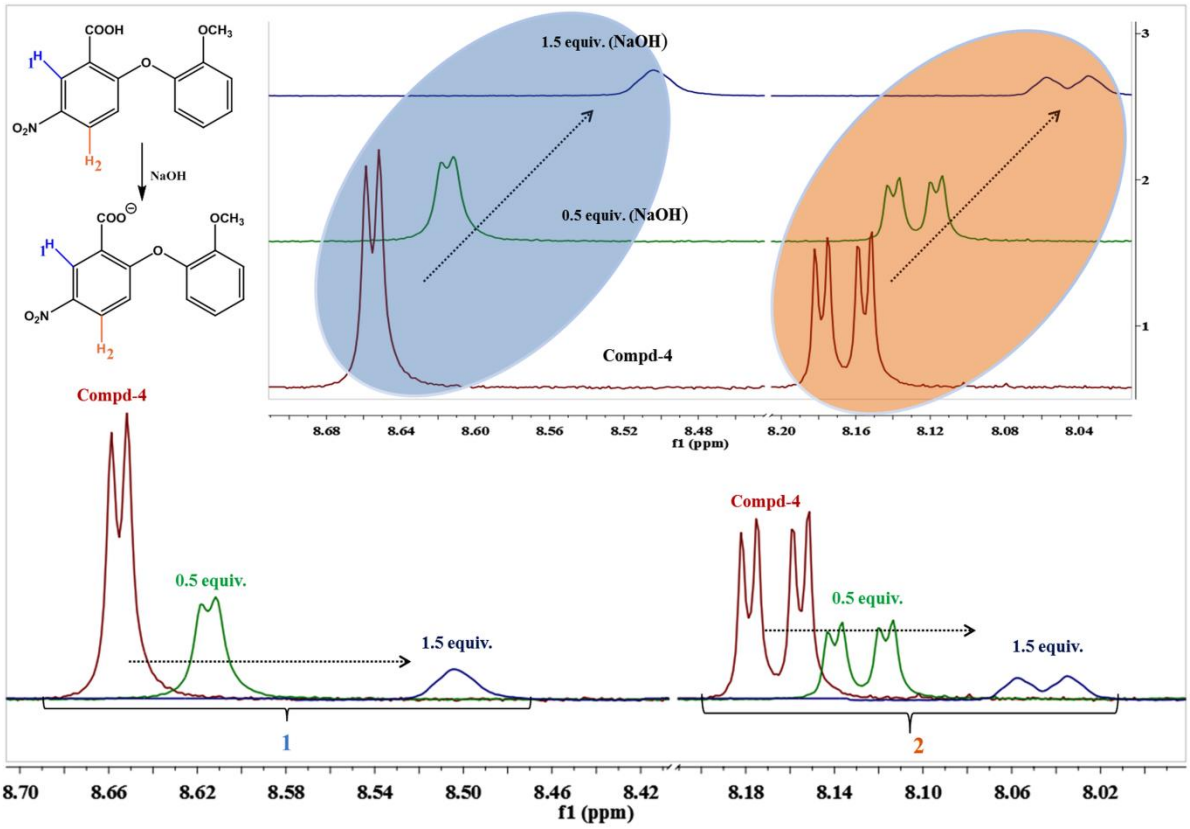

Figure-6.11: ^{1}H NMR titration of compound-**4** with 0.5 and 1.5 equivalents of the hydroxide ions to validate the cyanide pattern observed with the up field shift via carboxylate formation.

It accompanied a shift of the C=O signal from 1614 cm^{-1} to 1570 cm^{-1} due to the carboxylate anion formation.[23] Thus, the peaks of HCN and the carboxylate ions in the IR spectra supported the deprotonating mechanism.

6.8. Theoretical Studies

The exceptional ability of compound-**4** compared with positional isomer (compound-X) to selectively detect cyanide ions in the aqueous medium (**Sr. No. 1 & 6, Table 6.2**) required further exploration. Therefore, the minimum energy of both compounds was calculated with Gaussian-16 software using the B3LYP method and the 6-31*G (d) basis set.

Further, stereochemistry-based analysis of compound-**4** suggested two conformations assigned as **OH-IN** and **OH-OUT**, as shown in **Table-6.4**. Of all the three structures, including compound-**X**, the zero-point energy was minimum for compound-**4** (**OH-IN**), as

shown in **Table-6.4.** The **OH-IN** conformer was 290 kcal/mol, more stable than the OH-OUT conformer suggesting its prominent existence.

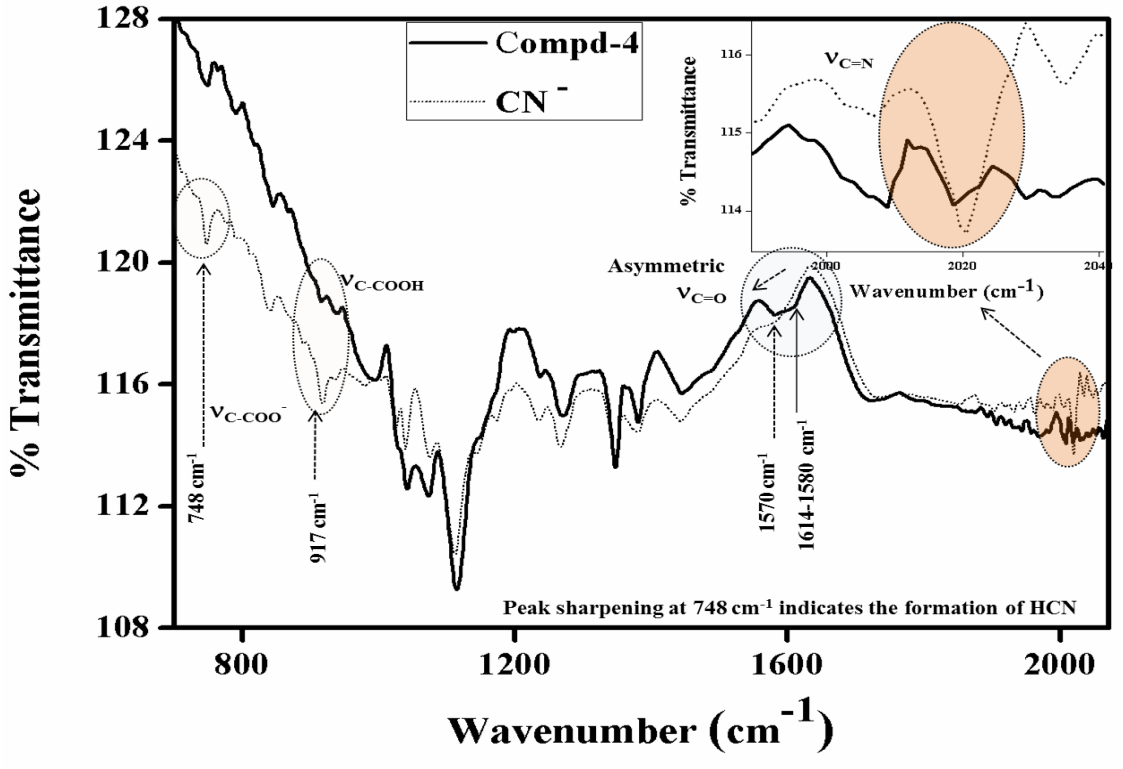

Figure-6.12: IR spectra of the compound-**4** (diethyl ether solution) upon addition of 1 equivalent of the cyanide ions (dotted line) compared to its native (continuous line)

Table-6.4: Comparative zero-point energy calculation for all the three conformers **OH-IN**, **OH-OUT** or **Compound-X**.

S.No.	Compounds	E+ZPE (Hartree)	
1.	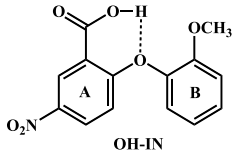 OH-IN	-1045.907707	$\Delta E_{(OH\text{-}IN)\text{-}(OH\text{-}OUT)}$ = 0.333 (209 kcal/mol)
2.	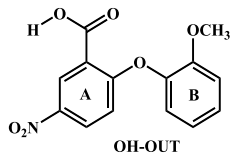 OH-OUT	-1045.574411	
3.	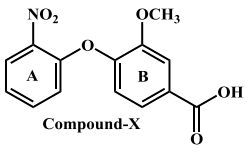 Compound-X	-1045.889509	NA

The above results were further complemented by calculating the energies of the HOMO-LUMO orbitals for the conformers **OH-IN** and **OH-OUT** along with compound-**X**, as shown

in **Figure-6.13**. The **ΔE** for the HOMO-LUMO of the three structures were 96.41 kcal/mol ($\Delta E_{OH\text{-}IN}$), 82.09 kcal/mol ($\Delta E_{OH\text{-}OUT}$) and 83.99 kcal/mol. The maximum value of **ΔE** for the **OH-IN** conformer further corroborated the above observation suggesting its maximum stability.

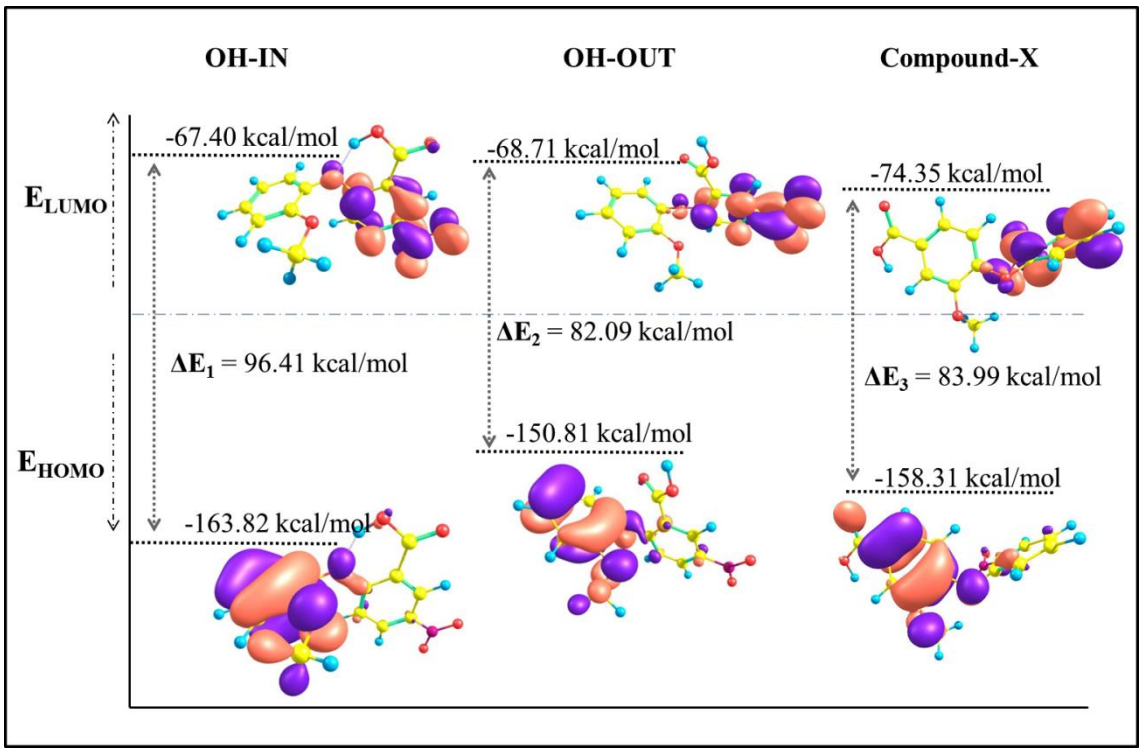

Figure-6.13: Minimum energy diagram of HOMO-LUMO orbitals for three conformers **OH-IN**, **OH-OUT** and compound-**X.**

As evident from minimized structures, the exceptional stability and the ability of the compound-**4,** compared to compound-**X**, to respond selectively in an aqueous medium can be attributed to the intramolecular hydrogen bonding between ethereal oxygen and carboxylic acid proton, as shown in **Figure-6.14**.

Further, the solvation behaviour was studied using theoretical calculation of both compounds in the presence of a water molecule. Interestingly, while carboxylic acid proton in compound-**X** displayed interaction with the water molecule **[Figure-6.14 (e)]**, no such interaction was observed for compound-**4,** as shown in **Figure-6.14 (d)**. It was due to the engagement of the carboxylic acid proton with the diphenyl ether's ethereal oxygen, thus complementing the above conclusions. Experimental results to calculate the pKa for both the compounds in an aqueous medium further confirmed the less lability of acidic proton for compound-**4** (pK_a = 6.65) compared to compound-X (pK_a = 6.22) due to the intramolecular hydrogen bonding.

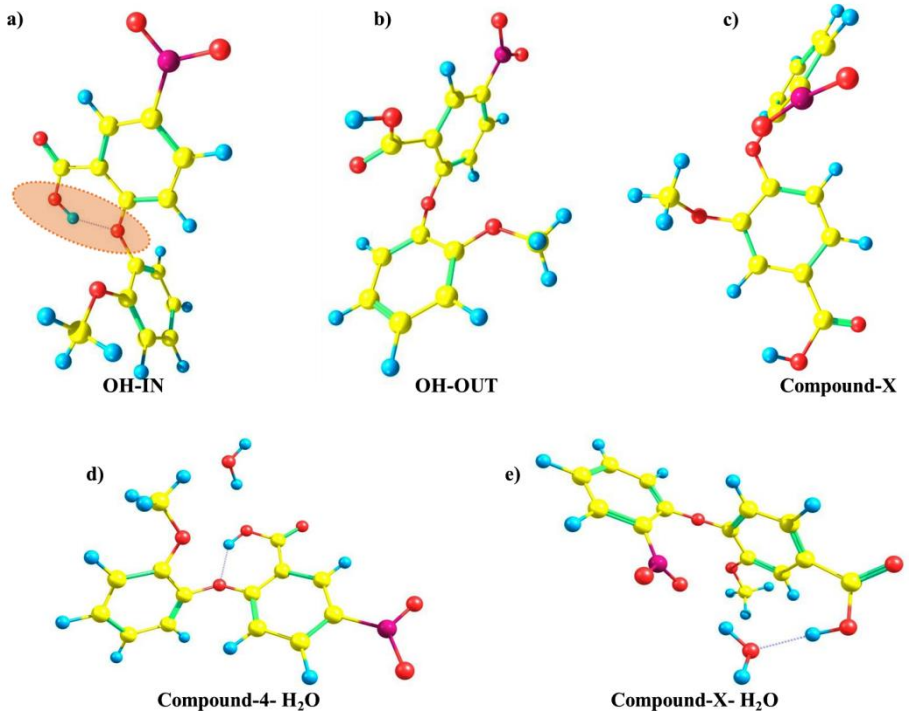

Figure-6.14: Optimized conformers indivisually **a) OH-IN**, **b) OH-OUT**, **c) compound-X,** and solvation interaction of **d) OH-IN** or **Compound-X** with water molecule.

Thus, the above studies highlighted the role of intramolecular hydrogen bonding in compound-**4** to respond in an aqueous medium.

6.9. Conclusion

The optimization of compound-4 under different pH and solvent systems gave conditions for the selective detection of cyanide ions. The pH studies suggested broader applicability for anion detection in the neutral pH range of 7.0 to 8.0 and a notable detection limit of 100 nM for the cyanide ions selectively in 5% aqueous ACN system. Except for the highly acidic sulphate ions, none of the anions (F^-, Cl^-, Br^-, I^-, CN^-, OAc^-, HPO_4^-, HSO_4^- and ClO_4^-) interfered in the detection of cyanide ions. The titration studies in the optimized solvent system gave an isosbestic point at 319 nm with a minimum detection limit of 100 nM and a binding constant equal to 0.5 $x10^5$ M^{-1}. The cyanide ions interacted with compound-**4** in a ratio of 1:1. Emission studies corroborated the above results but were not taken up further due to their weak intensity.

As proposed in the previous chapter, the proton abstraction mechanism for interaction with cyanide ions was explored by comparing similar studies with two new synthesized compounds, **4a** and **X**. The methyl ester derivative **(4a)** did not respond to any of the anions.

Compound-**X,** however, lost its ability to detect fluoride, acetate and cyanide ions when 5% aqueous ACN replaced the pure ACN solvent system.

Additionally, ^{1}H NMR titrations in the presence of cyanide ions also validated the proton abstraction mechanism for compound-**4** by the upfield shift of aromatic ring protons bearing the carboxylic acid group. The shifting matched proton abstraction by a base (NaOH) on titration against compound-**4,** authenticating the proposed mechanism. Similarly, using IR spectroscopy for compound-**4** before and after the addition of cyanide ions displayed movement of the carboxylic carbonyl group from 1614 cm^{-1} to 1570 cm^{-1} and the appearance of a new signal corresponding to HCN also corroborated the proton abstraction mechanism.

Further, the exceptional response of the compound-**4** in an aqueous medium compared to its positional isomer **(**compound-**X**) was reasoned via Gaussian-16 software. Calculations for the minimum energy and HOMO-LUMO gap suggested **OH-IN** as the most stable conformer for compound-**4** that edged over compound-**X** due to its exceptional ability to form an intramolecular hydrogen bond with ethereal oxygen. Comparative solvation studies gave an undissociated product for compound-**4** and a dissociated one for compound-**X** led to the above conclusion that was verified experimentally by finding the pKa value in each case.

Thus, the work presented here optimized the selective detection of the cyanide ions by compound-**4** in a neutral semi-aqueous medium. The limitation to recognizing anions in the alkaline medium prevented using compound-**4** for the real-life sampling. Nonetheless, the mechanistic study based on evidence highlights the proton abstraction mechanism.

Reference

1. Pourreza, N.; Golmohammadi, H.; Naghdi, T.; Yousefi, H., *Biosens. and Bioelectron.* **2015,** *74*, 353-359.
2. Jaszczak, E., Polkowska, Z.; Narkowicz, S.; Namiesnik, J., *Environ. Sci. Pollut. Res. Int.* **2017,** *24*, 15929.
3. Kuyucak, N.; Akcil, A., *Miner. Eng.* **2013,** *50*, 13-29.
4. Edition, F., Guidelines for drinking-water quality. *WHO chron.* **2011,** *38*, 104-108.
5. Orojloo, M.; Amani, S., *C. R. Chim.* **2017,** *20*, 415-423.
6. Egekeze, J. O.; Oehme, F. W., *Vet. Q.* **1980,** *2*, 104-114.
7. Ng, P. C.; Hendry-Hofer, T. B.; Witeof, A. E.; Mahon, S. B.; Brenner, M.; Boss, G. R.; Bebarta, V. S., *Ann. Emerg. Med.* **2019,** *74*, 423-429.
8. Ma, J.; Dasgupta, P. K., *Anal. chim. Acta* **2010,** *673*, 117-125.
9. Kundu, A.; Hariharan, P.; Prabakaran, K.; Anthony, S. P., *Sens. Actuators B Chem.* **2015,** *206*, 524-530.
10. Hu, J.-H.; Sun, Y.; Qi, J.; Li, Q.; Wei, T.-B., *Spectrochim. Acta A Mol. Biomol. Spectrosc.* **2017,** *175*, 125-133.
11. Li, Z.; Liu, C.; Wang, S.; Xiao, L.; Jing, X., *Spectrochim. Acta A Mol. Biomol. Spectrosc.* **2019,** *210*, 321-328.
12. Tang, L.; Cai, M., *Sens. Actuators B: chem.* **2012,** *173*, 862-867.
13. Yu, Y.; Shu, T.; Yu, B.; Deng, Y.; Fu, C.; Gao, Y.; Dong, C.; Ruan, Y., *Sens. Actuators B: chem.* **2018,** *255*, 3170-3178.
14. Jeyasingh, V.; Murugesan, K.; Lakshminarayanan, S.; Liyakathali, M. A.; Nadarajan, V. P.; Muniyandi, D. K.; Selvapalam, N.; Das, G.; Piramuthu, L., *J. Photochem. Photobiol.* **2021,** *6*, 100018-100029.
15. Jayasudha, P.; Manivannan, R.; Ciattini, S.; Chelazzi, L.; Elango, K. P., *Sens. Actuators B: chem.* **2017,** *242*, 736-745.
16. Schramm, A. D.; Menger, R.; Machado, V. G., *J. Mol. Liq.* **2016,** *223*, 811-818.
17. Padghan, S. D.; Wang, C.-Y.; Liu, W.-C.; Sun, S.-S.; Liu, K.-M.; Chen, K.-Y., *Dyes Pigm.* **2020,** *183*, 108724-108730.
18. Wu, C.; Wang, J.; Shen, J.; Zhang, C.; Wu, Z.; Zhou, H., *Tetrahedron* **2017,** *73*, 5715-5719.
19. Kaur, K.; Mittal, S. K.; SK, A. K.; Kumar, A.; Kumar, S., *Anal. Methods* **2013,** *5*, 5565-5571.
20. Gupta, S.; Mittal, S. K.; Chhibber, M., *J. Electrochem. Soc.* **2020,** *167*, 167506.
21. Kumar, A.; Chhibber, M., *ChemistrySelect* **2022,** *7*, e202104386.
22. Pliego J. R.; Riveros, J. M., *Phy. Chem. Chem. Phy.* **2002**, *4*, 1622-1627.
23. Dunn, G.; McDonald, R., *Can. J. Chem.* **1969,** *47*, 4577-4588.

Conclusion

The work presented here demonstrates the synthesis and characterization of diphenyl-based molecules and their use for detecting environmentally and biologically important ions. The synthesized molecules were explored both for detecting cations and anions using photophysical methods.

A systematic study in **section II** describes the detection of cations. A pH variation using an aqueous medium gave initial detection for the Hg^{2+}, Pb^{2+} and Cu^{2+} ions. The system was further optimized by synthesizing new thio-based diphenyl ether **(Compound-5)** to improve selectivity and the detection limit. The final results were validated by use of NMR titration and IR comparison. The receptor was further optimized to detect Hg^{2+} in the urine sample in the micro-molar range.

Section-III highlights the proton abstraction mechanism for the anion detection using seven diphenyl ethers that contained one or two acidic protons. The solvent played a vital role in this study where pure ACN medium initially detected three ions namely F^-, CN^- and CH_3COO^-. Optimization of the solvent conditions led us to use a 5% aqueous ACN system for the selective detection of CN^- ions

Overall, the work demonstrates the use of diphenyl ethers for the detection of ions using simple UV-Visible spectroscopy and the role of different functional groups on the motif in manipulating the detection capabilities of the receptors.